Dissertation

submitted to the

Combined Faculties for the Natural Sciences and Mathematics

of the Ruperto-Carola University of Heidelberg, Germany

for the degree of

Doctor of Natural Science

presented by

M.Sc. Isabel Hinsenkamp

born in Speyer, Germany

Oral examination: 14.09.2018

The role of DLC1 in *Helicobacter*-related gastric disease

Referees: Prof. Dr. Michael Wink

Prof. Dr. Ilse Hofmann

„Phantasie ist wichtiger als Wissen, denn Wissen ist begrenzt.“
- Albert Einstein

Table of Contents

Publications

Parts of this study have been published as follows:

Hinsenkamp, I., Schulz, S., Roscher, M., Suhr, A.-M., Meyer, B., Munteanu, B., Fuchser, J., Schoenberg, S.O., Ebert, M.P., Wängler, B., Hopf, C., Burgermeister, E. (2016). Inhibition of Rho-Associated Kinase 1/2 Attenuates Tumor Growth in Murine Gastric Cancer. Neoplasia *18*, 500-511.

Summary

DLC1 is a tumor suppressor protein downregulated in gastric cancer. It is a negative regulator of *RHOA*, which is the major oncogenic driver mutation of human diffuse gastric cancer. *Helicobacter* infection leads to chronic gastric inflammation, which is a risk factor for the development of carcinoma. The *Helicobacter* toxin CagA activates numerous signaling pathways including RHOA. The role of DLC1 in *Helicobacter*-related gastric disease is unknown and was analyzed by this thesis.

$DLC1^{gt/+}$ mice showed increased gastric inflammatory infiltration. Involvement of DLC1 in the regulation of the immune response was confirmed by RT-qPCR analyses. Furthermore, DLC1 was shown to be localized to enterochromaffin-like cells. Quantitative gene expression analyses verified a crucial role of the tumor suppressor in homeostasis of gastric acid *in vivo*, thereby preventing the development of gastric cancer.

This study further demonstrates an interaction between DLC1 and CagA. DLC1 was transcriptionally downregulated by CagA and the two proteins fulfilled antagonizing functions by complex formation. DLC1 counters the oncogenic signaling of CagA *in vitro* by promoting adhesion, suppressing proliferation and antagonizing CagA concerning the hypoxic stress response. DLC1 furthermore inhibited CagA-mediated G-protein-coupled RHOA activation.

In vivo therapy of a preclinical model for human gastric cancer with an inhibitor of the RHO/ROCK-pathway efficiently reduced tumor growth. These findings propose inhibition of this pathway as a novel treatment strategy for human gastric cancer.

In summary, this thesis postulates a protective role of DLC1 in initial steps of gastric disease by antagonizing CagA-mediated oncogenic signaling. Transcriptional downregulation of DLC1 by CagA promotes oncogenic effects and constitutes DLC1 as an early molecular marker for *Helicobacter*-related gastric disease. Due to the involvement of CagA and DLC1 in the regulation of RHOA, *Helicobacter*-related gastric disease can be assigned to diffuse genomically stable gastric cancer. This represents a new risk stratification for *Helicobacter*-infected gastric cancer patients. Suppression of tumor growth using an inhibitor of the RHOA downstream effector ROCK proposes DLC1 as a future druggable target in human gastric cancer.

Zusammenfassung

Der Tumorsuppressor DLC1 zeigt eine verminderte Expression in Magenkrebs und ist ein negativer Regulator von *RHOA*, welches das bedeutendste Onkogen in diffusem Magenkrebs darstellt. Eine *Helicobacter*-Infektion resultiert in einer chronischen Entzündung des Magens und erhöht das Risiko für Magenkrebs. Das *Helicobacter* Toxin CagA aktiviert verschiedenste Signalwege einschließlich RHOA. Die Funktion von DLC1 bei der *Helicobacter*-assoziierten Erkrankung des Magens ist unbekannt und wurde in der vorliegenden Arbeit untersucht.

$DLC1^{gt/+}$ Mäuse zeigten eine verstärkte inflammatorische Infiltration des Magens. RT-qPCR Analysen bestätigten eine Regulierung der Immunantwort durch DLC1. Des Weiteren konnte eine Lokalisierung von DLC1 in enterochromaffin-ähnlichen Zellen festgestellt werden. Quantitative Genexpressionsanalysen verifizierten eine essentielle Rolle von DLC1 bei der Homöostase der Magensäure *in vivo*, wodurch DLC1 vor Magenkrebs schützt.
Weiterhin demonstriert diese Arbeit eine Interaktion zwischen DLC1 und CagA. Es konnte eine transkriptionelle Hemmung von DLC1 durch CagA nachgewiesen werden. Die Proteine zeigten eine Interaktion und agierten gegensätzlich. DLC1 wirkte *in vitro* den onkogenen Effekten von CagA durch Unterstützung der Adhäsion, Inhibition der Proliferation und antagonistischer Wirkung bezüglich der hypoxischen Stressantwort entgegen. Zusätzlich konnte eine Hemmung der CagA-vermittelten RHOA Aktivierung durch DLC1 gezeigt werden. Ein Inhibitor des RHO/ROCK-Signalweges reduzierte effektiv das Tumorwachstum in einem präklinischen Modell für Magenkrebs. Somit stellt die Inhibition dieses Signalweges eine neue Strategie zur Behandlung von Magenkarzinomen dar.

Zusammenfassend zeigt diese Arbeit eine Schutzfunktion von DLC1 in initialen Stadien vor der Entstehung von Magenkrebs durch Inhibition der onkogenen CagA-Signalwirkung. Die transkriptionelle Hemmung von DLC1 durch CagA identifiziert DLC1 als frühen molekularen Marker für die *Helicobacter*-vermittelte Erkrankung des Magens. Aufgrund der Beteiligung von CagA und DLC1 an der RHOA-Regulation kann *Helicobacter*-assoziierter Magenkrebs dem genetisch stabilen Subtypen zugeordnet werden. Hierdurch ergibt sich eine neue Risikostratifizierung *Helicobacter*-infizierter Magenkrebspatienten. Eine Hemmung des RHO/ROCK-Signalweges *in vivo* ergab ein reduziertes Tumorwachstum und legt DLC1 als einen zukünftigen therapeutischen Angriffspunkt bei der Behandlung von Magenkrebs dar.

Abbreviations

aa	Amino acid
AB	Antibody
AGS	Human gastric adenocarcinoma cell line
AKT-X	AKT Serine/Threonine Kinase X
Amp^R	Ampicillin resistance
APC	Adenomatous polyposis coli
APS	Ammonium peroxodisulfate
ARHGAP-X	RHO GTPase activating protein X
ARID1A	AT-rich interactive domain-containing protein 1A
ATCC	American Type Culture Collection
ATP	Adenosine triphosphate
β2M	β2-Microglobulin
BabA	Blood group antigen binding adhesin
BCOR	B-cell lymphoma 6 corepressor
bp	Base pair
BRAF	B-Raf proto-oncogene, serine/threonine kinase
BSA	Albumin Fraction V
C3T	*Clostridium botulinum* C3 toxin
cagA	Cytotoxin-associated gene A
CAV1	Caveolin-1
CD-X	Cluster of differentiation X
CDC42	Cell division control protein 42 homolog
CDH1	Cadherin-1

CDKN2A	Cyclin-dependent kinase inhibitor 2A
cDNA	Complementary desoxyribonucleic acid
CDX2	Homeobox protein CDX-2
ChrA	Chromogranin A
CIMP	CpG island methylator phenotype
CIN	Chromosomal instability
CLDN18	Claudin-18
CLR	C-type lectin receptor
CoIP	Co-immunoprecipitation
CpG	Cytosine-phosphate-Guanine
CRC	Colorectal cancer
CS	Cell Signaling (company)
C-Terminus	Carboxy-Terminus
DAB	3,3'-Diaminobenzidine
DAMP	Damage-associated molecular pattern
DAPI	4,6-Diamidino-2-phenylindol dihydrochloride
DLC-X	Deleted in liver cancer X
DMEM	Dulbeccos Modified Eagle medium
DMSO	Dimethyl sulfoxide
DNA	Desoxyribonucleic acid
dNTP	Desoxyribonucleoside triphosphate
DSMZ	Leibniz-Institut DSMZ-Deutsche Sammlung von Mikroorganismen und Zellkulturen GmbH
DTT	Dithiothreitol
DU	Duodenal ulcer
DupA	Duodenal ulcer promoting gene A

EBV	Eppstein-Barr Virus
ECL	Enterochromaffin-like
EDTA	Ethylenediamine tetraacetic acid
EF1A1	Eukaryotic elongation factor 1A1
EGFR	Epidermal growth factor receptor
EMT	Epithelial-Mesenchymal-Transition
EPIYA	Proline-Isoleucine-Tyrosine-Alanine
ER	Endoplasmatic reticulum
ERK	Extracellular signal-regulated kinase
EtOH	Ethanol
EV	Empty vector
[^{18}F]-FDG	Radioactively labeled fluorodeoxyglucose
5-FU	Fluorouracil
F4/80	EGF-like module-containing mucin-like homone receptor-like 1
FACS	Fluorescence activated cell sorter
FAK	Focal adhesion kinase
FAT	Focal adhesion targeting
FCS	Fetal calf serum
FDG	Fluorodeoxyglucose
FLAG	FLAG octapeptide, proteintag
FOXP3	Forkhead-Box-Protein P3
Gα12/13	Guanine nucleotide binding protein alpha 12/13
GAP	GTPase-activating protein
GATA3	Guanine-adenine-thymine-adenine sequence-binding protein 3
GC	Gastric cancer

GDI	Guanine nucleotide dissociation inhibitor
GDP	Guanosine diphosphate
GEF	Guanine nucleotide exchange factor
GFP	Green fluorescent protein
GI	Gastrointestinal
GOF	Gain of function
GS	Genomic stability
GST	Glutathione-S-transferase
gt	Gene trap
GTP	Guanosine triphosphate
H&E	Hematoxylin & Eosin
H_2O_2	Hydrogen peroxide
HCl	Hydrochloric acid
HDAC	Histone deacetylase
HEK293T	Human embryonic kidney cell line, T-Antigen
HEPES	4-(2-Hydroxyethyl)-1-piperazine ethanesulfonic acid
HER-X	Human epidermal growth factor receptor-X
HIF1α	Hypoxia-inducible factor 1α
H^+K^+-ATPase	Hydrogen potassium ATPase
HMGB2	High mobility group protein B2
HRE	Hypoxia responsive element
HRP	Horseradish peroxidase
HSP90	Heat shock protein 90
IARC	International Agency for Research on Cancer
IB	Immunoblotting
IF	Immunofluorescence

IFNγ	Interferon gamma
IHC	Immunohistochemistry
IgX	Immunoglobulin class X
IL-X	Interleukin group X
iNOS	Inducible nitric oxide synthase
IP	Immunoprecipitation
IPTG	Isopropyl-β-D-1-thiogalactopyranoside
i.p.	Intraperitoneal
i.v.	Intravenous
JAK2	Janus kinase 2
Kan^R	Kanamycin resistance
kb	Kilo base
KCl	Potassium chloride
kDa	Kilo Dalton
Ki67	Cellular marker for proliferation
KO	Knockout
LOF	Loss of function
LOH	Loss of heterozygosity
LPS	Lipopolysaccharide
MALDI-MS	Matrix Assisted Laser Desorption Ionization-Mass Spectrometry
MALT	Mucosa-associated lymphoid tissue
MAPK	Mitogen-activated protein kinase
MEK	Mitogen-activated protein kinase kinase
MES	2-(N-Morpholino)ethanesulfonic acid
MET	Mesenchymal-Epithelial-Transition

$MgCl_2$	Magnesium chloride
MHC	Major histocompatibility complex
MKN45	Human gastric adenocarcinoma cell line derived from metastatic site: liver
MLC/MYL2	Myosin light chain 2
MLH1	MutL homolog 1
MMR	Mismatch repair
mRNA	Messenger RNA
MSI	Microsatellite instability
MTT	3-(4,5-Dimethylthiazol-2-yl)-2,5-diphenyltetrazolium bromide
MUC-X	Mucin X
Na_3VO_4	Sodium orthovanadate
NaCl	Sodium chloride
NaOH	Sodium hydroxide
NCBI	National Center of Biotechnology Information
NFκB	Nuclear factor kappa-light-chain-enhancer of activated B cells
NLR	Nod-like receptor
NLS	Nuclear localization signal
NNC	N-Nitroso compounds
NOD1	Nucleotide-binding oligomerization domain-containing protein 1
n.s.	Not significant
NT	Normal tissue
N-Terminus	Amino-Terminus
OD_{600}	Optical density measured at a wavelength of 600nm
OMP	Outer membrane protein

p38	P38 mitogen-activated protein kinase
p44/42	ERK, extracellular signal-regulated kinase
PAI	Pathogenicity island
PAMP	Pathogen-associated molecular pattern
PBS	Phosphate buffered saline
PCR	Polymerase chain reaction
PD-1	Programmed cell death protein 1
PD-LX	Programmed death-ligand X
PET/CT	Positron emission tomography/computed tomography
PFA	Paraformaldehyde
PGN	Peptidoglycan
PH	Pleckstrin homology
PIK3CA	Phosphatidylinositol 3-kinase catalytic subunit alpha
PLA	Proximity ligation assay
PPARγ	Peroxisome proliferator activated receptor gamma
PRR	Pattern recognition receptor
pT	pTarget empty vector
PTEN	Phosphatase and tensin homologue
pUC19	pUC19 empty vector
RAC1	Ras-related C3 botulinum toxin substrate 1
RAS	Rat sarcoma, oncogene
RBD	RHOA binding domain
RHO-X	RAS homolog gene family, member X
RLR	RIG-like receptor
RNA	Ribonucleic acid
RNF-X	Ring finger domain X

ROCK	RHO-associated coiled-coil containing protein kinase
RORG2T	RAR-related orphan receptor gamma, tissue specific isoform
ROS	Reactive oxygen species
rpm	Revolutions per minute
RPMI	Roswell Park Memorial Institute Medium
RT	Room temperature
RTK	Receptor tyrosine kinase
RT-qPCR	Real time-quantitative PCR
S100A10	S100 calcium-binding protein A10
SabA	Sialic acid-binding adhesin
SAM	Sterile α motif
SC	Santa Cruz (company)
SDS-PAGE	Sodium dodecyl sulfate-polyacrylamide gel electrophoresis
S. E.	Standard Error of the Mean
Src	Proto-oncogene tyrosine-protein kinase Src
SRE	Serum response element
SREBP1	Sterol regulatory element-binding protein 1
StAR	Steroidogenic acute regulatory protein
START	StAR-related lipid-transfer
STAT3	Signal transducer and activator of transcription 3
SUV	Standard uptake volume
SYBR	DNA intercalating cyanine dye
T4SS	Type IV secretion system
TAE	Tris-acetate EDTA
Taq polymerase	*Thermus aquaticus* DNA polymerase
TBET	T-box expressed in T-cells

T_c cell	Cytotoxic T cell
TEMED	Tetramethylethylene diamine
T_h cell	T helper cell
TKI	Tyrosine-kinase inhibitor
TLR	Toll-like receptor
TOP 10	*Escherichia coli* strain
TP53	Tumor protein 53
TPBS	Tween-PBS
T_{reg} cell	Regulatory T cell
TRIS	Tris(hydroxymethyl)aminomethane
tsA201	Cell line human embryonal kidney, SV40 transformed
TU	Tumor tissue
UreB	Urease B
VacA	Vacuolating cytotoxin A
VEGF	Vascular endothelial growth factor
v/v	Volume per volume
WB	Western Blot
WHO	World Health Organization
WNT	Wingless-type MMTV integration site family
WT	Wild type
w/v	Weight per volume
X-Gal	5-Bromo-4-chloro-indolyl-β-D-galactopyranoside
YKL40	Human cartilage glycoprotein-39, glycosyl hydrolase

Nomenclature

Human genes are written in italic capital letters (e.g. *DLC1*), whereas mouse genes are indicated in italic letters and only the first letter is upper-case (e.g. *Dlc1*). Human and mouse protein names are in capital letters (e.g. DLC1).

Bacterial genes are indicated as small italic letters (e.g. *cagA*). Bacterial protein names are not italicized and the first letter is upper-case (e.g. CagA).

1 Introduction

1.1 Gastric cancer

1.1.1 Epidemiology

Gastric cancer (GC) is the fifth most frequent cancer entity and the third leading cause of cancer related deaths worldwide (Tan and Yeoh, 2015). Due to nonspecific symptoms such as abdominal fullness or heartburn in early stages, gastric malignancies are usually detected in advanced stages resulting in a very poor prognosis. Symptoms of advanced stages include anemia, weight loss, vomiting and a general impairment of health (Catalano et al., 2009; Nagini, 2012). This results in an increased case-fatality ratio compared with other malignancies (Jemal et al., 2011). In Europe, 159,900 new cases and 118,200 cases of death have been reported in 2006 for GC (Jackson et al., 2009). The 5-year survival rate of GC in US and European countries is only 10-20% (Catalano et al., 2009; Karimi et al., 2014; Strathmann and Simon, 1991). Nevertheless, a decline in both, incidence and mortality, has been observed (Bosetti et al., 2013; Fox and Wang, 2007; Nagini, 2012).

Incidence of GC increases with age showing a peak at 60-80 years (Nagini, 2012). In almost all countries, there is a male predominance. In males, rates of stomach cancer are two to four times higher compared with females (Jemal et al., 2011; Karimi et al., 2014; Nagini, 2012). GC shows highest incidence rates in Eastern Asia, Eastern Europe and South America. Lowest incidence rates have been recorded in North America and Africa (Howe et al., 2006; Karimi et al., 2014). Furthermore, the incidence of GC shows significant variations among different ethnic groups living in the same area (Parkin, 2004).

Adenocarcinomas develop in proximal (cardia) and distal (non-cardia) stomach regions. Distal GC is most common in developing countries, among Afro-Americans and lower socio-economic groups. Proximal tumors predominate in developed countries, among whites and higher socio-economic classes. While distal stomach cancer preponderates in Japan, proximal tumors show an increasing prevalence in the rest of the world and poorer prognosis compared with distal GC (Catalano et al., 2009; Crew and Neugut, 2006).

1.1.2 Pathogenesis

GC shows a multifactorial disease pattern. Several risk factors for gastric carcinogenesis are known. Almost all cases of GC are associated with an infection with *Helicobacter pylori* (*H. pylori*). The bacterium was classified as a type I carcinogen in humans by the International Agency for Research on Cancer (IARC) in 1994. *H. pylori* infection results in a two-fold increased risk of GC. Nevertheless, *H. pylori* infection alone is not sufficient for the development of gastric malignancies (Catalano et al., 2009; Crew and Neugut, 2006; De Falco et al., 2015; Karimi et al., 2014; Nagini, 2012).

Nutrition and food play a significant role in the progression of GC. High starch and low protein diet are suggested to cause nitrosation and thereby attack the gastric mucosa. Prolonged consumption of salt-preserved foods such as soy sauce, pickled vegetables, processed meat and salted fish is known to increase the risk for GC development. Salt is proposed to induce mutations, cause proliferation of epithelial cells and loss of parietal cells. Furthermore, intake of salt-preserved foods enforces *H. pylori* infection and directly damages the gastric mucosa. Dietary nitrates are also associated with an elevated risk of GC. Gastric acid converts dietary nitrates into carcinogenic N-nitroso compounds (NNC). Dietary nitrates can be found naturally in foods (e.g. carrots, radish, beets, spinach), synthesized by bacterial reactions or added artificially during preservation. Moreover, *H. pylori*-mediated gastritis facilitates colonization of the stomach with nitrosating bacteria. Furthermore, cooking practices such as smoking, roasting, grilling, sun drying, pickling, salting and curing of meat are known to increase the risk for GC (Catalano et al., 2009; Crew and Neugut, 2006; IARC Press, 2014; Karimi et al., 2014; Nagini, 2012).

A significant dose-dependent relationship exists between tobacco consumption and the development of GC. Approximately 18% of all GCs are associated with smoking. A combination of excessive use of cigarettes (> 20/day) and alcohol (> 5 occasions/2 weeks) resulted in a five-fold increased risk of distal GC. Furthermore, smokers have an increased chance for *H. pylori* infection and gastroduodenal inflammation compared with non-smokers (Catalano et al., 2009; Crew and Neugut, 2006; Nagini, 2012).

Obesity is another risk factor, which promotes gastro-esophageal reflux disease and Barrett's esophagus. It has been found that obesity is responsible for a 2.3-fold increased chance for proximal GC (Crew and Neugut, 2006; Karimi et al., 2014).

Another risk factor for GC represents a positive family history. Approximately 10% of all GCs are hereditary. First degree relatives of patients have a two- to three-fold elevated risk of GC (Catalano et al., 2009; Crew and Neugut, 2006; Nagini, 2012).

Minor risk factors for GC include radiation, blood type A, Epstein-Barr Virus infection or several occupations. An increased risk of GC has been recognized for occupations such as mining, refining, farming and fishing due to exposure to dust, rubber or asbestos (Crew and Neugut, 2006; Karimi et al., 2014; Nagini, 2012).

1.1.3 Genetic background

Gastric carcinogenesis is a result of multiple genetic and epigenetic changes, which are responsible for activation of oncogenic pathways and inactivation of tumor suppressors. The majority of GCs are adenocarcinomas. They are classified into two distinct histological types, also known as intestinal- and diffuse-type GC, according to the Laurén classification (Cancer Genome Atlas Research, 2014).

Intestinal GC is characterized by a gastritis focused on the corpus. It is more frequent in men, Afro-Americans and older patients. Furthermore, intestinal-type tumors have a better prognosis compared to diffuse-type GC (Nagini, 2012). Intestinal-type GC develops through well-differentiated sequential stages from chronic gastritis, atrophy, intestinal metaplasia and dysplasia to carcinoma (Yuasa, 2003). Atrophic gastritis describes a histological step characterized by a complete loss of parietal (acid producing) and chief (pepsinogen producing) cells as well as a variable gland loss and infiltration of inflammatory cells into glandular zones (Fox and Wang, 2007; Polk and Peek, 2010). During intestinal metaplasia, gastric mucosa changes to an intestinal phenotype by columnar elongation and formation of goblet (mucin producing) cells. Abnormal activation of the intestine-specific transcription factor CDX2 leading to expression of intestine-specific genes including *MUC2*, *sucrose/isomaltase* or *carbonic anhydrase I* is believed to be responsible for this event

(Yuasa, 2003). Cell proliferation and cellular/nuclear atypia can be observed during dysplasia (Catalano et al., 2009; Fox and Wang, 2007).

Diffuse-type GC is histologically undifferentiated and develops from single-cell changes localized at the mucous-neck region of gastric glands, which proliferate and invade into the lamina propria (Catalano et al., 2009; Yuasa, 2003). Diffuse-type GC is characterized by a pan-gastritis affecting the whole stomach without atrophy. It is more common in women and younger people living in endemic areas (Fox and Wang, 2007; Nagini, 2012). *H. pylori* infection is known to be a risk factor for both histological types of GC (Uemura et al., 2001).

Besides the Laurén classification, the Cancer Genome Atlas Research Network has classified 295 GC patient samples into four molecular subtypes (Fig. 1.1). First, the tumor samples were categorized by Epstein-Barr Virus (EBV) positivity (9%) and microsatellite instability (MSI)-high status (22%). The remaining tumors were classified by grade of aneuploidy (gain/loss of chromosome parts or whole chromosomes) into genomically stable (GS; 20%) and chromosomally instable (CIN; 50%) tumors (Cancer Genome Atlas Research, 2014).

EBV-positive tumors are mainly present in the fundus or the body of the stomach. All EBV-positive cases showed an extreme CpG island methylator phenotype (CIMP). 5‘-Cytosine-phosphate-Guanine-3‘ (CpG) sites are promoter regions where cytosine is followed by a guanine nucleotide. CpG islands are accumulations of CpG sites and methylation results in epigenetic repression of specific genes. The Cancer Genome Atlas Research Network determined increased DNA hypermethylation for EBV-positive tumors compared with all other cancers including promoter hypermethylation of the tumor suppressor *CDKN2A*. Furthermore, EBV-positive GC showed activating mutations of the oncogenes *PIK3CA* and *BCOR*, but also inactivating mutations of the tumor suppressors *ARID1A* and *TP53*. Moreover, enriched amplification of 9p24.1 at the locus possessing *JAK2*, *CD274* and *PDCD1LG2* was observed. The JAK2 protein represents a receptor tyrosine kinase, which is a putative therapeutic target. *CD274* and *PDCD1LG2* encode the two immunosuppressant proteins PD-L1 and PD-L2. Strong IL-12 mediated signaling indicates a solid immune cell presence in EBV-positive tumors (Cancer Genome Atlas Research, 2014; Figueiredo et al., 2013; Garattini et al., 2017; Wang et al., 2014).

MSI tumors are predominantly of the intestinal type and can be found in all stomach regions. MSI results from impaired DNA replication and is characterized by extension or reduction of microsatellite repeats (short repeated DNA sequences) as a result of insertion or deletion of repeats (Yuasa, 2003). MSI cases show increased hypermethylation of *MLH1* promoter (DNA mismatch repair gene) in the context of CIMP. Furthermore, cytosine-adenine repeat instability and loss of heterozygosity (LOH, loss of a complete gene and its surrounding chromosomal region) of the tumor suppressor gene *APC* have been reported leading to activation of the WNT signaling pathway by stabilization of β-catenin and subsequent activation of oncogenes (Nagini, 2012; Yuasa, 2003). Just as EBV-positive GC, MSI tumors show silencing of *ARID1A* and lack of *TP53.* Further mutations of MSI tumors represent *MUC6* and *RNF43*. *MUC6* encodes gastric mucin and its inactivation is suggested to enhance chronic mucosal injury and carcinogenic progression. *RNF43* encodes the E3 ubiquitin ligase and acts as a negative regulator of the WNT pathway (Cancer Genome Atlas Research, 2014; Figueiredo et al., 2013; Garattini et al., 2017; Nagini, 2012; Wang et al., 2014; Yuasa, 2003).

CIN tumors are characterized by increased occurrence at the cardia and an intestinal histology. They show numerous DNA copy number variations resulting in gains of diverse chromosomal regions. This molecular subtype shows increased mutation of *TP53* and cytosine-adenine repeat instability. Further hallmarks of CIN tumors represent genomic amplification of receptor tyrosine kinases (RTKs) and RAS signaling including HER-2, BRAF and EGFR. Moreover, CIN GC is associated with genome-wide demethylation and somatic mutations (Cancer Genome Atlas Research, 2014; Figueiredo et al., 2013; Garattini et al., 2017; Wang et al., 2014).

Tumors of the GS subtype are present throughout the stomach and show a diffuse histology. Increased *CDH1* somatic mutations were observed in GS tumors. *CDH1* encodes E-cadherin, a tumor suppressor protein. There are several studies, which identified mutations of the *RAS homolog gene family A* (*RHOA*) as oncogenic drivers in 14-25% of diffuse-type GC (Cancer Genome Atlas Research, 2014; Kakiuchi et al., 2014; Wang et al., 2014). RHO is a member of the rat sarcoma (RAS)-related family of small molecular weight GTP-binding proteins. It regulates cytoskeletal organization, apoptosis, cell adhesion, gene transcription and cell cycle progression. GTP-bound active RHOA is known to promote tumorigenesis through diverse effectors such as the RHO-associated coiled-coil containing kinase (ROCK), mDIA or

Protein Kinase N (Cancer Genome Atlas Research, 2014; Julian and Olson, 2014). Modulated RHOA is suggested to be responsible for characteristics of diffuse tumors such as a dissimilar growth pattern and defects in cellular coherence. Furthermore, *RHOA* mutations are proposed to play an essential role in initial stages of cancer progression. The Cancer Genome Atlas Research Network observed enriched interchromosomal translocation resulting in *CLDN18-ARHGAP26/6* fusions in GS tumors. CLDN18 is part of the tight junction adhesion structures. ARHGAPs catalyze transformation from active GTP-bound to inactive GDP-bound RHOA. The CLDN18-ARHGAP26/6 fusion transcript can be affected in RHOA regulation and the function of CLDN18 concerning cellular adhesion (Cancer Genome Atlas Research, 2014; Garattini et al., 2017). Somatic mutations are distributed across the whole *RHOA* gene. Highly conserved mutational hotspots affecting the Tyr42, Arg5 and Gly17 residues in RHOA and, hence, its functional domains, were identified (Kakiuchi et al., 2014). *RHOA* mutations further promote resistance to anoikis, which is a hallmark of diffuse-type GC (Wang et al., 2014).

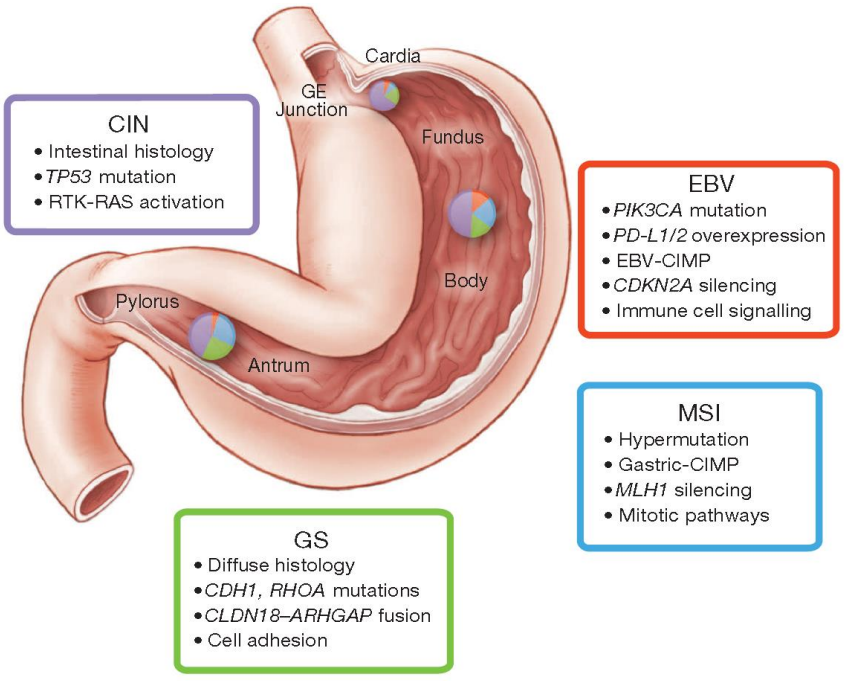

Fig. 1.1: Main features of the four molecular GC subtypes. Inset charts represent the distribution of each molecular subtype in tumors obtained from the different regions of the human stomach (copied from Cancer Genome Atlas Research, 2014).

1.1.4 Treatment

Gastric malignancies are usually detected in advanced stages due to mild and nonspecific symptoms in early stages. Primary prevention is very important to improve prognosis. Modifying risk factors for GC, such as high salt intake, low consumption of fresh fruits and vegetables, smoking and *H. pylori* eradication therapy may result in a decrease of GC incidence and mortality. Due to the high risk of GC in Japan, a national endoscopic surveillance program helped to detect about half of GCs at early stages (Catalano et al., 2009; Crew and Neugut, 2006; Nagini, 2012). Endoscopy is the most effective, accurate and rapid diagnose method to detect GC. A major advantage of endoscopy is the ability to perform biopsy of gastric lesions or ulcers in one step (Catalano et al., 2009; Karimi et al., 2014).

The treatment of choice for GC is the surgical resection of primary tumors. Chemo- or radiotherapy can be applied as adjuvant therapy strategies. Neoadjuvant therapy is used to reduce the size of inoperable tumors enabling resection. In case of metastatic disease, the treatment of GC is symptomatic or palliative (Catalano et al., 2009).

A widely used chemotherapeutic drug for treatment of advanced GC is 5-Fluorouracil (5-FU), which is an analogue of uracil. 5-FU is able to enter cells rapidly and is converted to active metabolites intracellularly. These disrupt RNA and DNA synthesis and impair the function of the nucleotide synthetic enzyme thymidylate synthase (Longley et al., 2003). A similar mode of action is known for platinum compounds, such as cisplatin (*cis*-Diamino-dichloro-platinum). Cisplatin-induced DNA damage activates cell cycle checkpoints resulting in apoptosis (Siddik, 2003).

The response rate of chemotherapy constitutes only 20-40% and serious side effects cannot be ignored. This is why attention has been focused on molecular targeted therapy. Molecular targeted inhibitors negatively regulate overexpressed molecules and pathways involved in tumor development. Big advantages of targeted therapy are improved specificity, decreased non-selective toxicity and reduced resistance. Molecular targeted therapy affects a number of mechanisms associated with GC, such as regulation of epidermal growth factor (EGF), angiogenesis or immune-checkpoint blockade. Monoclonal antibodies used for treatment of advanced GC targeting the EGF-receptor (EGFR)-family are cetuximab,

trastuzumab or pertuzumab. The EGFR family consists of four members: HER-1 (EGFR), HER-2 (Neu), HER-3 and HER-4. In contrast to trastuzumab and pertuzumab targeting HER-2 receptor, cetuximab avoids the binding of natural ligands to HER-1. This inhibits activation of EGFR and downstream RAS/MEK signaling pathway, leading to a reduced cell proliferation and increased apoptosis. Moreover, cancer progression, invasion and metastasis are vascular-dependent. Monoclonal antibodies, such as bevacizumab, targeting vascular EGF (VEGF) affecting tumor angiogenesis and downstream signaling are commonly used for the treatment of advanced GC. Furthermore, tyrosine kinase inhibitors (TKIs) are applied in GC treatment to inhibit key molecules, such as EGFR and VEGFR (The Angiogenesis Foundation, 2015; Xu et al., 2016). There are also monoclonal antibodies targeting PD-1 or PD-L1. These antibodies are used to block multiple immune-checkpoints resulting in the avoidance of tumor escape from immunologic cytotoxicity (Xu et al., 2016). Moreover, epigenetic alterations contribute to gastric carcinogenesis. Modifications in DNA methylation and histone acetylation results in divergent gene expression and silencing of tumor suppressor genes. Increased expression levels of histone deacetylases (HDACS) have been observed in GC. Thus, HDAC inhibition represents an effective treatment strategy for GC (Regel et al., 2012). Another attractive drug target for the treatment of GC represents ROCK1/2 downstream the oncogenic driver RHO. In China and Japan, fasudil (1-[5-Isoquinoline sulfonyl]-homopiperazine), a potent ROCK1/2 inhibitor, is already permitted for the treatment of cerebral vasospasms. Anti-tumor efficacy of fasudil was confirmed in rodent xenograft studies investigating myeloma, melanoma, glioblastoma, breast, lung and head-and-neck cancer (Deng et al., 2010; Miyamoto et al., 2012; Xia et al., 2015; Ying et al., 2006).

A major obstacle in treatment of GC is the non-response due to resistance mechanisms. Due to this fact, there is a high medical need for novel drug targets and treatment strategies for GC (Siddik, 2003; The Angiogenesis Foundation, 2015; Xu et al., 2016).

1.2 *Helicobacter pylori*

An infection with *H. pylori* is known to be associated with the development of gastric diseases, such as chronic gastritis, peptic ulcer disease, Mucosa associated lymphoid tissue (MALT) lymphoma, mucosal atrophy and GC (Carbo et al., 2013). The discovery of *H. pylori* in

1982 by Robin Warren and Barry Marshall was a milestone for the treatment of these diseases. This is why they earned the Nobel Prize in 2005. In 1994, *H. pylori* has been classified as a class I human carcinogen by the International Association for Research on Cancer (IARC) (De Falco et al., 2015; Fox et al., 2000; Hatakeyama, 2004; Morales-Guerrero et al., 2013; Salama et al., 2013; Suerbaum and Josenhans, 2007; Yamaoka, 2010).

The gram-negative, helical, rod-shaped, microaerophilic bacterium colonizes the human stomach as its ecological niche. This demonstrates that the stomach is not a sterile organ as supposed for a long time. The pathogen shows a remarkable genetic heterogeneity enabling the bacteria to adapt to the host and its microniches. Bacterial diversity is generated by significantly increased endogenous mutation rates compared with other bacteria, which is advantaged by a lack of mismatch-repair systems. Intra- and intergenomic recombination due to natural competence of *H. pylori* for uptake of DNA from other bacteria are further mechanisms to facilitate chronic persistence and adaption to the host (Blaser and Atherton, 2004; Salama et al., 2013; Suerbaum and Josenhans, 2007).

1.2.1 Epidemiology

H. pylori colonizes the stomachs of at least half of the human population. It is suggested that the bacteria have co-evolved with humans since they migrated out of Africa 58,000 years ago (Blaser and Atherton, 2004; Salama et al., 2013; Suerbaum and Josenhans, 2007; Yamaoka, 2010). *H. pylori* infection shows a higher prevalence in developing countries compared with developed countries. There, approximately 80% of the middle-aged adults are estimated to be infected (De Falco et al., 2015). Prevalence not only varies with geographic regions, but also with age, educational level, socio-economic status, living environment and occupation. Infection mainly occurs during childhood and can persist for decades or even a whole lifetime. The pathogen is transmitted vertically via direct human-to-human contact by fecal-oral or oral-oral routes of infection usually within families (De Falco et al., 2015; Hatakeyama, 2004; Morales-Guerrero et al., 2013; Suerbaum and Josenhans, 2007).

1.2.2 Colonization factors

The first step for a successful infection is the colonization of the human stomach by *H. pylori*. The production of gastric acid results in a pH of 1-2, thus, limiting bacterial colonization of the human stomach. *H. pylori* can only survive for a short time in the gastric lumen and needs to migrate to the epithelial surface. This is enabled by flagellar-based chemotaxis, which further allows penetration of the mucus. Ammonium production by the bacterial enzyme urease (UreB) plays an essential role in acid resistance by locally increasing the pH. Moreover, urease-catalyzed ammonium production facilitates bacterial motility by solubilizing the mucus layer, which usually forms a viscous gel for protection against bacteria. The helical cell shape of *H. pylori* is supposed to function as a corkscrew and thereby alleviates motility through viscous media (De Falco et al., 2015; Morales-Guerrero et al., 2013; Salama et al., 2013).

Once they have reached the gastric epithelium, the bacteria need to attach to the host cells to enforce infection and to be protected against clearance by liquid flow or peristaltic movement (De Falco et al., 2015). Attachment is mediated by outer membrane proteins (OMPs), named adhesins, which recognize glycan structures of gastric epithelial cells (Fig. 1.3). The most popular adhesins are blood group antigen binding adhesion (BabA) and sialic acid-binding adhesion (SabA). BabA recognizes fucosylated blood group antigens, whereas SabA binds to silylated carbohydrate structures of neutrophils and induces oxidative burst in these cells (De Falco et al., 2015; Morales-Guerrero et al., 2013; Salama et al., 2013).

1.2.3 Virulence factors

There are two types of *H. pylori* strains: strains harboring a *cag* pathogenicity island (PAI) and *cag* PAI-negative strains. This PAI is a genomic region composed of 31 genes including the *cytotoxin-associated gene A* (*cagA*) and a *type IV secretion system* (*T4SS*). The T4SS injects CagA into the epithelial host cell by forming a needle-like structure. Subsequently after translocation into the host cell, CagA localizes to focal adhesions and can be subjected to tyrosine phosphorylation of its C-terminal glutamate-proline-isoleucine-tyrosine-alanine (EPIYA) motif by Src or Abl kinases (De Falco et al., 2015; Morales-Guerrero et al., 2013; Salama et al., 2013; Yamaoka, 2010). EPIYA motifs are repeat regions and are classified into EPIYA-A, -B, -C and -D. Western-type CagA features EPIYA-A, -B and -C segments, whereas

East Asian-type CagA possesses EPIYA-A, -B and -D segments (Fig. 1.2). The number of EPIYA-C segments positively correlates to virulence of CagA due to multimerization sequences, which are known to be important for the interaction of CagA with diverse cellular targets. Compared with Western-type CagA, East Asian-type CagA is supposed to be more virulent. The polymorphism concerning the EPIYA motifs explains a variable size of the CagA protein of 120-145 kDa (Morales-Guerrero et al., 2013; Yamaoka, 2010). In the host cell cytoplasm, phosphorylated and unphosphorylated CagA interacts with diverse host proteins thereby activating downstream signaling pathways, such as RAS/mitogen-activated protein kinase (MEK)/extracellular signal-regulated kinase (ERK), nuclear factor κB (NFκB), β-catenin or RHOA. This causes deregulation of epithelial cell polarity (cell elongation, "hummingbird" phenotype), pro-inflammatory cytokine expression, disruption of tight junctions and cell apical junction complex (Blaser and Atherton, 2004; De Falco et al., 2015; Morales-Guerrero et al., 2013; Yamahashi and Hatakeyama, 2013; Yamaoka, 2010). Moreover, CagA interacts with the apoptosis-stimulating protein of p53 (ASPP2) thereby causing an anti-apoptotic response. These oncogenic processes enforce malignant transformation suggesting that CagA-positive *H. pylori* strains are more virulent than CagA-negative strains and significantly contribute to the development of gastric malignancies (De Falco et al., 2015).

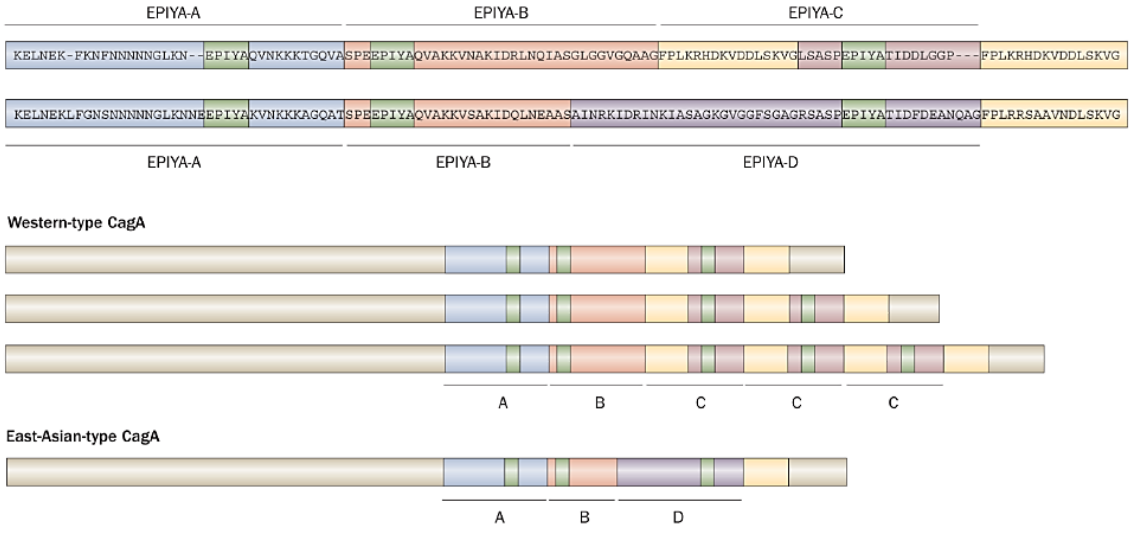

Fig. 1.2: Structure of *Helicobacter pylori* CagA protein. Western-type CagA contains EPIYA-A, -B and -C segments, whereas East Asian-type CagA contains EPIYA-A, -B, and -D segments. EPIYA motifs (green) in each segment represent the tyrosine phosphorylation sites of CagA (copied from Yamaoka, 2010) .

Another extensively studied *H. pylori* virulence factor is the vacuolating cytotoxin A (VacA), which is expressed by the majority of all *H. pylori* strains (Suerbaum and Josenhans, 2007). The *vacA* gene encodes a 140 kDa pro-toxin. After cleavage, the pore-forming virulent 88 kDa toxin arises and inserts itself into the host cell membrane (De Falco et al., 2015; Morales-Guerrero et al., 2013; Palframan et al., 2012). *VacA* is a polymorphic gene possessing three variable regions: the signal sequence region (*s*-region), the mid-region (*m*-region) and the intermediate-region (*i*-region). Besides induction of vacuolation, VacA has a series of further effects on the host cells, such as inhibition of mitochondrial functions, promotion of apoptosis, formation of membrane-channels, impeding T-cell proliferation and disruption of tight junctions (Morales-Guerrero et al., 2013; Palframan et al., 2012; Yamaoka, 2010). Loss of epithelial junctions allows nutrients to enter the gastric lumen where the bacteria are living (Blaser and Atherton, 2004; De Falco et al., 2015). The physiological importance of vacuolation during *H. pylori* infection is not fully understood, but it is suggested to intermit protein trafficking pathways and, thus, affecting host cell functions (Palframan et al., 2012).

Further *H. pylori* virulence factors include the heat shock protein B (HspB) and the duodenal ulcer promoting protein A (DupA). HspB inhibits the antioxidant response of infected cells and influences cellular proliferation and apoptosis (De Falco et al., 2015). DupA is associated with stimulation of mononuclear inflammatory cells and IL-8 production (Yamaoka, 2010). The bacterial cell wall components lipopolysaccharide (LPS) and peptidoglycan (PGN) represent further *H. pylori* virulence factors. *H. pylori* LPS is less bioactive than LPS of other gram-negative bacteria. It is not recognized by toll-like receptor 4 (TLR4) and, thus, prevents a pro-inflammatory immune response (Salama et al., 2013). PGN leads to Nod1-mediated activation of NFκB signaling resulting in expression of pro-inflammatory genes. PGN furthermore enhances PI3K-AKT signaling causing carcinogenesis related phenotypes, such as protection from apoptosis and cell migration (Morales-Guerrero et al., 2013).

The activities of the most important colonization and virulence factors of *H. pylori* are illustrated in figure 1.3.

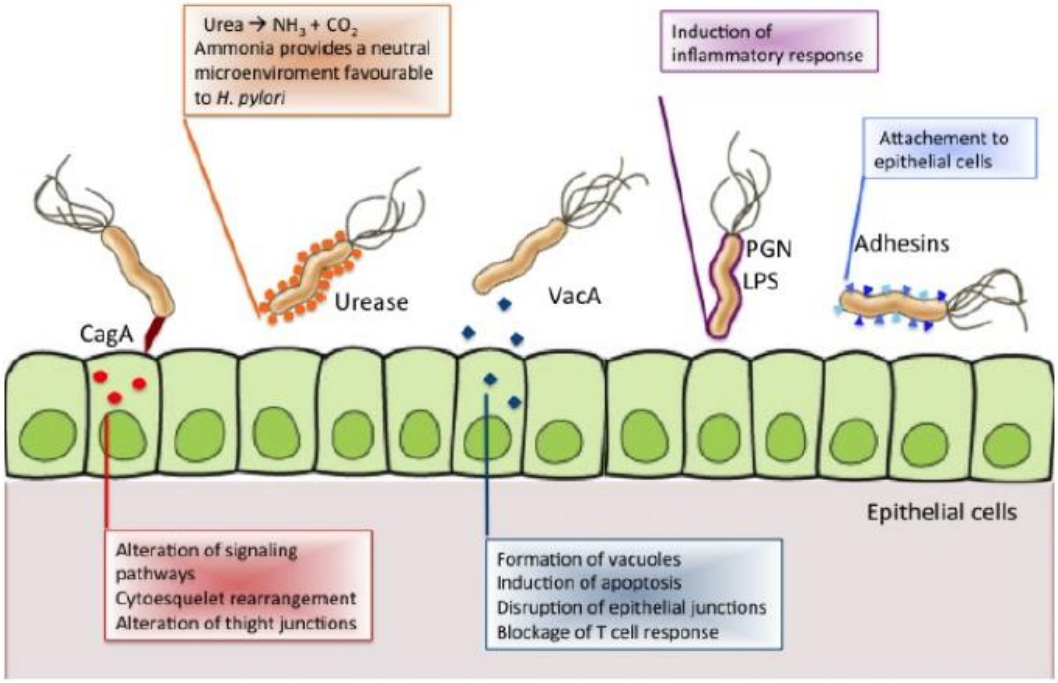

Fig. 1.3: *Helicobacter pylori* virulence and colonization factors. Besides the most popular *H. pylori* virulence factors CagA and VacA, further proteins cause damage to the host cells (copied from Morales-Guerrero et al., 2013).

1.2.4 Pathogenesis of *H. pylori*-related diseases

H. pylori infection first induces an inflammation (gastritis) of the gastric mucosa, which is often asymptomatic but can develop into different disease patterns (Portal-Celhay and Perez-Perez, 2006). About 10% of all infected persons show severe gastric lesions, such as peptic ulcer disease, 1-3% develop GC and 0.1% progress to MALT (De Falco et al., 2015). The disease outcome depends on the interplay between the gastritis phenotype and acid secretion by parietal cells. *H. pylori*-induced gastritis is classified into antrum-predominant or corpus-predominant gastritis, which is host-specific. Antrum-predominant gastritis shows an increased acid secretion, whereas acid secretion of a corpus-predominant inflammation is impaired (hypochlorhydria) or even lost (achlorhydria) (Blaser and Atherton, 2004; Malfertheiner, 2011).

An antrum-predominant gastritis increases the risk for duodenal ulcer (DU). Hormonal as well as neural mechanisms can contribute to an increased acid production. Increased gastrin levels (hypergastrinemia) result from alkalization surrounding the G cells, which is caused by

H. pylori urease activity. The G cells then constitutively release gastrin (Calam, 1999). Hypergastrinemia can also be the result of decreased somatostatin levels caused by *H. pylori* (Moss et al., 1992). Furthermore, *H. pylori* infection disrupts the antral-fundic connections thereby impairing the neural axis, which controls acid secretion. All these events lead to an increased acid-secretion, which spreads out to the duodenum. The intestinal epithelium begins to transform into gastric metaplasia, which shows an increased resistance against the harmful acid and enables *H. pylori* to colonize the duodenal bulb (Blaser and Atherton, 2004; Malfertheiner, 2011)

Several bacterial and host-derived molecules are involved in the control of acid production. The pro-inflammatory cytokines interleukin (IL)-1β and TNFα show an inhibitory effect on gastric acid secretion. This occurs indirectly by inhibiting enterochromaffin-like (ECL) cell histamine production or directly by suppressing parietal cell function (Blaser and Atherton, 2004). Inhibition of acid secretion over a long time period facilitates *H. pylori* colonization, which further suppresses acid production in a positive feedback loop and results in a corpus-predominant gastritis. This is associated with the development of GC. Atrophy of the corpus mucosa with loss of parietal cells leads to an irreversible hypo- or achlorhydria. Furthermore, the *H. pylori* cag PAI gene products are known to downregulate H^+K^+-ATPase expression by parietal cells also resulting in an inhibition of acid secretion (Calam, 1999; Malfertheiner, 2011).

1.2.5 Effects of *H. pylori* on hormones involved in appetite and satiety

H. pylori infection leads to changes in the levels of gastric hormones. The bacteria mainly affect the expression of leptin and ghrelin, which are both hormones regulating appetite and satiety. Leptin is secreted from adipose tissue and the gastric mucosa, where it is produced by chief and parietal cells to signal satiety. Leptin is an antagonist of ghrelin, which is produced in oxyntic glands stimulating gastric acid production and release of gastrin. Infection with *H. pylori* results in decreased gastrin as well as circulating ghrelin levels and increased somatostatin-mediated gastric leptin levels. Circulating leptin amounts are not affected by an infection. Decreased ghrelin levels in *H. pylori*-infected patients are associated with low serum levels of pepsinogen. These hormonal changes can be reversed by *H. pylori*

eradication therapy resulting in an increased body weight (Blaser and Atherton, 2004; Weigt and Malfertheiner, 2009). Moreover, an animal study in mice showed that immunity to *H. pylori* positively correlates with an upregulation of adipocytic genes, such as adiponectin (Mueller et al., 2003).

1.2.6 Effects of *H. pylori* infection on the host immune response

1.2.6.1 General overview of the immune system

An infection with pathogens usually evokes an innate and adaptive host immune response. Innate immunity is characterized by a rapid response but a lack of specificity and the risk to affect normal tissue. Adaptive immunity is more precise and features memory capacity, but it is a process that develops more slowly. Borders between innate and adaptive immunity are blurry, since their components are interacting (Parkin and Cohen, 2001).

Besides physical, chemical and microbiological barriers, innate immunity also involves elements of the immune system (neutrophils, macrophages, complement, cytokines). Highly conserved pathogen-associated molecular patterns (PAMPs) are recognized by pattern recognition receptors (PRRs) at the surface of epithelial and immune cells resulting in the activation of the immune response. This mode of pathogen recognition only works for extracellular organisms, such as bacteria, and not for intracellular organisms (e.g. viruses, mycobacteria, protozoa) (Parkin and Cohen, 2001). There are four classes of PRRs - RIG-like helicase receptors (RLRs), C-type lectin receptors (CLRs) and Nod-like receptors (NLRs), but the most popular ones are the toll-like receptors (TLRs) initiating NFκB signaling and cell activation. TLR4 is known to recognize LPS in contrast to TLR2, which binds lipoteichoic acid and lipoproteins. TLR3 is involved in recognition of dsDNA, TLR5 detects flagellin and TLR9 identifies unmethylated CpG (Blaser and Atherton, 2004; Parkin and Cohen, 2001; Salama et al., 2013; Wilson and Crabtree, 2007). The pro-inflammatory stimulation of host cells by bacterial products leads to the release of chemoattractants, such as cytokines, to recruit immune cells to the site of inflammation. Thus, cellular communication is indispensable. Recruited neutrophil granulocytes finally kill pathogens by phagocytosis. Further components of the innate immune system are eosinophile and basophile granulocytes. Eosinophile granulocytes are involved in the immune response to parasites, whereas

basophile granulocytes play a key role in anaphylaxis. The complement represents also a part of the innate immunity. It is composed of about 20 glycoproteins and is known to be activated for lysis of gram-negative bacteria, opsonization and recruitment of other immune cells. Natural killer cells are able to recognize abnormal cells due to modified major histocompatibility complex I (MHC I) levels compared with normal host cells or bind antibody-coated targets, both leading to cell lysis (Parkin and Cohen, 2001).

Adaptive immunity is activated if a pathogen is able to evade the innate immune system. The adaptive immune response is based on antigen-specific reactions mediated by T and B lymphocytes. Activated T cells are subsequently migrating to the inflammation site (cellular response), whereas activated B cells secrete antibodies to neutralize antigens (humoral response). Antigens can be presented MHC-dependent by macrophages, dendritic cells or B cells. If the antigen is processed endogenously, it is complexed with MHC I. Exogenous antigen can be incorporated by specialized antigen-presenting cells and re-expressed with MHC II for recognition by T cells. Naïve T cells develop in the thymus and possess a series of diverse T cell receptors. The co-receptors CD4 and CD8 are important for T cell activation. Naïve T cells are negative for both co-receptors before they become double positive due to self-peptide-MHC signaling. $CD4^+$ T helper cells (T_h cells) are only able to bind antigens in complex with MHC II, whereas $CD8^+$ cytotoxic T cells (T_c cells) can only recognize antigens presented with MHC I. Activated T_c cells directly cause apoptosis of virus-infected cells via perforin and granzymes. T_h cells function as activators of immune cells, in particular B lymphocytes. Precursor T_h cells can differentiate into T_h1, T_h2, T_h17 and regulatory T (T_{reg}) cells due to their specific cytokine production, cell surface marker expression and expression of transcription factors. T_h1 cells produce IL-2 leading to T cell proliferation and cytotoxicity as well as interferon gamma (IFNγ), which stimulates macrophages and natural killer cells to eliminate pathogens. IFNγ furthermore causes enhanced T_h1 and inhibited T_h2 differentiation. T_h2 cells secrete IL-4, IL-5, IL-6, IL-10 and IL-13 resulting in antibody production. In addition, IL-4 enforces T_h2 response and suppresses T_h1 differentiation. Expression of the transcription factors STAT3 and RORγt lead to T_h17 differentiation, whereas expression of the transcription factor FOXP3 is responsible for the development of T_{regs}, which is a crucial factor for immunological balance. At the end of a successful immune

response, some activated T cells stay in the lymph nodes to act as memory cells (Buchholz et al., 2016; Carbo et al., 2013; Parkin and Cohen, 2001; Wilson and Crabtree, 2007).

1.2.6.2 Modulation of the host immune response by *H. pylori*

To ensure persistence and avoid clearance, *H. pylori* has evolved diverse mechanisms to evade the host immune system. To this end, *H. pylori* is enabled to survive without tissue invasion in the gastric lumen where the bacteria cannot be recognized by the immune system. Innate and acquired immunity are only activated when bacterial proteins are entering the epithelial barrier, but *H. pylori* is able to minimize TLR stimulation by diverse mechanisms. In this context, TLR5 is not able to recognize *H. pylori* flagella and TLR9 is not stimulated by the hypermethylated DNA of *H. pylori*. Unusual for enteric bacteria, *H. pylori* LPS is almost anergic due to lipid A modifications. Due to this fact, *H. pylori* LPS is not recognized by gastric epithelial TLR4 (Blaser and Atherton, 2004; Salama et al., 2013). *H. pylori* rather triggers TLR2 and TLR9 thereby evoking an anti-inflammatory response dominant over pro-inflammatory signals activated by other TLRs (Salama et al., 2013). Thus, *H. pylori* evades innate immunity but causes a strong anti-microbial response leading to inflammation and tissue damage by the release of reactive oxygen species (ROS) and cytokines (Wilson and Crabtree, 2007). *H. pylori* also modulates the adaptive immune system by suppression of proliferation/activation of T cells and induction of T cell apoptosis. In addition, asymptomatic *H. pylori* carriers show increased levels of FOXP3, suggesting an enhanced T_{reg} response to ensure survival of the bacterium paralleled by the prevention of a destructive inflammation. *H. pylori* further provokes a predominant T_h1 response, which is a crucial factor in pathogenesis of the bacteria. Mice showing a T_h1 predominance develop increased gastric inflammation compared to mice with a predominant T_h2 response. Inhibition of GATA3 in T cells is an indicator of the T_h1 phenotype. In addition, *H. pylori* arginase ensures the survival of the bacteria by competing with the host macrophage concerning the inducible nitric oxide synthase (iNOS) substrate L-arginine. The macrophage response to *H. pylori* is further affected by the ability of *H. pylori* to process cholesterol of the host's cell membrane, which efficiently inhibits phagocytosis of the bacteria. In addition, *H. pylori* causes apoptosis of macrophages further inhibiting phagocytosis (Blaser and Atherton, 2004; Carbo et al., 2013; Salama et al., 2013; Wilson and Crabtree, 2007).

1.3 Deleted in liver cancer 1

The RHO family of small GTPases is part of the RAS superfamily (Durkin et al., 2007; Popescu and Goodison, 2014). In total, 23 RHO proteins have been identified in humans. The best characterized RHO proteins are RHOA, RAC1 and CDC42 (Braun and Olayioye, 2015; Lukasik et al., 2011). These small GTPases are involved in the regulation of diverse cellular processes, such as cell cycle progression, cytoskeleton formation, apoptosis, migration, adhesion, polarity and transcriptional regulation. Hence, deregulation of small GTPases is supposed to contribute to tumorigenesis and metastasis (Braun and Olayioye, 2015; Du et al., 2012; Durkin et al., 2007; Ko and Ping Yam, 2014; Lukasik et al., 2011; Sabbir et al., 2010). The mode of action of small GTPases is based on a cycling between an inactive GDP-bound state and an active GTP-bound conformation (Durkin et al., 2007; Lukasik et al., 2011; Sabbir et al., 2010). The switch between these two states is mediated by three classes of regulatory proteins. Guanine nucleotide dissociation inhibitors (GDI) prevent a nucleotide exchange by binding to the GDP-conformation of small GTPases. Guanine nucleotide exchange factors (GEF) catalyze the exchange of GDP for GTP. GTPase-activating proteins (GAP) stimulate the hydrolysis of GTP to GDP (Braun and Olayioye, 2015; Du et al., 2012; Durkin et al., 2007; Ko and Ping Yam, 2014; Lukasik et al., 2011; Popescu and Goodison, 2014). The inactivation of RHOGAPs represents the most common modification for RHO regulators in cancer development (Lukasik et al., 2011).

The human genome encodes about 70 RHOGAPs under which the Deleted in liver cancer (DLC) protein family, if inactivated, plays a crucial role in cancer progression (Braun and Olayioye, 2015; Lukasik et al., 2011). The human genome encodes three members of the DLC protein family: DLC1, DLC2 and DLC3. They are all characterized by a multidomain organization but differ in their subcellular localization and functions. DLC1 is the best characterized member of the DLC protein family. It was first identified in 1998 as a tumor suppressor candidate from hepatocellular carcinoma (HCC) and is mapped to chromosome 8p21.3-22 (Braun and Olayioye, 2015; Du et al., 2012; Durkin et al., 2007; Ko and Ping Yam, 2014; Low et al., 2011; Lukasik et al., 2011; Popescu and Goodison, 2014). DLC1 is ubiquitously expressed in normal tissues but is frequently silenced or lost in tumor tissues. Besides liver, these include breast, lung, ovarian, kidney, colon, prostate and gastric

carcinoma. Deletion or silencing of DLC1 may refer to genomic deletion, somatic mutations or epigenetic inactivation, such as promoter hypermethylation (Durkin et al., 2007; Ko and Ping Yam, 2014; Low et al., 2011; Lukasik et al., 2011; Popescu and Goodison, 2014; Sabbir et al., 2016; Sabbir et al., 2010). DLC1 fulfills a number of tumor suppressor functions including inhibition of cell proliferation, migration, invasion and induction of apoptosis. It can act as cytoplasmatic and nuclear tumor suppressor. Translocation of DLC1 into the nucleus is mediated by a nuclear localization signal (NLS) and can be a spatial regulatory mechanism (Braun and Olayioye, 2015; Ko and Ping Yam, 2014; Low et al., 2011; Popescu and Goodison, 2014).

There have been four isoforms of DLC1 identified in humans (Fig. 1.4). They show the same protein domain structure and mainly differ in their N-terminal sequences. DLC1.1 is the longest of all isoforms (1528 aa) showing a molecular size of 170 kDa. DLC1.2 has a size of 1091 aa and a predicted molecular weight of 120 kDa. DLC1.3 is the shortest isoform showing only 498 aa and is therefore predicted to be non-functional. DLC1.4 consists of 1125 aa with a molecular size of 123 kDa and is characterized by a putative mitochondrial targeting sequence. DLC1.1 and DLC1.3 share a promoter and are silenced in almost all cancer cell lines, whereas DLC1.2 and DLC1.4 use different promoters and are frequently downregulated (Durkin et al., 2007; Hitkova et al., 2013; Low et al., 2011; Lukasik et al., 2011; Popescu and Goodison, 2014). In mice, also four transcripts are known for DLC1. Isoform 1 of mouse DLC1 encodes a 127 kDa protein, which is equivalent to human DLC1.2. Mouse isoform 2 shows a size of 123 kDa and structurally resembles isoform 1, whereas isoform 3 is the largest one and is equivalent to human DLC1.1. The shortest DLC1 isoform in mice represents transcript 4 encoding a very small protein equivalent to human isoform 3 (Sabbir et al., 2010).

The DLC1 protein consists of mainly three functional domains (Fig. 1.4). A sterile α motif (SAM) is localized at the N-terminus and mediates protein-protein interactions. It is also suggested to act as an autoinhibitory domain for the RHOGAP activity. The highly conserved RHOGAP domain is located to the middle of the protein and promotes hydrolysis of GTP to GDP to inactivate RHO GTPases via an arginine finger. The GAP domain of DLC1 inactivates RHOA, -B and -C, but it shows no activity on RAC1 and only low activity on CDC42 *in vitro*. Studies in HCC cells showed that an inactivation of RHO by DLC1's GAP activity negatively

regulates ROCK/myosin light chain (MLC) pathway, hence, regulating the vascular tone and endothelial permeability. In addition, DLC1 overexpressing cells showed a rounded morphology and RHOGAP defective mutants were not able to inhibit stress fiber formation *in vitro.* The C-terminal steroidogenic acute regulatory protein (StAR) related lipid-transfer (START) domain functions as a lipid-binding domain. Since RHO signaling occurs at membranes, it is not surprising that lipid interaction is crucial for DLC1 activity. The long unstructured serine-rich linker region between the SAM and RHOGAP domain is also known as the focal adhesion targeting (FAT) domain and contains a phosphorylation-independent binding site (Braun and Olayioye, 2015; Du et al., 2012; Durkin et al., 2007; Ko and Ping Yam, 2014; Low et al., 2011; Lukasik et al., 2011; Popescu and Goodison, 2014; Sabbir et al., 2016; Sabbir et al., 2010).

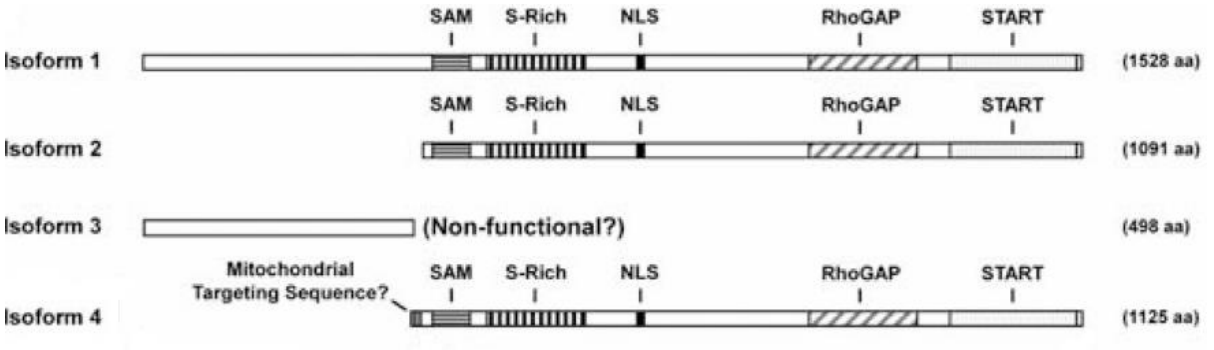

Fig. 1.4: Structure of human DLC1 isoforms. Isoforms 1, 2 and 4 share the same multi domain organization including a SAM, Serine-rich (S-Rich) region, NLS, RHOGAP and START domain. Isoform 3 is suggested to be non-functional and isoform 4 is the only one possessing a mitochondrial targeting sequence. Schemes are not drawn to scale (adapted from Low et al., 2011).

DLC1 has a wide range of interaction partners, which regulate DLC1 at a cellular level (Ko and Ping Yam, 2014; Lukasik et al., 2011; Popescu and Goodison, 2014). Tensins are members of the family of focal adhesion proteins and include four members: tensin 1, 2, 3 and 4. They function as scaffold proteins of the cytoskeleton and are involved in signal transduction and cellular transformation. Tensin 2 was the first identified DLC1 interacting partner giving first evidence for localization of DLC1 to focal adhesions. Perturbation of the binding of DLC1 to tensin 2, 3 and 4 resulted in reduced RHOGAP activity. Increased GAP activity of DLC1 in case of tensin 3 binding is due to the disruption of the intramolecular autoinhibitory interaction between the SAM and the GAP domain (Braun and Olayioye, 2015; Durkin et al., 2007; Ko

and Ping Yam, 2014; Popescu and Goodison, 2014; Sabbir et al., 2016). Thus, interaction with tensins and localization to focal adhesions are suggested to play a crucial role for tumor suppressor functions of DLC1 (Durkin et al., 2007; Ko and Ping Yam, 2014; Lukasik et al., 2011). Furthermore, DLC1 is known to bind eukaryotic elongation factor 1A1 (EF1A1) and the phosphatase and tensin homologue (PTEN) via its SAM domain to regulate cell migration. The FAT domain of DLC1 was shown to interact with talin and focal adhesion kinase (FAK) supporting localization of DLC1 to focal adhesions. The formation of a complex between DLC1 and α-catenin resulted in a stabilization of adherens junctions and a reduction of active RHO. The interaction between the DLC1 linker region and the pro-inflammatory and tumor cell invasion promoting protein S100A10 (S100 calcium-binding protein) is known to inhibit cell migration, invasion and colony formation (Braun and Olayioye, 2015; Du et al., 2012; Ko and Ping Yam, 2014; Popescu and Goodison, 2014; Sabbir et al., 2016; Tripathi et al., 2012). Furthermore, DLC1 forms a complex with the tumor suppressor caveolin-1 (CAV1) in the caveolae mediated by a CAV1-binding motif of the START domain (Braun and Olayioye, 2015; Durkin et al., 2007; Ko and Ping Yam, 2014; Lukasik et al., 2011; Popescu and Goodison, 2014). Hitkova et al. showed that CagA-proficient *H. pylori* strains promote the recruitment of a DLC1.4 mutant to CAV1 in human gastric epithelial cells. CAV1 thereby enforces the tumor suppressor activity of DLC1 (Hitkova et al., 2013). A deletion of the CAV1-binding site resulted in decreased inhibition of cell migration and clonogenic growth, despite RHOA activity was suppressed. This gives evidence for RHOGAP-independent modes of action of DLC1. DLC1 activity can further be regulated by phosphorylation, but the physiological stimuli of the phosphorylators are still unclear. For example, S549 phosphorylation of DLC1 by protein kinase A results in a dimerization of DLC1 and, consequently, an increased RHOGAP activity (Ko and Ping Yam, 2014; Popescu and Goodison, 2014).

Mice with a heterozygous gene trap of *Dlc1* showed no physical abnormalities, whereas homozygous mice were not viable and died at about day 10 post coitus due to severe defects in a series of organs. This demonstrates that the other two DLC members are insufficient to compensate for the functions of DLC1, probably due to different temporal or tissue specific expression during embryonic development. Hence, DLC1 needs to be in balance to interact with other signaling proteins in a complex (Braun and Olayioye, 2015; Durkin et al., 2007; Ko and Ping Yam, 2014; Lukasik et al., 2011; Sabbir et al., 2010).

Due to its tumor suppressive functions and downregulation in tumor tissue, DLC1 became a putative drug for targeted therapy. Hypermethylation of the DLC1 promoter may be a useful future biomarker for diagnosis, staging and prediction of malignancies. Reactivation of DLC1 expression could be of therapeutic utility. Epigenetic approaches manipulating DNA methyltransferases and histone deacetylases aiming for restoration of DLC1 expression in cancer cells represent promising therapeutic strategies in cancer treatment (Popescu and Goodison, 2014). Preliminary studies in human GC cells showed an increased DLC1 expression by treatment with the histone deacetylase inhibitor trichostatin A or the methyltransferase inhibitor 5-aza-2'-deoxycytidine (Durkin et al., 2007). Inhibition of the RHO/ROCK pathway represents a further auspicious alternative for therapeutic intervention in the DLC1-regulated pathway (Popescu and Goodison, 2014).

1.4 Objective

GC is often diagnosed in advanced stages where survival prognosis is poor. Thus, it is the third most common cause of cancer-related death worldwide (Tan and Yeoh, 2015). Due to non-response caused by resistance mechanisms, there is a high medical need for new therapeutic approaches. *Helicobacter*-infection significantly increases the risk for GC by activating pro-tumor pathways including RHO, which has been corroborated as a major oncogenic driver in diffuse human GC. The RHO-inhibitor DLC1 is frequently silenced or even lost in GC. The role of DLC1 in *Helicobacter*-related gastric disease is unknown and was investigated by this thesis.

This thesis aimed to characterize in depth the function of DLC1 in gastric disease. For this purpose, $DLC1^{gt/+}$ mice with reduced expression of DLC1 isoform 2 were used to determine the causative role of DLC1 deficiency in gastric carcinogenesis. Furthermore, interaction between DLC1 and the *Helicobacter* toxin CagA was clarified on the protein and DNA level. *In vitro* assays were performed to investigate the functional antagonism of the two proteins. *In vivo* therapy with an inhibitor of the RHO downstream effector ROCK was applied to reduce GC tumor growth.

The summarized major goals of this thesis were:

1) Detailed characterization of DLC1 and analysis of its role in *Helicobacter*-related gastric disease
2) Elaboration of DLC1 as an early diagnostic marker in *Helicobacter*-associated gastric malignancies
3) Identification of novel targets such as RHO/ROCK-inhibitors in human GC and
4) Classification of *Helicobacter*-related carcinogenesis into one of the four molecular subtypes of human GC.

2 Materials & Methods

2.1 Materials

Table 2.1: General chemicals, reagents and solutions.

Chemical/reagent/solution	Company	Catalog number
Acetic acid	Sigma Aldrich Chemie GmbH, Steinheim, Germany	45740
Acrylamide solution Rotiphorese Gel 30	Roth GmbH, Karlsruhe, Germany	3029.2
Agarose	Biozym Scientific GmbH Hess. Oldendorf, Germany	840004
Albumin Fraktion V (BSA)	Merck KGaA, Darmstadt, Germany	12659
Alexa Fluor® 488 Phalloidin	Thermo Fisher Scientific, Inc., Surrey, UK	A12379
Alexa Fluor® 594 Phalloidin	Thermo Fisher Scientific, Inc., Surrey, UK	A12381
Ammoniumperoxodisulfat (APS)	Roth GmbH, Karlsruhe, Germany	9592.3
Antigen unmasking solution	Vector Laboratories, Inc., Burlingame, USA	H-3300
Aqua (dH_2O)	B. Braun Melsungen AG, Melsungen, Germany	750082479E
Bacto™ Tryptone	BD Biosciences, Heidelberg, Germany	211705
β-Glycerophosphate (disodium salt hydrate)	Sigma Aldrich Chemie GmbH, Steinheim, Germany	010M45131
Boric acid	Sigma Aldrich Chemie GmbH, Steinheim, Germany	B7901
Brain Heart Infusion Broth	Sigma Aldrich Chemie GmbH, Steinheim, Germany	53286
Bromophenol Blue	Sigma Aldrich Chemie GmbH, Steinheim, Germany	B5525
Brucella broth base	Sigma Aldrich Chemie GmbH, Steinheim, Germany	B3051
Chloroform	Merck KGaA, Darmstadt, Germany	1.02445.1000
Cobalt chloride	Sigma Aldrich Chemie GmbH, Steinheim, Germany	60818
Columbia Blood Agar Base	Thermo Fisher Scientific, Inc., Surrey, UK	CM0331
Complete Mini Protease Inhibitor Cocktail Tablets	Roche Diagnostics GmbH, Mannheim, Germany	04 693 124 062

Chemical/reagent/solution	**Company**	**Catalog number**
4',6-Diamidino-2-phenylindole (DAPI)	Roth GmbH, Karlsruhe, Germany	6335.1
Deoxycholic acid	Sigma Aldrich Chemie GmbH, Steinheim, Germany	D2510
1,4-Dithiothreitol (DTT)	Merck KGaA, Darmstadt, Germany	1.114.740.004
DNA loading dye 6x	Thermo Fisher Scientific, Inc., Surrey, UK	R0611
Ethanol absolute for analysis (EtOH)	Merck KGaA, Darmstadt, Germany	1.00983.2500
Ethanol 96% (v/v) technical (EtOH)	Roth GmbH, Karlsruhe, Germany	T171.4
Ethidium bromide (10 mg/ml)	Thermo Fisher Scientific, Inc., Surrey, UK	15585-011
Ethylendiaminetetraacetic acid (EDTA)	Sigma Aldrich Chemie GmbH, Steinheim, Germany	E 5134
Eukitt	Sigma Aldrich Chemie GmbH, Steinheim, Germany	03989
[^{18}F]-FDG	Zyklotron AG, Karlsruhe, Germany	
Fasudil	Selleck Chemicals LLC, Houston, USA	HA-1077
Fluorescence mounting medium	Dako North America, Inc., Carpinteria, USA	S302380-2
Gene Ruler™ 50bp DNA ladder	Thermo Fisher Scientific, Inc., Surrey, UK	SM1133
Gene Ruler™ 100bp DNA ladder	Thermo Fisher Scientific, Inc., Surrey, UK	SM1143
Gene Ruler™ 1kb DNA ladder	Thermo Fisher Scientific, Inc., Surrey, UK	SM1163
Glutathione Sepharose 4 Fast Flow	GE Healthcare GmbH, Solingen, Germany	17513201
Glycerol	Sigma Aldrich Chemie GmbH, Steinheim, Germany	200-289-5
Glycine	Roth GmbH, Karlsruhe, Germany	3908.3
Goat serum	Sigma Aldrich Chemie GmbH, Steinheim, Germany	G9023
Hematoxylin	Sigma Aldrich Chemie GmbH, Steinheim, Germany	H9627
Horse Blood	Thermo Fisher Scientific, Inc., Surrey, UK	SR0048
Hydrochloric acid (HCl)	Merck KGaA, Darmstadt, Germany	1.090.571.000
Hydrogen peroxide (H_2O_2) 30%	Merck KGaA, Darmstadt, Germany	1.085.971.000
IGEPAL® CA-630	Sigma Aldrich Chemie GmbH, Steinheim, Germany	I3021
Isofluorane	Abbvie Deutschland GmbH & Co. KG, Ludwigshafen, Germany	4831850
Isopropyl-β-D-1-thiogalactopyranoside (IPTG)	Sigma Aldrich Chemie GmbH, Steinheim, Germany	I5502

Chemical/reagent/solution	**Company**	**Catalog number**
LB-Agar (Lennox)	Roth GmbH, Karlsruhe, Germany	X965.1
LB-Medium (Lennox)	Roth GmbH, Karlsruhe, Germany	X964.1
Luminol	Sigma Aldrich Chemie GmbH, Steinheim, Germany	A8511
Lipopolysaccharide (LPS) from *E. coli* O111:B4	Merck KGaA, Darmstadt, Germany	LPS25
Magnesium chloride ($MgCl_2$)	Merck KGaA, Darmstadt, Germany	5833 1000
2-Mercaptoethanol	Sigma Aldrich Chemie GmbH, Steinheim, Germany	M7522
2-(N-Morpholino)ethanesulfonic acid (MES)	Roth GmbH, Karlsruhe, Germany	4256.3
Methanol ≥ 99,8%	Sigma Aldrich Chemie GmbH, Steinheim, Germany	32213
Milk powder blotting grade	Roth GmbH, Karlsruhe, Germany	T145.2
Nuclease-free water	Promega Corporation, Madison, USA	P1193
Paraformaldehyde	Roth GmbH, Karlsruhe, Germany	4979.2
PBS Dulbecco	Merck KGaA, Darmstadt, Germany	L 182-50
p-Coumaric acid	Sigma Aldrich Chemie GmbH, Steinheim, Germany	C9008
Pefablock	Roche Diagnostics GmbH, Mannheim	11585916001
Phosphatase Inhibitor Cocktail II	Sigma Aldrich Chemie GmbH, Steinheim, Germany	P5726
Potassium chloride (KCl)	Merck KGaA, Darmstadt, Germany	1.04936.1000
2-Propanol	Merck KGaA, Darmstadt, Germany	1.096.341.000
Protein A/G PLUS-Agarose	Merck KGaA, Darmstadt, Germany	IP05
Ponceau S solution	Sigma Aldrich Chemie GmbH, Steinheim, Germany	P7170
Rabbit serum	Sigma Aldrich Chemie GmbH, Steinheim, Germany	R9133
Rotiphorese® Gel 30	Roth GmbH, Karlsruhe, Germany	3029.2
Roti®-Mark Tricolor, protein marker prestained	Roth GmbH, Karlsruhe, Germany	8271.1
Sodium dodecyl sulfate (SDS)	Roth GmbH, Karlsruhe, Germany	2326.2
Sodium chloride (NaCl)	Sigma Aldrich Chemie GmbH, Steinheim, Germany	31434
Sodium orthovanadate (Na_3VO_4)	Sigma Aldrich Chemie GmbH, Steinheim, Germany	S6508
Sodium hydroxid (NaOH)	Merck KGaA, Darmstadt, Germany	1.09137.1000
TEMED	Roth GmbH, Karlsruhe, Germany	2367.3
TRIS PUFFERAN ≥ 99,9% Ultra	Roth GmbH, Karlsruhe, Germany	5429.3

Chemical/reagent/solution	Company	Catalog number
Triton® X-100	Merck KGaA, Darmstadt, Germany	1.122.980.101
Trizma base ≥ 99,9%	Sigma Aldrich Chemie GmbH, Steinheim, Germany	T1503
Tween® 20	Roth GmbH, Karlsruhe, Germany	9127.1
5-Bromo-4-chloro-indolyl-β-D-galactopyranoside (X-Gal)	Sigma Aldrich Chemie GmbH, Steinheim, Germany	B4252
Xylol (Isomere) ≥ 98,5%	Roth GmbH, Karlsruhe, Germany	CN80.1
Yeast Extract	Roth GmbH, Karlsruhe, Germany	2363.3

Table 2.2: Consumables.

Consumable	Company	Catalog number
1.5ml safe lock tubes	Eppendorf AG, Hamburg, Germany	0030 120.086
2.0ml safe lock tubes	Eppendorf AG, Hamburg, Germany	0030 123.344
200µl PCR Tubes "Multiply®-µStrip Pro 8-strip"	Sarstedt AG & Co. KG, Nümbrecht, Germany	72.991.002
10µl Pipette Tips TipOne®	STARLAB GmbH, Hamburg, Germany	S1111-3000
200µl Pipette Tips TipOne®	STARLAB GmbH, Hamburg, Germany	S1111-0006
1000µl Pipette Tips TipOne®	STARLAB GmbH, Hamburg, Germany	S1111-6001
5ml serological pipette	Greiner Bio-One GmbH, Frickenhausen, Germany	606 160
10ml serological pipette	Greiner Bio-One GmbH, Frickenhausen, Germany	607 180
25ml serological pipette	Greiner Bio-One GmbH, Frickenhausen, Germany	760 160
50ml serological pipette	Greiner Bio-One GmbH, Frickenhausen, Germany	768 160
13ml Falcon for bacterial culture	Sarstedt AG & Co. KG, Nümbecht, Germany	62.515.006
15ml Falcon tubes	Greiner Bio-One GmbH, Frickenhausen, Germany	188 271
50ml Falcon tubes	Greiner Bio-One GmbH, Frickenhausen, Germany	227 261
25 cm² Cellstar Cell Culture Flask	Greiner Bio-One GmbH, Frickenhausen, Germany	690 175
75 cm² Cellstar Cell Culture Flask	Greiner Bio-One GmbH, Frickenhausen, Germany	658 175

Consumable	Company	Catalog number
6-well Cellstar Cell Culture Plate	Greiner Bio-One GmbH, Frickenhausen, Germany	657 160
6-well Cellstar Suspension Culture Plate	Greiner Bio-One GmbH, Frickenhausen, Germany	657 185
96-well Cellstar Cell Culture Plate	Greiner Bio-One GmbH, Frickenhausen, Germany	655 180
96-well Cellstar Cell Culture Plate, white	Greiner Bio-One GmbH, Frickenhausen, Germany	655 073
Amersham Protran 0.2µm NC Nitrocellulose Blotting Membrane	GE Healthcare GmbH, Solingen, Germany	10600001
Coverslips 24x60mm	Roth GmbH, Karlsruhe, Germany	H878
Counting chamber	neoLab Migge GmbH, Heidelberg, Germany	C-1003
Cryotubes CRYO.S™	Greiner Bio-One GmbH, Frickenhausen, Germany	122 280
GasPak™ EZ Anaerobe Container System	BD Biosciences, Heidelberg, Germany	260678
LightCycler® 480 Multiwell Plate 96, white	Roche Diagnostics GmbH, Mannheim	04729692001
Petri Dish Falcon®	Corning Laser Technologies GmbH, Krailling, Germany	351029
Pipettes	Eppendorf AG, Hamburg, Germany	
SuperFrost® Plus microscope slides	VWR International GmbH, Darmstadt, Germany	631-0108
TC-Dish 60, Cell+	Sarstedt AG & Co. KG, Nümbrecht, Germany	83.3901.300
Whatman 3mm CHR	GE Healthcare GmbH, Solingen, Germany	3030-917

Table 2.3: Cell culture reagents and solutions.

Reagent/Solution	Company	Catalog number
0.25% Trypsin-EDTA	Thermo Fisher Scientific, Inc., Surrey, UK	25200056
3-(4,5-Dimethylthiazol-2-yl)-2,5-diphenyltetrazolium bromide (MTT)	Sigma Aldrich Chemie GmbH, Steinheim, Germany	M5655
Dimethyl sulfoxide (DMSO)	Sigma Aldrich Chemie GmbH, Steinheim, Germany	D8418
DMEM Medium	Thermo Fisher Scientific, Inc., Surrey, UK	41966-029

Reagent/Solution	Company	Catalog number
DMEM/F-12 Medium	Thermo Fisher Scientific, Inc., Surrey, UK	11320033
Fasudil Y-27632	Merck KGaA, Darmstadt, Germany	688000
Fetal Calf Serum (FCS)	Thermo Fisher Scientific, Inc., Surrey, UK	SV30 160.03
Fetal Calf Serum (FCS)	PAN-Biotech GmbH, Aidenbach, Germany	P40-37100M
L-Glutamin	Thermo Fisher Scientific, Inc., Surrey, UK	25030024
PBS pH 7.4 1x	Thermo Fisher Scientific, Inc., Surrey, UK	10010056
RPMI 1640 Medium	Thermo Fisher Scientific, Inc., Surrey, UK	21875091
Trypanblue 0,4%	Thermo Fisher Scientific, Inc., Surrey, UK	15250-061
TurboFect™ Transfection Reagent	Thermo Fisher Scientific, Inc., Surrey, UK	R0531

Table 2.4: Cell lines.

Cell line	Description	Company	Catalog number
AGS	Human gastric adenocarcinoma, primary tumor, epithelial	ATCC, Manassas, USA	CRL-1739
HCT116	Human colorectal carcinoma	ATCC, Manassas, USA	CCL-247
HEK293T	Human embryonic kidney, SV40 transformed, mesenchymal	ATCC, Manassas, USA	CRL-3216
HepG2	Human hepatocellular carcinoma	ATCC, Manassas, USA	HB-8065
Jurkat	Human T cell leukemia, suspension	DSMZ, Braunschweig, Germany	ACC 282
MKN45	Human gastric adenocarcinoma, derived from metastatic site: liver	DSMZ, Braunschweig, Germany	ACC 409
NCI-N87	Human gastric carcinoma, derived from metastatic site: liver, epithelial	ATCC, Manassas, USA	CRL-5822
SW480	Human colorectal adenocarcinoma	ATCC, Manassas, USA	CCL-228
tsA201	Human embryonic kidney, SV40 transformed	ECACC, Salisbury, United Kingdom	96121229

Table 2.5: Bacteria.

Strain	Genotype	Company/Origin	Catalog number
E. coli DH5α competent cells	F- ø80*lac*ZΔM15 Δ(*lac*ZYA-*arg*F)U169 *rec*A1 *end*A1 *hsd*R17(r_K-, m_K+) *pho*A *sup*E44 *thi*-1 *gyr*A96 *rel*A1 λ-	Thermo Fisher Scientific, Inc., Surrey, UK	18265017
E. coli Top10 One Shot competent cells	F- *mcrA* Δ(*mrr-hsd*RMS-*mcr*BC) Φ80*lac*ZΔM15 Δ *lac*X74 *rec*A1 *ara*D139 Δ(*araleu*)7697 *gal*U *gal*K *rps*L (StrR) *end*A1 *nup*G	Thermo Fisher Scientific, Inc., Surrey, UK	C404003
E. coli Rosetta™ (DE3) competent cells	F- *ompT hsdS*$_B$(r_B- m_B-) *gal dcm* (DE3) pRARE (CamR)	Merck KGaA, Darmstadt, Germany	70954
H. pylori G27	Clinical isolate, *cagA*$^+$, *vacA*$^+$	(Covacci et al., 1993; Xiang et al., 1995)	
H. pylori SS1	Clinical isolate, *cagA*$^+$, *vacA* (s2-m2), mouse adapted	(Lee et al., 1997; Van Doorn et al., 1999)	
H. felis	Cat isolate, *cagA*$^-$	ATCC, Manassas, USA	51211

Table 2.6: Animals.

Mouse	Genotype	Origin
DLC1$^{gt/+}$	Hypomorphic knock-down (KD) of the DLC1 protein via gene trap (gt). Heterozygous state of mutation ($^{gt/+}$), because homozygous ($^{gt/gt}$) would be embryonic lethal.	(Sabbir et al., 2010)
CEA424-SV40 TAg (TCEA)	Overexpression of the viral "large T-antigen" (T-Ag) oncogene under control of the human "carcinoembryonic antigen" (CEA) promoter in gastric epithelial cells induces tumor formation in the lower part of the stomach (pylorus).	(Thompson et al., 2000)
Wildtype (WT)	B6129SF2/J	Jackson Laboratory, Bar Harbor, USA

Table 2.7: Enzymes.

Enzyme	Company	Catalog number
GoTaq® Green Master Mix	Promega Corporation, Madison, USA	M7121
HindIII restriction enzyme 20U/µl	New England Biolabs GmbH, Frankfurt, Germany	R0104
JumpStart™ REDTaq® ReadyMix™	Sigma Aldrich Chemie GmbH, Steinheim, Germany	P0982
KpnI restriction enzyme 10U/µl	New England Biolabs GmbH, Frankfurt, Germany	R0142
KpnI restriction enzyme 10U/µl	Thermo Fisher Scientific, Inc., Surrey, UK	ER0521
Power SYBR® Green Master Mix	Thermo Fisher Scientific, Inc., Surrey, UK	4368577
Proteinase K	Roche Diagnostics GmbH, Mannheim	03 115 887 001
RNase-free DNase Set	QIAGEN GmbH, Hilden, Germany	79254
SacI restriction enzyme 10U/µl	Thermo Fisher Scientific, Inc., Surrey, UK	ER1132
T4 Ligase 5U/µl	Thermo Fisher Scientific, Inc., Surrey, UK	EL0014

Table 2.8: Antibiotics.

Antibiotics	Company	Catalog number
Ampicillin	Roth GmbH, Karlsruhe, Germany	K029.1
Amphotericin B	Sigma Aldrich Chemie GmbH, Steinheim, Germany	A4888
β-Cyclodextrin	Sigma Aldrich Chemie GmbH, Steinheim, Germany	C4805
Cefsulodin sodium salt hydrate	Sigma Aldrich Chemie GmbH, Steinheim, Germany	C8145
Cycloheximide	Sigma Aldrich Chemie GmbH, Steinheim, Germany	C7698
Kanamycin	Sigma Aldrich Chemie GmbH, Steinheim, Germany	60615
Penicillin/Streptomycin (Pen/Strep)	Thermo Fisher Scientific, Inc., Surrey, UK	15140122

Antibiotics	Company	Catalog number
Polymyxin B sulfate salt	Sigma Aldrich Chemie GmbH, Steinheim, Germany	P1004
Trimethoprim	Sigma Aldrich Chemie GmbH, Steinheim, Germany	T7883
Vancomycin hydrochloride	Sigma Aldrich Chemie GmbH, Steinheim, Germany	V2002

Table 2.9: Kits.

Kit	Company	Catalog number
Avidin/Biotin Blocking Kit	Vector Laboratories, Inc., Burlingame, USA	SP-2001
Cellular Reactive Oxygen Species Detection Assay Kit (Deep Red Fluorescence)	Abcam plc, Cambridge, UK	ab186029
DAB Peroxidase Substrate Kit	Vector Laboratories, Inc., Burlingame, USA	SK-4100
DNeasy@ Blood & Tissue Kit	QIAGEN GmbH, Hilden, Germany	69504
Dual-Luciferase® Reporter Assay System	Promega Corporation, Madison, USA	E1960
Duolink® In Situ Red Starter Kit	Sigma Aldrich Chemie GmbH, Steinheim, Germany	DUO92101-1KT
HiSpeed® Plasmid Midi Kit	QIAGEN GmbH, Hilden, Germany	12643
peqGold Total RNA Kit	VWR International GmbH, Darmstadt, Germany	12-6834-02
Pierce BCA™ Protein Assay Kit	Thermo Fisher Scientific, Inc., Surrey, UK	23225
Pure Yield™ Plasmid Miniprep System	Promega Corporation, Madison, USA	A1222
QIAquick Gel Extraction Kit	QIAGEN GmbH, Hilden, Germany	28704
RhoA/Rac1/Cdc42 Activation Assay Combo Kit	Cell Biolabs, Inc., San Diego, USA	STA-405
TOPO TA Cloning Kit	Thermo Fisher Scientific, Inc., Surrey, UK	45-0641
Vectastain® ABC Kit	Vector Laboratories, Inc., Burlingame, USA	PK-4001

Table 2.10: Antibodies.

Antibody	Company	Catalog number
Alexa Fluor® 594 donkey anti-mouse IgG	Thermo Fisher Scientific, Inc., Surrey, UK	A-21203
Alexa Fluor® 594 donkey anti-rabbit IgG	Thermo Fisher Scientific, Inc., Surrey, UK	A-21207
Alexa Fluor® 594 donkey anti-goat IgG	Thermo Fisher Scientific, Inc., Surrey, UK	A-11058
Alexa Fluor® 488 donkey anti-goat IgG	Thermo Fisher Scientific, Inc., Surrey, UK	A-11055
Alexa Fluor® 488 donkey anti-rabbit IgG	Thermo Fisher Scientific, Inc., Surrey, UK	A-21206
Alexa Fluor® 488 goat anti-chicken	Thermo Fisher Scientific, Inc., Surrey, UK	A-11039
Anti-rabbit IgG, HRP-linked antibody	Cell Signaling Technology, Inc., Danvers, USA	7074
β-Actin Clone AC-15	Sigma Aldrich Chemie GmbH, Steinheim, Germany	A1978
Biotinylated anti-rat IgG	Vector Laboratories, Inc., Burlingame, USA	BA-9401
H. pylori	PD Dr. Roger Vogelmann, Mannheim	
ChrA (H-300)	Santa Cruz Biotechnology, Inc., Heidelberg, Germany	sc-13090
DLC1 C-terminal	Abcam plc, Cambridge, UK	ab180697
DLC1	Thermo Fisher Scientific, Inc., Surrey, UK	PA5-18290
Donkey anti-goat IgG, HRP-linked Antibody	Santa Cruz Biotechnology, Inc., Heidelberg, Germany	Sc-2020
ECL™ Anti-mouse IgG, HRP-linked Antibody	GE Healthcare UK	NA931V
F4/80 clone BM8	Thermo Fisher Scientific, Inc., Surrey, UK	MF 48000
FLAG	Abcam plc, Cambridge, UK	ab8112
FLAG	Sigma Aldrich Chemie GmbH, Steinheim, Germany	F1804
GFP	Roche Diagnostics GmbH, Mannheim, Germany	11 814 460 001
HIF1α	Cell Signaling Technology, Inc., Danvers, USA	3716
HSP 90α/β (H-114)	Santa Cruz Biotechnology, Inc., Heidelberg, Germany	sc-7947
Ki67	BD Biosciences, Heidelberg, Germany	550609
Ki67	Novus Biologicals Europe, Abingdon, UK	NB600-1252

Antibody	Company	Catalog number
MYL2 (C-17) (MLC2)	Santa Cruz Biotechnology, Inc., Heidelberg, Germany	sc-34490
NFκB	Cell Signaling Technology, Inc., Danvers, USA	3033
Phospho-NFκB	Cell Signaling Technology, Inc., Danvers, USA	8242
p38	Cell Signaling Technology, Inc., Danvers, USA	9212
Phospho-p38	Cell Signaling Technology, Inc., Danvers, USA	4511
p44/42 MAPK (ERK1/2)	Cell Signaling Technology, Inc., Danvers, USA	4695
Phospho-p44/42 MAPK (Phospho- ERK1/2)	Cell Signaling Technology, Inc., Danvers, USA	9101
Phospho-Myosin Light Chain 2 (Ser19) (Phospho-MLC2)	Cell Signaling Technology, Inc., Danvers, USA	3671
RhoA (26C4)	Santa Cruz Biotechnology, Inc., Heidelberg, Germany	sc-418
ROCKII	BD Biosciences, Heidelberg, Germany	610624
ROCK2 (phospho T249)	Abcam plc, Cambridge, UK	ab83514

Table 2.11: Oligonucleotides; hu = human, m = mouse.

Oligonucleotide	Sequence (5‘ -> 3‘)	Product size (bp)
RT-qPCR hormones		
5-m*Somatostatin*	GAGCCCAACCAGACAGAGAA	150
3-m*Somatostatin*	GAAGTTCTTGCAGCCAGCTT	
5-m*ChromograninA*	CCAATACCCAATCACCAACC	148
3-m*ChromograninA*	ACAGCCTCCTCTTCCTCCTC	
5-m*Hisdecarboxylase*	CTCATCCCGGCTACTATCCA	118
3-m*Hisdecarboxylase*	CAAGGTTAGCAGCCTCTTGG	
5-m*Tryptophanhydroxylase*	CATCAGCCGAGAACAGTTGA	184
3-m*Tryptophanhydroxylase*	TTCGGATCCATACAACAGCA	
5-m*Adiponectin*	GTTGCAAGCTCTCCTGTTCC	120
3-m*Adiponectin*	ATCCAACCTGCACAAGTTCC	
5-m*Ghrelin*	CCATCTGCAGTTTGCTGCTA	178
3-m*Ghrelin*	GCTTGTCCTCTGTCCTCTGG	
5-m*Intrinsic factor*	CTTGGCCCTGACCTGTATGT	191
3-m*Intrinsic factor*	TAGGTTGCTCAGGTGTCACG	

Oligonucleotide	**Sequence (5‘ -> 3‘)**	**Product size (bp)**
5-m*PepsinogenC*	CCAACCTGTGGGTGTCTTCT	187
3-m*PepsinogenC*	TTAGGGACCTGGATGCTTTG	
5-mH^+K^+-*ATPase*	GTTCCTGATGCTGTGCTCAA	118
3-mH^+K^+-*ATPase*	TGCCCTCTGAGATGATACCC	
RT-qPCR immunotyping		
5-m*Foxp3*	TTCATGCATCAGCTCTCCAC	185
3-m*Foxp3*	CTGGACACCCATTCCAGACT	
5-m*Cd4*	AGGAAGTGAACCTGGTGGTG	107
3-m*Cd4*	CTCCTGCTTCAGGGTCAGTC	
5-m*Cd8*	TATGGCTTCATCCCACAACA	190
3-m*Cd8*	GACTGGCACGACAGAACTGA	
5-m*iNOS*	CACCTTGGAGTTCACCCAGT	170
3-m*iNOS*	ACCACTCGTACTTGGGATGC	
5-m*Arg1*	AAAGCTGGTCTGCTGGAAAA	122
3-m*Arg1*	ACAGACCGTGGGTTCTTCAC	
5-m*Ifnγ*	GCGTCATTGAATCACACCTG	129
3-m*Ifnγ*	TGAGCTCATTGAATGCTTGG	
5-m*Gata3*	CCGAAACCGGAAGATGTCTA	131
3-m*Gata3*	AGATGTGGCTCAGGGATGAC	
5-m*Rorc*	TGCAAGACTCATCGACAAGG	177
3-m*Rorc*	AGGGGATTCAACATCAGTGC	
RT-qPCR RHO-pathway components		
5-m*RhoA*	CGCTTTTGGGTACATGGAGT	125
3-m*RhoA*	ACAAGATGAGGCACCCAGAC	
5-m*Rock2*	CCTGTCAAGCGTGGTAGTGA	191
3-m*Rock2*	TCCAGGGTCATCTGGAGTTC	
5-m*Rock1*	CAAAGCACGCCTAACTGACA	111
3-m*Rock1*	TCTGCCTTCTCTCGAGCTTC	
General PCR *Helicobacter* genotyping		
5-*vacA*	AGCCAGCTCTACGGTTTTGA	164
3-*vacA*	AATACGCTCCCACGTATTGC	
5-*cagA*	AGCAAAAAGCGACCTTGAAA	257
3-*cagA*	GGGTTCCATTCACACCATTC	
5-*ureB*	CATAAGCCGCTTGAGACACA	144
3-*ureB*	GCGGGTTCATTGCATTAAGT	
H276F	CTATGACGGGTATCCGGC	382
H676R	ATTCCACCTACCTCTCCCA	
P25F	ATGGGTAAGAAAATAGCAAAAAGATTGCAA	705
P25R	CTATTTCATATCCATAAGCTCTTGAGAATC	
P17F	ATGGAACAGATAAAGATTTTAAAGCAACTT	435
P17R	CTATGCAAGTTGTGCGTTAAGCAT	

Oligonucleotide	**Sequence (5‘ -> 3‘)**	**Product size (bp)**
5-HP-Cluster2	GGCGTTATCAACAGAATGGC	992-1548
3-HP-B1J99	CTCAGTTCGGATTGTAGGCTGC	
5-*H. felis*	GTGAAGCGACTAAAGATAAACAAT	241
3-*H. felis*	GCACCAAATCTAATTCATAAGAGC	
General PCR		
5-Nhu*DLC1*	CTTTCTCTGGAAGCCAGCAC	213
3-Nhu*DLC1*	ACCAGCTATTCCCCAGGAGT	
5-Chu*DLC1*	CCCTCACTCTGGAAGCACTC	268
3-Chu*DLC1*	TCCCAGAGGTGCTGTTCTTT	
5-Nm*DLC1*	GGGGAAGAGCGGTTTCTATC	188
3-Nm*DLC1*	TGCATGGTGGACAGTGTCTT	
5-Cm*DLC1*	CGTATTGAGGACCTGGAGGA	293
3-Cm*DLC1*	TCGTGTCCTTGCTTTCAGTG	
5-hu*RHOA*	TATCGAGGTGGATGGAAAGC	172
3-hu*RHOA*	TTCTGGGGTCCACTTTTCTG	
5-hu*ROCK2*	TGAAGCCTGACAACATGCTC	178
3-hu*ROCK2*	TCTCGCCCATAGAAACCATC	
5-hu*ROCK1*	AGGAAAATCGAAAGCTGCAA	186
3-hu*ROCK1*	GTTTAGCACGCAATTGCTCA	
Cloning		
5-*Kpnpv1hDLC1*	ATGGTACCCCATATTCTAACAGAAATATGCAAAC	1148
3-*Sacpv1hDLC1*	ATGAGCTCGTCATCATAGTTTAACAACAGACAGA	
5-*Kpnpv4hDLC1*	ATGGTACCAAGTGCTCCTTCCAGCCATATCTT	658
3-*Hindpv4hDLC1*	ATAAGCTTCCGCTCGCAGACGCCTTCAGC	
Sequencing		
T7	TAATACGACTCACTATAGGG	
M13 FP	TGTAAAACGACGGCCAGT	
M13 RP	CAGGAAACAGCTATGACC	
5Fseq-pGL3luc	CTAGCAAAATAGGCTGTCCC	
5Rev-EGFPC15seq	CATTTTATGTTTCAGGTTCAGGG	

Table 2.12: Plasmids.

Plasmid	**Characteristics**	**Origin**
pCR2.1 TOPO	Cloning vector, Amp^R, Kan^R	Thermo Fisher Scientific, Inc., Surrey, UK
pEGFP	Cloning vector, Kan^R, Neo^R	BD Biosciences, Heidelberg, Germany

Plasmid	**Characteristics**	**Origin**
pEGFP_CagA	Contains full length *cagA* of *H. pylori* G27, Kan^R, Neo^R	PD Dr. Roger Vogelmann, Mannheim
pEGFP_CagA _838-1216	Contains bp 838-1216 of *H. pylori* G27 *cagA*, Kan^R, Neo^R	PD Dr. Roger Vogelmann, Mannheim
pEGFP_CagA *A*_1-877	Contains bp 1-877 of *H. pylori* G27 *cagA*, Kan^R, Neo^R	PD Dr. Roger Vogelmann, Mannheim
pTRE-Tight	Cloning vector, Amp^R	BD Biosciences, Heidelberg, Germany
pTRE_CagA _1029-1216	Contains bp 1029-1216 of *H. pylori* G27 *cagA*, Amp^R, GFP fused	PD Dr. Roger Vogelmann
pGL3	Reporter plasmid, *luc+*, Amp^R	Promega Corporation, Madison, USA
pGL3_*SRE*	*luc+*, Amp^R, contains five serum responsive elements (*SRE*)	Stratagene Inc., La Jolla, USA
pGL3_*HRE*	*luc+*, Amp^R, contains HMGB2 promoter and hypoxia responsive element (*HRE*)	Promega Corporation, Madison, USA
pGL3_*DLC1.1p*	Contains promoter of *DLC1.1*, *luc+*, Amp^R	this study
pGL3_*DLC1.4p*	Contains promoter of *DLC1.4*, *luc+*, Amp^R	this study
pTarget	Expression vector, CMV Enhancer/Promoter, Amp^R, Neo^R	Promega Corporation, Madison, USA
pT_DLC1.1	Contains *DLC1.1*, CMV Enhancer/Promoter, Amp^R, Neo^R, FLAG tagged	Jan Philipp Köhler
pT_DLC1.4	Contains *DLC1.4* ΔSAM, CMV Enhancer/Promoter, Amp^R, Neo^R, FLAG tagged	Dr. Ivana Hitkova
pUC19	Cloning vector, Amp^R	Thermo Fisher Scientific, Inc., Surrey, UK
pGEX-2T-TRBD	Contains GST fusion proteins with a thrombin site and rhotekin RHO-binding domain (amino acids 7-89), Amp^R	Ren and Schwartz (2000)
pRL.TK	Luciferase control reporter vector; the HSV-thymidine kinase promoter is located upstream of *renilla* luciferase	Promega Corporation, Madison, USA

Plasmid	Characteristics	Origin
p*SRE*.L	Contains a mutated serum response element (*SRE*), which is deficient for the c-Fos ternary complex-binding site resulting in a more specifically respond to active RHOA than wild type *SRE* promoter.	Dianqing Wu, University of Rochester, USA
pcDNA_C3T	CMV Enhancer/Promoter, Amp^R, Neo^R, contains C3 toxin of *Clostridium botulinum*	Prof. Dr. Dr. Klaus Aktories, Freiburg
pcDNA_G13qL	CMV Enhancer/Promoter, Amp^R, Neo^R, contains G-protein α subunit Gα13	(Strathmann and Simon, 1991)

Table 2.13: Equipment and devices.

Equipment/device	Company
ABI PRISM Real Time 7900HT Sequence Detection System	Thermo Fisher Scientific, Inc., Surrey, UK
Agarose electrophoresis chamber	neoLab Migge GmbH, Heidelberg, Germany
Autoclave Systec V-150	Systec GmbH, Linden, Germany
Cabinet dryer FunctionLine	Heraeus Holding GmbH, Hanau, Germany
Centrifuge 5424R	Eppendorf AG, Hamburg, Germany
Centrifuge 5415C	Eppendorf AG, Hamburg, Germany
Centrifuge 5804R	Eppendorf AG, Hamburg, Germany
Centrifuge 3K12	Sigma Laborzentrifugen GmbH, Osterode am Harz, Germany
Centrifuge ROTANTA/RP	Andreas Hettich GmbH & Co. KG, Tuttlingen, Germany
FACSCanto™	BD Biosciences, Heidelberg, Germany
Fusion Solo	PEQLAB Biotechnologie GmbH, Erlangen, Germany
Homogenisator IKA® T10 basic ULTRA-TURRAX®	IKA-Werke GmbH & Co. KG, Munich, Germany
Incubator HERAcell® 240	Heraeus Holding GmbH, Hanau, Germany
Microscope AxioVert 25	Carl Zeiss MicroImaging GmbH, Göttingen, Germany
Microscope Axio Imager	Carl Zeiss MicroImaging GmbH, Göttingen, Germany
Microscope DM IRB	Leica Microsysteme Vertrieb GmbH, Wetzlar, Germany
Microtome RM 2145	Leica Microsysteme Vertrieb GmbH, Wetzlar, Germany

Equipment/device	Company
Microplate reader Tecan Infinite M200	Tecan Group AG, Männedorf, Switzerland
Microwave	Siemens AG, Munich, Germany
Multi-animal transport system	Bruker Biospin GmbH, Karlsruhe, Germany
Mini Trans-Blot® Electrophoretic Transfer Cell	Bio-Rad Laboratories GmbH, Munich, Germany
Mini-PROTEAN® Tetra Cell	Bio-Rad Laboratories GmbH, Munich, Germany
Overhead shaker REAX 2	Heidolph Instruments GmbH & Co. KG, Schwabach, Germany
pH-Meter 766	Knick Elektronische Messgeräte GmbH & Co. KG, Berlin, Germany
Power supply PowerPac Basic	Bio-Rad Laboratories GmbH, Munich, Germany
Power supply Consort Ev 245	Biophoretics, Sparks, USA
Safety cabinet for cell culture HERAsafe® KS	Heraeus Holding GmbH, Hanau, Germany
Shaker ROCKY®	Labortechnik Fröbel GmbH, Lindau, Germany
Shaker IKA®-VIBRAX-VXR	IKA-Werke GmbH & Co. KG, Munich, Germany
Sonifier®Cell Disrupter 250, Branson Ultrasonics	Emerson Electronic Co., St. Louis, USA
Spectrophotometer NanoDrop® ND-1000	PEQLAB Biotechnologie GmbH, Erlangen, Germany
Thermomixer compact	Eppendorf AG, Hamburg, Germany
Thermocycler GeneAmp® 9700	Thermo Fisher Scientific, Inc., Surrey, UK
Tri-modal Bruker Albira II small-animal PET/SPECT/CT	Bruker Biospin GmbH, Karlsruhe, Germany
Thermocycler PEQSTAR	PEQLAB GmbH, Erlangen, Germany
UV Transilluminator	Biometra GmbH, Göttingen, Germany
Vortexer REAX 2000	Heidolph Instruments GmbH & Co. KG, Schwabach, Germany
Water bath Certomat® WR	B. Braun Melsungen AG, Melsungen, Germany
Weighing machine Sartorius research R180D	Sartorius AG, Göttingen, Germany

Table 2.14: Software.

Software	Company
AxioVision Rel. 4.4	Carl Zeiss MicroImaging GmbH, Halbergmoss, Germany
AxioVision Rel. 4.7.2	Carl Zeiss MicroImaging GmbH, Halbergmoss, Germany
FACSDIVA™	BD Biosciences, Heidelberg, Germany
FusionCapt Advance Solo 4	VILBER LOURMAT GmbH, Eberhardzell, Germany

Software	Company
ImageJ 1.45s	Wayne Rasband NIH, MD, USA
PRISM GraphPad 7	GraphPad Software, Inc., La Jolla, USA

2.2 Methods

2.2.1 Cell culture

2.2.1.1 Cell growth conditions

HEK293T, AGS, SW480 and tsA201 cells were grown in DMEM medium, whereas MKN45, NCI-N87 and Jurkat cells were cultivated in RPMI 1640 medium at 37°C under 5% CO_2 in a humidified incubator. All media were supplemented with 1% Pen/Strep, 1% L-glutamine and 10% FCS (Thermo Fisher Scientific).

2.2.1.2 Splitting of cells

Cells were split at 80-90% confluency. For this purpose, cells were washed with PBS to remove all FCS (2ml in 25cm² cell culture flask and 5ml in 75cm² cell culture flask). The cells were coated with 0.25% Trypsin EDTA (1ml in 25cm² cell culture flask and 2ml in 75cm² cell culture flask) and incubated at 37°C until they were detached. To neutralize the trypsin, growth medium was added and the cells were resuspended and split appropriately (1:30 for HEK293T and tsA201, 1:10 for AGS and SW480, 1:3-1:5 for MKN45 and NCI-N87).

2.2.1.3 Preparing cell stocks

For preparation of cell stocks, cells were trypsinized at a confluency of 90% in a 75 cm² cell culture flask and centrifuged (5min, 1000g, RT). The pellet was resuspended in 3ml freezing medium (10% (v/v) DMSO and 90% (v/v) FCS) and split into three cryotubes. Cell stocks were incubated at -80°C for at least 24h and finally frozen in liquid nitrogen.

2.2.1.4 Counting cells

For determination of the cell number, cells were trypsinized and stained with trypan blue. To this end, 10µl cell suspension was added to 10µl trypan blue. Trypan blue accumulates in perforated dead cells and allows a differentiation between vital and dead cells. The stained cell suspension served for determination of the cell number via light microscopy using a counting chamber.

2.2.1.5 Transient transfection of cells

To insert plasmid DNA into eukaryotic cells, cells were seeded in 6-well plates overnight (500 000 cells per well for HEK293T and tsA201, 750 000 cells per well for AGS, SW480, NCI-N87 and MKN45). Then, cells were transiently transfected in growth medium without FCS, L-glutamine and Pen/Strep using TurboFect™ according to the manufacturer's instructions. After 6h incubation time at 37°C, the medium was changed (supplemented with 10% FCS, 1% L-glutamine and 1% Pen/Strep).

2.2.1.6 Stimulation of cells

Cells were seeded in 6-well plates, transiently transfected as described in 2.2.1.5 and stimulated with 1µg/ml LPS for up to 60 min (0, 15, 30, 60 min) 48h after transfection to analyze NFκB expression. For analysis of HIF1α expression, cells were treated with 0.1mM $CoCl_2$ for 4h one day after transfection.

2.2.1.7 MTT Assay

This method is based on the metabolization of thiazolyl blue tetrazolium bromide by living cells, resulting in the formation of a blue dye called formazan, which indicates cell viability. Cells were seeded in 100µl growth medium and treated with increasing concentrations of fasudil or PBS as vehicle control in 96-well plates when cells were attached. After two days of incubation, MTT reagent (5 mg/ml in 1x PBS, 10µl per well) was added and the plate was incubated at 37°C for 4h. Afterwards, the reaction was stopped using 100µl MTT lysis buffer (10% (w/v) SDS and 0.01N HCl) per well. An overnight incubation at 37°C ensured complete

lysis of the cells and solubilization of the formed formazan. Released blue dye was then measured at 570-650nm by a plate reader.

2.2.2 Microbiological methods

2.2.2.1 Cultivation of *H. pylori*

Frozen Stocks of *H. pylori* were thawed on ice. About 100µl of bacterial suspension were plated on freshly prepared and pre-warmed horse blood agar plates.

For preparing horse agar plates, 44g Columbia Agar Base was dissolved in 950ml dH_2O and autoclaved for 15min. Afterwards, the solution was incubated at 50°C for 1h. Horse blood was pre-warmed at RT and 25ml were added to the agar solution. Antibiotics were prepared as follows and 2.5ml 200x antibiotics, 0.5ml 1000x antibiotics and 5ml β-cyclodextrin (1g in 5ml DMSO) were added to the agar solution.

200x antibiotics

component	**amount**
Vancomycin hydrochloride	100mg
Cefsulodin sodium salt hydrate	50mg
Polymyxin B sulfate salt	3.3mg
Cycloheximide	500mg
dH_2O	Add 50ml, filter sterilize

1000x antibiotics

component	**amount**
Trimethoprim	100mg
Amphotericin B	160mg
DMSO	Add 20ml, filter sterilize

The inoculated plates were incubated in an airtight closed box together with GasPak™ at 37°C for 48-72h to remove elemental oxygen gas and thus produce an anaerobic environment.

For preparing stocks, bacteria were taken off the agar plate with a sterile cotton bud and resuspended in 0.5-1ml freezing medium (10% FCS, 20% glycerol, 70% BHI medium). BHI medium was prepared by dissolving and autoclaving 3.7g Brain Heart Infusion Broth in 100ml dH_2O.

2.2.2.2 Genotyping of *Helicobacter*

For isolation of bacterial DNA of frozen bacterial stocks, the DNeasy@ Blood & Tissue Kit was used according to the manufacturer's instructions. Genotyping of the bacterial strains was done by performing general PCR as described in 2.2.4.6.

2.2.2.3 Infection of eukaryotic cells with *H. pylori* for immuno-fluorescence staining

For infection of eukaryotic cells with *H. pylori*, AGS cells were grown to 80% confluency in a 75cm^2 cell culture flask and washed 3x with warm PBS before 8ml *H. pylori* cultivation medium (DMEM/F12, 10% FCS (PAN-Biotech), 10% Brucella Broth medium (14.05g Brucella Broth Base in 500ml dH_2O), 1µg/ml vancomycin) were added to the cells. Bacteria were taken off the agar plate using a sterile cotton bud and resuspended in 2ml *H. pylori* cultivation medium. Vitality of the bacteria was validated by light microscopy and the bacterial suspension was added to the cells. The cells were incubated at 37°C under 5% CO_2 in a humidified incubator. After 24h of incubation, the cell culture supernatant was collected in a tube and centrifuged for 5min at 4000rpm. The pellet was resuspended in 2ml *H. pylori* cultivation medium and used for infection of overnight grown AGS cells on glass slides in a 6-well plate. The next day, immunofluorescence staining was performed as described in 2.2.5.1.

2.2.3 Protein preparation and analysis

2.2.3.1 Preparation of total cell lysate

Cells were washed with PBS before adding SDS lysis buffer (50mM Tris-HCl, pH 7.4, 1% SDS, 1mM sodium orthovanadate, 1mM dithiothreitol, Protease Inhibitor Complete®). The cells

were scraped and transferred into 1.5ml tubes. For purification, the lysate was sonicated for 20sec and centrifuged at maximum speed for 10min at 4°C. The supernatant was collected and stored at -80°C until determination of protein concentration.

2.2.3.2 Preparation of total tissue lysate

For protein extraction of tissue, either normal tissue lysis buffer or RIPA buffer was used.

normal tissue lysis buffer

component	concentration
HEPES	20mM, pH 7.4
EDTA	1mM
β-Glycerophosphate	50mM
Glycerol	10% (v/v)
Triton X-100	1% (v/v)
Sodium orthovanadate	1mM
Dithiothreitol	1mM
Protease Inhibitor Complete®	1 Tablet per 50ml

RIPA buffer

component	concentration
Tris-HCl	50mM, pH 7.2
NaCl	250mM
Nonidet P40	2% (v/v)
EDTA	2.5mM
SDS	0.1% (w/v)
Deoxycholic acid (DOC)	0.5% (w/v)
Phosphatase inhibitor cocktail II	1:100
Protease Inhibitor Complete®	1 Tablet per 50ml

Frozen tissue (2-3mm³) was added to 400µl of ice-cold lysis buffer. Afterwards, the tissue was homogenized using the Homogenisator IKA® T10 basic ULTRA-TURRAX® and incubated on ice for 40min (RIPA) or 60min (normal buffer), respectively. Samples lyzed with RIPA buffer were additionally incubated for 10min at RT. After centrifugation at maximum speed for 10min at 4°C, the supernatant was collected and stored at -80°C until determination of protein concentration.

2.2.3.3 Western Blot

Preparation of samples

The BCA™ Protein Assay Kit was used to measure protein concentration according to the manufacturer's protocol. The protein samples were diluted in dH_2O to reach the same concentration for each sample and boiled in 5x SDS loading buffer (62.5mM Tris-base pH 10, 10% (w/v) SDS, 5% (v/v) β-mercaptoethanol, 50% (v/v) glycerol, bromphenol blue) for 10min at 99°C. After a short centrifugation, the samples were used for Western Blot analysis or stored at -20°C.

SDS-polyacrylamide gel electrophoresis (SDS-PAGE)

SDS-PAGE was performed to separate the proteins according to their molecular weight. Acrylamide gels (12.5%, 10% or 7.5%) were prepared as follows:

Component	Separating gel			Stacking gel
	12.5%	**10%**	**7.5%**	**4%**
H_2O	2.59ml	3.29ml	3.99ml	1.53ml
Acrylamide (30%)	3.5ml	2.8ml	2.1ml	333µl
1.5M Tris-HCl, pH 8.8	2.1ml	2.1ml	2.1ml	-
0.5M Tris-HCl, pH 6.8	-	-	-	625µl
SDS (10%)	83µl	83µl	83µl	25µl
APS (10%)	42µl	42µl	42µl	12.5µl
TEMED	2.8µl	2.8µl	2.8µl	2.5µl

The protein samples were loaded in equal amounts and the gel was run at constant 15mA in running buffer (192mM glycine, 25mM Tris-base, 0.1% (w/v) SDS) using the Mini-PROTEAN® Tetra Cell system.

Protein transfer and detection

Transfer of the separated proteins to a nitrocellulose membrane was achieved by the Mini trans-Blot® Electrophoretic Transfer Cell for 1h at 100V in transfer buffer (192mM glycine, 25mM Tris-base, 20% (v/v) methanol). The membrane was then blocked for 1h in 5% (w/v) BSA or milk in T-PBS (0.1% (v/v) Tween 20 in PBS) on a shaker at RT and incubated overnight in primary antibody solution at 4°C while gentle shaking. The next day, the membrane was washed in T-PBS 3x 10min before adding peroxidase-labelled secondary antibody solution (1:5000). After 1h incubation time, the membrane was washed again 3x 10min and immunodetection was performed using Enhanced Chemiluminescence Detection Reagent A and B 1:1 (A: 3µl H_2O_2 in 5ml 0.1M Tris-HCl, pH 8.5; B: 50µl luminol and 22µl p-coumaric acid in 5ml 0.1M Tris-HCl, pH 8.5) using the Fusion Solo device.

Table 2.15: Antibody dilutions used for Western Blot analysis.

Antibody	Company	blocking	dilution
Primary antibody			
β-Actin Clone AC-15, A1978	Sigma Aldrich Chemie GmbH, Steinheim, Germany	5% milk/ 5% BSA	1:1000 in T-PBS
DLC1, PA5-18290	Thermo Fisher Scientific, Inc., Surrey, UK	5% milk	1:1000 in 2.5% milk
DLC1 C-terminal, ab180697	Abcam plc, Cambridge, UK	5% milk	1:500 in 2.5% milk
p44/42 MAPK (ERK1/2), #4695	Cell Signaling Technology, Inc., Danvers, USA	5% milk	1:1000 in 2.5% milk
FLAG, ab8112	Abcam plc, Cambridge, UK	5% milk	1:1000 in 2.5% milk
FLAG, F1804	Sigma Aldrich Chemie GmbH, Steinheim, Germany	5% milk	1:1000 in 2.5% milk
GFP, #11 814 460 001	Roche Diagnostics GmbH, Mannheim, Germany	5% milk	1:1000 in 2.5% milk
HIF1α, #3716	Cell Signaling Technology, Inc., Danvers, USA	5% milk	1:1000 in 2.5% milk
HSP 90α/β (H-114), sc-7947	Santa Cruz Biotechnology, Inc., Heidelberg, Germany	5% milk/ 5% BSA	1:1000 in T-PBS
MYL2 (C-17), sc-34490	Santa Cruz Biotechnology, Inc., Heidelberg, Germany	5% milk	1:1000 in 2.5% milk
NFκB, #3033	Cell Signaling Technology, Inc., Danvers, USA	5% milk	1:1000 in 5% BSA
Phospho-NFκB, #8242	Cell Signaling Technology, Inc., Danvers, USA	5% BSA	1:1000 in 5% BSA

Antibody	Company	blocking	dilution
Primary antibody			
Phospho-Myosin Light Chain 2 (Ser19), #3671	Cell Signaling Technology, Inc., Danvers, USA	5% milk	1:1000 in 5% BSA
RhoA (26C4), sc-418	Santa Cruz Biotechnology, Inc., Heidelberg, Germany	5% milk	1:1000 in 2.5% milk
ROCKII, #610624	BD Biosciences, Heidelberg, Germany	5% milk	1:1000 in 2.5% milk
ROCK2 (phospho T249), ab83514	Abcam plc, Cambridge, UK	5% BSA	1:500 in 1% BSA
Secondary antibody			
Anti-rabbit IgG, HRP-linked antibody, #7074	Cell Signaling Technology, Inc., Danvers, USA	5% milk/ 5% BSA	1:5000 in BSA/ milk
Donkey anti-goat IgG, HRP-linked Antibody, sc-2020	Santa Cruz Biotechnology, Inc., Heidelberg, Germany	5% milk/ 5% BSA	1:5000 in BSA/ milk
ECL™ Anti-mouse IgG, HRP-linked Antibody, NA931V	GE Healthcare UK	5% milk/ 5% BSA	1:5000 in BSA/ milk

2.2.3.4 (Co)-Immunoprecipitation

Immunoprecipitation (IP) was done to enrich a specific protein out of solution using an antibody that specifically binds to that antigen. The antibody needs to be coupled to a solid substrate. Co-immunoprecipitation (CoIP) was performed to analyze protein-protein interactions. This method is based on the interaction of an antibody with a known protein, which is suggested to be part of a protein complex. Co-IP aims to precipitate the entire protein complex out of solution and later to identify unknown components of the complex by immunoblot (IB).

To perform CoIP, cells were grown to 90% confluency on a TC-dish 60 and transiently transfected as described in 2.2.1.5. For hypotonic lysis, 1ml lysis buffer (10mM Tris-HCl, pH 7.4, 2mM EDTA, 2mM $MgCl_2$, 1mM sodium orthovanadate, 1mM DTT, Protease Inhibitor Complete®) was added. The cells were scraped and transferred to a 2.0ml tube. For complete lysis, the cells were incubated on ice for 20min, homogenized by pipetting up and down 20 times until foaming and centrifuged for 10min at 13200rpm at 4°C. All following steps were performed on ice. The supernatant was mixed with 10µl Protein A/G PLUS-Agarose and incubated for 1h at 4°C under rotation. After centrifugation for 10min at 13200rpm and 4°C, 80µl of the supernatant were separated as input controls and stored at -

20°C, whereas 400µl of the supernatant were mixed with 4µg primary antibody (GFP #11 814 460 001 for CagA constructs, DLC1 PA5-18290 for DLC1.1 and FLAG, ab8112 for DLC1.4). Furthermore, 400µl of each sample were left without antibody as negative controls. The samples were incubated overnight at 4°C under rotation. The next day, 60µl Protein A/G PLUS-Agarose were added and incubated for 2h at 4°C under rotation. Beads were pelleted by centrifugation for 1min, 13200rpm at 4°C followed by three washing steps with 1ml wash buffer (lysis-buffer supplemented with 150mM NaCl) and subsequent centrifugation for 2min and 13200rpm at 4°C. For elution, the supernatant was mixed with 50µl of 100mM glycine (pH 2.2) and incubated on ice for 2min. The reaction was stopped by adding 10µl of 1.5mM Tris-HCl (pH 8.8). The eluate was collected after further centrifugation for 1min, 13200rpm at 4°C and supplemented with 10µl 5x SDS-loading buffer. The input controls were supplemented with 20µl 5x SDS-loading buffer and all samples were boiled for 10min at 99°C for Western Blot analysis.

To perform IP, frozen mouse liver tissue (2-3mm³) was added to 1ml hypotonic lysis buffer for tissue (1M Tris pH7.4, 0.5M EDTA, 1M $MgCl_2$, 1mM sodium orthovanadate, 1mM DTT, Protease Inhibitor Complete®). The tissue was homogenized using the Homogenisator IKA® T10 basic ULTRA-TURRAX® and incubated on ice for 1h. After resuspension and centrifugation for 10min at 4°C and 13200rpm, the supernatant was transferred into a new tube. All following steps were performed on ice according to the protocol for CoIP.

2.2.3.5 RHO Pulldown Assay

Analysis of RHOA activity was done using the RhoA/Rac1/Cdc42 Activation Assay Combo Kit. This method uses agarose beads linked to the RHO-binding domain (RBD) of rhotekin. Only active RHOA (RHOA-GTP) binds to rhotekin-RBD and can be precipitated and used for Western Blot analysis. Cells were grown to 90% confluency on a TC-dish 60 and transiently transfected as described in 2.2.1.5. After 72h of incubation, cells were starved in DMEM medium without supplements for 16h. Cells were incubated for 5min in DMEM medium supplemented with 20% FCS. The medium was aspirated and the cells were washed with ice-cold PBS twice before addition of 1ml 1x Assay/Lysis Buffer (supplemented with 1mM sodium orthovanadate, 1mM DTT, Protease Inhibitor Complete®). The cells were scraped

with a cell scraper and collected in 2.0ml tubes for incubation on ice for 15min to ensure complete cell lysis. All following steps were performed on ice. Centrifugation for 10min, 13200rpm at 4°C separated the cell debris from the protein containing supernatant. For input controls, 80µl supernatant were separated. Remaining samples were supplemented with 40µl RBD-agarose beads and incubated at 4°C under rotation. After 1h of incubation, samples were centrifuged for 1min at 13200rpm at 4°C and the supernatant was discarded. The pellet was washed three times using 0.5ml 1x Assay/Lysis Buffer followed by centrifugation for 2min, 13200rpm at 4°C. The supernatant was completely removed and 30µl of 1M Tris-buffer (pH 7.4) were added. The samples were supplemented with 10µl 5x SDS-loading buffer, whereas the input controls were supplemented with 20µl 5x SDS-loading buffer. All samples were boiled for 5min at 99°C and subjected to Western Blot analysis.

For analysis of RHOA activity in mouse tissue, 1ml 1x Assay/Lysis Buffer (supplemented with 1mM sodium orthovanadate, 1mM DTT, Protease Inhibitor Complete®) was added to a piece of frozen tissue (2-3mm²). The tissue was homogenized and incubated on ice for 1h. After centrifugation at maximum speed for 10min at 4°C, supernatant was collected and all steps were performed as previously described for cells.

In cooperation with Prof. Wieland (Experimental Pharmacology, Medical Faculty Mannheim of University Heidelberg, Mannheim, Germany), RHOA pulldown assay was performed in tsA201 cells to assess the interplay between CagA and DLC1 concerning RHOA activation. The principle of this assay is similar to that of the RhoA/Rac1/Cdc42 Activation Assay Combo Kit and is based on the binding of active RHOA to the RHOA-GTP-interacting protein domain of rhotekin, which is linked to glutathione sepharose by GST-tag. The glutathione sepharose beads were kindly provided by the group of Prof. Wieland.

GST-Rhotekin-RBD was expressed in competent *E. coli* Rosetta™ cells and linked to glutathione sepharose. To this end, RBD was cloned in pGEX2T vector encoding the protein in combination with GST. An overnight culture of bacteria was added to 800ml 2x YT medium supplemented with 100µg/ml ampicillin.

2x YT medium

component	concentration
Bacto™ Tryptone	16g
Yeast extract	10g
NaCl	5g
dH_2O	ad 1l

Bacteria were grown until OD_{600} of 0.6 at 37°C under rotation. Protein synthesis was induced via addition of 1mM IPTG at 25°C for 1h under rotation. Centrifugation for 10min at 3000g and 4°C was followed by resuspension of the pellet using 10ml ice cold PBS and lysis by sonification (5x30sec). After centrifugation for 10min at 20000g and 4°C, the supernatant was added to 800µl equilibrated glutathione sepharose and incubated on ice for 45min under rotation. Samples were centrifuged for 2min at 1000g and 4°C and washed twice with 50ml ice cold PBS. Protein concentration was determined and 50µg glutathione sepharose were supplemented with 100µl freezing buffer and stored at -80°C.

Freezing Buffer

component	concentration
Tris-HCl	50mM, pH 7.5
NaCl	150mM
$MgCl_2$	5mM
DTT	1mM
Triton X-100	0.5% (v/v)
Glycerol	10% (v/v)
Pefablock	1:1000

For pulldown assay, cells were grown to 90% confluency in a 6-well plate, transiently transfected as described in 2.2.1.5 and incubated in DMEM medium supplemented with 0.5% FCS overnight. All steps of the RHOA pulldown assay were performed in a cooling room. All substances, solutions and materials were pre-chilled. The cell medium was completely aspirated and 500µl GST-Fish buffer was added per well for cell lysis.

GST-Fish buffer

component	concentration
Tris-HCl	50mM, pH 7.4
NaCl	150mM
$MgCl_2$	4mM
Glycerol	10% (v/v)
Igepal® CA-630	1% (v/v)

Cells were detached using a cell scraper and transferred into an Eppendorf tube for centrifugation at maximum speed for 2min. For determination of general RHOA level, 60µl of the supernatant were transferred into a second tube. The remaining lysate was added to 90µl glutathione sepharose and incubated in a tube on ice for 1h under rotation using an overhead shaker. The samples were centrifuged at maximum speed for 2min and the supernatant was aspirated until about 50µl were left. Sepharose was washed by adding 1ml GST-Fish buffer and samples were vortexed. Centrifugation and the washing step were repeated and the supernatant was aspirated until 15-20µl were left. Samples were centrifuged finally and prepared for Western Blot analysis by adding 5x SDS loading buffer without glycerol and boiling for 5min at 95°C under rotation. Samples were vortexed carefully and centrifuged briefly. The complete supernatant of the pulldown samples and 20µl of the input controls were subjected to Western Blot analysis.

2.2.3.6 Luciferase Activity Assay

For determination of *DLC1* promoter activity, the promoters of human isoforms 1 and 4 were linked to the luciferase gene. The expression of luciferase was now under control of the corresponding *DLC1* promoter. To analyze the functional antagonism between CagA and DLC1, luciferase reporter plasmids containing *SRE* (serum response element, pGL3_*SRE*) and *HRE* (hypoxia response element under control of the promoter of HMGB2, high mobility group protein B2, pGL3_*HRE*) were co-transfected with pEGFP_CagA, pT_DLC1.1 or a combination of both. For analysis of RHOA activity, p*SRE*.L luciferase reporter plasmid was co-transfected with pEGFP_CagA, pT_DLC1.1, pT_DLC1.4 or a combination of pEGFP_CagA and the respective DLC1 plasmid. Luciferase catalyzes the oxidation of luciferin resulting in

the generation of chemiluminescence, which can be measured by a plate reader using a white 96-well Cellstar Cell Culture Plate.

Cells were transiently transfected as described in 2.2.1.5. After 48h (HEK293T) or 24h (AGS, NCI-N87) of incubation, the medium was aspirated and 150µl 1x passive lysis buffer were added. The 6-well plate was incubated for 10min at RT on a shaker and cells were transferred into tubes for centrifugation at maximum speed for 10min at 4°C to remove cell debris. For determination of *firefly* luciferase activity, 10µl lysate was mixed with 35µl luciferin and the measured values were normalized to the according protein concentration.

Specificity of p*SRE*.L for active RHOA was verified by control plasmids in cooperation with the group of Prof. Wieland (Dept. of Experimental Pharmacology, Medical Faculty Mannheim of University Heidelberg, Mannheim, Germany). For this purpose, RHOA activators (pcDNA_G13qL) or RHOA inhibitors (pcDNA_C3T) were co-transfected with DLC1 or CagA, respectively, in addition to the luciferase reporter plasmids p*SRE*.L and pRL.TK. The reporter plasmid pRL.TK encodes a luciferase under control of the constitutively active Herpes Simplex thymidine kinase (HSV-TK) promoter and served for determination of *renilla* luciferase. TsA201 cells were transiently transfected in duplicates with a total of 125ng plasmid DNA in a 96-well plate. The quantity of reporter plasmids amounted to 25ng and was made of six parts of p*SRE*.L and one part of pRL.TK. After an incubation time of 24h, luciferase activity was measured using the Dual Luciferase Reporter Assay System. Cells were lyzed by shaking for 10min using 25µl buffer per well and 25µl substrate buffer was added to 10µl lysate for measurement. *Firefly* luciferase (p*SRE*.L) was normalized to *renilla* luciferase activity (pRL.TK).

2.2.4 Nucleic acid preparation and analysis

2.2.4.1 Transformation of plasmid DNA

For amplification of plasmid DNA, the *E. coli* strains DH5α and Top10 were used. For transformation, a 50µl aliquot of chemically competent cells was thawed on ice and 1µl (approx. 200ng) plasmid was added and incubated for 30min on ice. After heat shock at 42°C for 90sec, the cells were cooled down on ice for 2min, mixed with 500µl LB-medium and

incubated for 1h at 37°C, 370rpm. Selective LB-agar plates were used for cultivation of 50µl bacteria suspension in an incubator at 37°C overnight.

2.2.4.2 Isolation of plasmid DNA

A single colony of transformed bacteria was picked from a selective LB-agar plate using a sterile pipette tip and transferred into 3ml LB-medium containing the corresponding selective antibiotic (100µg/ml). The bacterial culture was incubated overnight at 37°C, 370rpm. Suspension was centrifuged for 30sec at 13200rpm and the pellet was resuspended in 600µl nuclease-free water. Afterwards, plasmid DNA was isolated using the Pure Yield™ Plasmid Miniprep System kit according to the manufacturer's protocol.

To obtain higher amounts of plasmid DNA, a single colony was picked from a selective LB-agar plate using a sterile pipette tip and transferred into 5ml LB-medium containing the corresponding antibiotic (100µg/ml) for selection. The bacterial culture was incubated for 6h at 37°C, 370rpm. Afterwards, the suspension was added to 100ml LB-medium containing 100µg/ml of the corresponding selective antibiotic and incubated overnight at 37°C, 370rpm. Bacteria were centrifuged for 15min at 4000rpm and plasmid DNA was isolated according to the instructions of the HiSpeed® Plasmid Midi Kit.

2.2.4.3 RNA extraction of cells

Cells were seeded in 6-well plates and transiently transfected as described in 2.2.1.5. Medium was aspirated and 400µl of RNA Lyse buffer T were added. The cell lysates were mixed with an equal volume of 70% ethanol and transferred to a silica membrane of the RNeasy™ Mini Kit. RNA extraction was performed according to the manufacturer's instructions. DNA was digested by adding DNase I for 15min, pure RNA was eluted in nuclease-free water.

2.2.4.4 RNA extraction of tissue

Frozen tissue (2-3mm³) was added to 600µl of RNA Lyse buffer T and homogenized using the Homogenisator IKA® T10 basic ULTRA-TURRAX®. The samples were centrifuged for 10min at

4°C, 10000rpm and the supernatant was transferred to a silica membrane of the RNeasy™ Mini Kit. RNA was extracted as described in 2.2.4.3.

2.2.4.5 cDNA synthesis

Purified RNA (1µg) was used for reverse transcription into cDNA via the Verso™ cDNA Kit according to the manufacturer's instructions. Synthesized cDNA was filled up with nuclease-free water to a final volume of 50µl.

2.2.4.6 General polymerase chain reaction (PCR)

For amplification of DNA fragments, PCR was performed. The reaction setup was as follows:

Component	**Volume**
GoTaq® Green Master Mix/ JumpStart™ REDTaq® ReadyMix™	10µl
Forward primer (10µM)	2µl
Reverse primer (10µM)	2µl
DNA	2µl
Nuclease-free H_2O	4µl

An example for an amplification program is shown below.

Step	**Temperature**	**Holds**	**Number of cycles**
Initial denaturation	95°C	5min	1
Denaturation	95°C	2min	
Primer annealing	55°C	1min	40
Elongation	72°C	2min	
Final elongation	72°C	5min	1
Cooling	4°C	∞	

By increasing the number of cycles, the amount of PCR product can be increased, but this can also result in unspecific product. Optimal annealing temperature is important for specific primer annealing and elongation time depends on the size of the PCR product.

2.2.4.7 Quantitative real-time PCR (RT-qPCR)

RT-qPCR was performed for quantitative analysis of gene expression. The composition of the reaction mix is shown below.

Component	**Volume**
Power SYBR® Green Master Mix	10µl
Forward primer (10µM)	1µl
Reverse primer (10µM)	1µl
Nuclease-free H_2O	6µl

The reaction mix was completed by addition of 2µl cDNA. Each reaction was performed in duplicates in a LightCycler® 480 Multiwell Plate 96. The housekeeping gene ß2-microtubulin (*ß2M*) was used as reference. The plate was centrifuged for 1min at 1000rpm and amplification was done using the following program:

Step	**Temperature**	**Holds**	**Number of cycles**
Initial denaturation	95°C	5min	1
Cycling Stage	95°C	15sec	40
	60°C	1min	
Melting Curve Stage	95°C	15sec	1
	60°C	1min	
	95°C	15sec	

This method is based on the binding of SYBR® Green to double stranded DNA during amplification resulting in a fluorescence signal, which can be directly measured. Fluorescence intensity of SYBR® Green increases with the amount of the PCR product. For quantification, the CT-value (cycle threshold) was used. This value correlates to the number

of PCR cycles where fluorescence of amplified DNA can be distinguished from background fluorescence. There is an inverse correlation between the CT-value and the expression of a certain gene. The mean value of the duplicates of one gene and condition (individual, tumor, normal tissue, etc.) was calculated and the CT of the housekeeping gene was subtracted resulting in ΔCT. The mean of all ΔCTs for one gene and condition is also known as "calibrator". Subtraction of the "calibrator" from each ΔCT-value leads to ΔΔCT. Fold induction was calculated based on the formula $2^{-\Delta\Delta CT}$ (Tellmann and Geulen, 2006).

2.2.4.8 Agarose gel electrophoresis

PCR products were analyzed on 1-2% (w/v) agarose gels dependent on the size of the amplified PCR product. Agarose was added to 1x TAE buffer (40mM Tris-base, 1mM EDTA pH 8.0, 20mM acetic acid) and boiled in the microwave until all agarose was dissolved. Afterwards, 0.25 µg/ml ethidium bromide were added, and polymerized gels were run for at least 30min at 100V. DNA was detected using a UV transilluminator.

2.2.4.9 Molecular cloning

To investigate a putative transcriptional regulation of the human *DLC1* promoter, the promoter of human *DLC1.1* and *DLC1.4* were cloned into a luciferase reporter plasmid (pGL3) for luciferase activity assays. Human *DLC1* promoter from isoform 1 and 4 were amplified from 2µl HEK293T DNA by PCR as follows:

JumpStart™ REDTaq® ReadyMix™	10µl
Forward Primer	2µl
Reverse Primer	2µl
H_2O	4µl

Amplification of the product was performed using following program:

Step	Temperature	Holds	Number of cycles
Initial denaturation	95°C	5min	1
Denaturation	95°C	2min	
Primer annealing	55°C	2min	40
Elongation	72°C	2min	
Final elongation	72°C	5min	1
Cooling	4°C	∞	

The PCR products were analyzed on a 1% agarose gel. Bands showing the correct size were excised with a clean scalpel and DNA was extracted using the QIAquick Gel Extraction Kit according to the manufacturer's instructions. The purified PCR products were used for TOPO TA Cloning® according to the manufacturer's protocol. The reaction was composed as follows:

PCR product	4µl
Salt solution	1µl
TOPO® vector	1µl

The mixture was incubated for 15min at RT or 37°C, respectively, and 1µl of the TOPO TA Cloning® reaction was transformed into competent DH5α cells as described in 2.2.4.1. Colonies were grown overnight on selective agar plates supplemented with 0.5 mg/ml X-Gal for blue-white-selection. Single white colonies containing the TOPO® vector with inserted PCR product were used for colony PCR. To this end, colonies were picked with a yellow pipette tip, transferred to a selective LB agar plate and grown overnight as a backup at 37°C. Furthermore, the contaminated pipette tip was incubated in 50µl LB medium for 1h at 37°C under rotation. Colony PCR reaction was done as described above using 5µl bacteria culture as template. PCR reactions were loaded on a 1% agarose gel and plasmid preparation was done of colonies showing a band of the correct size. To this end, bacteria suspensions of positive clones were incubated in 3ml LB medium supplemented with 100µg/ml ampicillin overnight at 37°C, 300rpm. Plasmids were prepared using the Pure Yield™ Plasmid Miniprep

System according to the manufacturer's protocol. Afterwards, pGL3 and the TOPO® vector containing the PCR product were digested using the same restriction enzymes (*KpnI* and *SacI* from Thermo Fisher Scientific for cloning of the *DLC1.1* promoter; *KpnI* and *HindIII* from New England Biolabs for cloning of the *DLC1.4* promoter). The reaction setup was as follows:

TOPO_*DLC1.1p*	8µl	TOPO_*DLC1.4p*	8µl	pGL3	1µl
KpnI	0.5µl	*HindIII*	0.5µl	Enzyme 1	1µl
SacI	0.5µl	*KpnI*	0.5µl	Enzyme 2	1µl
10x *BamHI* buffer	1µl	10x NEBuffer *2.1*buffer	1µl	10x buffer	1µl
H_2O	-	H_2O	-	H_2O	6µl

The reaction mix was incubated for 1h at 37°C before heat inactivation for 20min at 65°C. The digestion was loaded on a 1% agarose gel. Inserts and linearized pGL3 were excised and purified using the QIAquick Gel Extraction Kit according to the manufacturer's instructions. Insert and pGL3 were subjected to ligation as follows:

T4 ligase	1µl
T4 buffer	1µl
insert	20ng
pGL3	20ng
H_2O	ad 10µl

The reaction mix was incubated overnight at 11°C and 5µl were used for transformation into competent DH5α bacteria as described in 2.2.4.1. Single colonies were picked using a yellow pipette tip, transferred to a selective LB agar plate and grown as a backup at 37°C overnight. Furthermore, the pipette tip was incubated in 50µl LB medium and incubated for 1h at 37°C under rotation. Colony PCR reaction was performed as previously described. Positive clones were sequenced by GATC service (GATC Biotech AG, Cologne).

2.2.5 Immunochemical methods

2.2.5.1 Immunofluorescence staining of cells

Immunofluorescence staining was performed to determine protein localization. To this end, cells were grown in 6-well plates overnight. The next day, cells were transiently transfected as described in 2.2.1.5 and seeded on sterile glass slides in a new 6-well plate. After overnight incubation, the medium was aspirated and the cells were washed with PBS before fixation with 4% paraformaldehyde (v/v) in PBS for 20min at RT. Cells were washed with PBS for 3x5min followed by blocking with 100% FCS for 30min at RT. Cell permeabilization was performed by adding permeabilization buffer (0.1% Triton® X-100 (v/v) in PBS) for 10min. The cells were washed again with PBS and incubated with primary antibody diluted in antibody dilution buffer (1% FCS (v/v) in PBS) overnight at 4°C in a humidified chamber. All following steps were carried out in the dark. The cells were washed again three times with PBS (HEK293T only once) and fluorescently labeled secondary antibody (1:250) or phalloidin (1:1000) was added in antibody dilution buffer for 1h at RT in a humid chamber. After washing with PBS, DAPI (1:5000 in PBS) was added for 10min to stain the nuclei. Cells were washed again and cover slips were placed upside-down on microscope slides with one drop of fluorescence mounting medium. The samples were stored at 4°C in the dark until fluorescence microscopy analysis. Primary antibody dilutions are listed in the table below.

Table 2.16: Primary antibody dilutions used for immunofluorescence staining of cells.

Antibody	Company	dilution
H. pylori	PD Dr. Roger Vogelmann, Mannheim	1:1000
DLC1 PA5-18290	Thermo Fisher Scientific, Inc., Surrey, UK	1:100

2.2.5.2 Proximity ligation assay (PLA)

PLA was performed for analysis of protein interactions. For this purpose, the Duolink® In Situ Red Starter Kit was used. This method is based on the specific binding of primary antibodies to the proteins of interest and the binding of oligonucleotide-labeled secondary antibodies to the corresponding primary antibody. If the secondary antibodies are in close proximity,

they generate a fluorescent signal by ligation of the oligonucleotides and rolling circle amplification using fluorescently labeled oligonucleotides. Protein interaction is then visualized as single red fluorescent spots.

HEK293T cells were transfected (as described in 2.2.1.5) with deletion series of defined sections of the *cagA* gene in combination with pT_DLC1.1 or pT_DLC1.4 and seeded on cover slips placed in a new 6-well plate after 6h of incubation. The next day, cells were washed once with PBS and fixed for 20min in 4% paraformaldehyde (v/v) in PBS at RT. After washing the cells with PBS for 5min, unspecific antibody binding was blocked by adding blocking solution for 30min at 37°C in a humidified chamber. Permeabilization took place using 0.1% Triton® X-100 in PBS for 10min at RT. Cells were washed once with PBS and incubated with primary antibodies 1:250 in antibody diluent overnight at 4°C in a humidified chamber. Slides were washed twice using 1x Wash Buffer A for 5min and incubated with the secondary oligonucleotide-labeled antibodies in antibody diluent for 1h at 37°C in a humidified chamber. Slides were washed twice with 1x Wash Buffer A for 5min and incubated with ligase solution for 30min at 37°C in a humid chamber. Washing the slides with 1x Wash Buffer A for 2x2min was followed by incubation with amplification polymerase solution for 100min at 37°C in a humid chamber. All following steps were performed in the dark. The slides were washed with 1x Wash Buffer B for 10min and incubated with DAPI (1:5000) or phalloidin (1:500) diluted in 1x Wash Buffer B. Slides were first washed with 1x Wash Buffer B for 10min and then with 0.01x Wash Buffer B for 2min before covering the dried slides with fluorescence mounting medium. Samples were stored at 4°C until fluorescence microscopy. The table below shows the antibodies used.

Table 2.17: Antibodies used for PLA.

construct	Primary antibody	Secondary antibody	company
All CagA constructs	GFP, 11 814 460 001	Mouse MINUS	Roche Diagnostics GmbH, Mannheim, Germany
pT_DLC1.1	DLC1 C-terminal, ab180697	Rabbit PLUS	Abcam plc, Cambridge, UK
pT_DLC1.4	FLAG, ab8112	Rabbit PLUS	Abcam plc, Cambridge, UK

2.2.5.3 Preparation of tissue

Mouse or human tissue samples were fixed in 4% (v/v) paraformaldehyde in PBS at 4°C for 24-48h. The tissue was dehydrated in an autotechnicon, embedded in paraffin and the blocks were stored at room temperature. Before cutting 2-5µm slices using a microtome, the blocks were transferred to -20°C for 1h.

2.2.5.4 Immunofluorescence staining of tissue

Paraffin sections were deparaffinized in Xylol and rehydrated in 96% EtOH, 80% EtOH, 70% EtOH (2x3min each) and dH_2O for 2min. Antigen retrieval was performed using Vectastain antigen unmasking solution (pH 6.0) 1:100 in dH_2O and heating the slides for 10min in the microwave without boiling. After cooling to RT, the slides were washed in dH_2O, PBS and dH_2O (2min each). Unspecific antibody binding was blocked by 100% FCS for 1h at RT and primary antibody or phalloidin (1:1000) was added in antibody diluent (10% FCS, 0.3% Triton® X-100 in PBS). After overnight incubation at 4°C in a humidified chamber, slides were washed in PBS for 3x5min. All following steps were carried out in the dark. Fluorescently labeled secondary antibody was added (1:350 in PBS supplemented with 10% FCS) for 1h at RT in a humidified chamber before washing the samples in PBS for 3x5min. Slides were incubated with DAPI (1:5000 in PBS) for 10min at RT to achieve nucleic staining. After a last washing step in PBS for 3x5min, the tissue sections were covered with one drop of Eukitt medium and a cover slip. Samples were stored at 4°C until fluorescence microscopy. Primary antibody dilutions are listed in the table below.

Table 2.18: Primary antibody dilutions used for immunofluorescence staining of tissue.

Antibody	Company	dilution
ChrA (H-300), sc-13090	Santa Cruz Biotechnology, Inc., Heidelberg, Germany	1:100
DLC1 PA5-18290	Thermo Fisher Scientific, Inc., Surrey, UK	1:150
DLC1 ab180697	Abcam plc, Cambridge, UK	1:100
p38, #9212	Cell Signaling Technology, Inc., Danvers, USA	1:50
Phospho-p38, #4511	Cell Signaling Technology, Inc., Danvers, USA	1:800
p44/42 MAPK, #4695	Cell Signaling Technology, Inc., Danvers, USA	1:100
Phospho-p44/42 MAPK, #9101	Cell Signaling Technology, Inc., Danvers, USA	1:200
RhoA (26C4), sc-418	Santa Cruz Biotechnology, Inc., Heidelberg, Germany	1:150

2.2.5.5 Immunohistochemistry

For immunohistochemical staining with Ki67 (Novus) and C-terminal DLC1 antibody paraffin sections were deparaffinized and antigen retrieval was performed as described in 2.2.5.4. After cooling to RT, the slides were washed in PBS for 3x2min. Afterwards, endogenous peroxidase activity was quenched using 3% (v/v) H_2O_2 in PBS for 20min. Washing the sections 3x2min in PBS was followed by blocking with 5% (v/v) normal goat serum in 1% (w/v) BSA-PBS for 1h in a humidified chamber at RT. Primary antibody was diluted 1:100 in 1% (w/v) BSA in PBS supplemented with 5% (v/v) normal serum and added to the slides for overnight incubation at 4°C in a humidified chamber. Slides were washed 3x2min with PBS, biotinylated secondary antibody was added 1:500 diluted in 1% (w/v) BSA-PBS and incubated for 1h at RT in a humidified chamber. Sections were washed again and ABC-mixture (freshly prepared 30min before use!) was added for incubation for 30min at RT in a humidified chamber. Washing 3x2min in PBS was followed by DAB-staining. Slides were incubated with freshly prepared DAB-solution for 1-7min until the tissue turned brown. Washing with dH_2O for 3x1min stopped the reaction and counterstaining with hematoxylin

for 3sec was performed. The color was washed out under tap water and sections were dehydrated in 70% EtOH, 80% EtOH, 96% EtOH and Xylol (2x3min each) and mounted using Eukitt.

For Ki67 staining using the antibody from BD Biosciences, the Vector® M.O.M.™ Immunodetection Kit was used according to the manufacturer's instructions.

For F4/80 staining, the paraffin sections were deparaffinized as described in 2.2.5.4. Antigen retrieval was performed using 20 µg/ml proteinase K in 10mM Tris/HCl pH8.0 for 15min at RT. After washing 2x2min in dH_2O, endogenous peroxidase activity was blocked using 3% (v/v) H_2O_2 in 1xPBS for 15min at RT. The slides were washed again 2min in 1xPBS, 2min in dH_2O, 2min in 1xPBS and unspecific antigen binding was blocked for 1h at RT in a humidified chamber using blocking solution (1ml 1xPBS, 4 drops of avidin, 50µl normal rabbit serum). Washing the tissue section 3x in 1xPBS was followed by overnight incubation at 4°C with primary antibody solution (1ml 1xPBS, 4 drops of biotin, 50µl normal rabbit serum, 10µl antibody) in a humidified chamber. The next day, the slides were washed 3x in 1xPBS and incubated for 1h at RT with secondary antibody solution (948µl 1xPBS, 50ml normal rabbit serum, 2µl biotinylated secondary antibody) in a humidified chamber. Sections were washed again 3x2min in 1xPBS and ABC-mixture (freshly prepared 30min before use!) was added for incubation for 30min at RT in a humid chamber. Washing 3x2min in dH_2O was followed by DAB-staining. Slides were incubated with freshly prepared DAB-solution for 1-7min until the tissue turned brown. Washing with dH_2O for 3x1min stopped the reaction and counterstaining with hematoxylin for 3sec was performed. The color was washed out under tap water and sections were dehydrated in 70% EtOH, 80% EtOH, 96% EtOH and Xylol (2x3min each) and mounted using Eukitt.

2.2.6 Fluorescence activated cell sorting (FACS)

FACS analysis was performed to determine the ROS status of CagA or DLC1 transfected cells. To this end, the Cellular Reactive Oxygen Species Detection Assay Kit (Deep Red Fluorescence) was used according to the manufacturer's protocol. HEK293T cells were seeded and transfected as described in 2.2.1.5. One day after transfection, the cells were trypsinized and the cell number was adjusted to 500 000 cells/ml. Treatment with tert-butyl hydrogen peroxide (TBHP) served as positive control and occurred at 37°C for 3h while

gentle shaking. The ROS Deep Red fluorescence dye was added 30-60min before measurement and samples were kept in the dark. The dye is cell permeable thereby ensuring analysis of viable cells and reacts with ROS in the cell generating a red fluorescent signal (Ex/Em=650/675nm). FACS analysis occurred by the FACSCanto™ device using the FACSDIVA™ software. The FACS device works via a laser and is able to sort a heterogeneous mixture of fluorescently labeled cells based upon their size, granularity and fluorescent characteristics as a single cell suspension. Dependent on the light scatter, cells can be subdivided into different populations. Forward scatter (FSC) and sideward scatter (SSC) determine size and granularity of the cells. Cell debris and dead cells are usually forward scatter (FSC)-low compared to live cells. This enables a differentiation between dead cells, cell clumps or doublets and viable, single cell events.

2.2.7 Therapy of CEA424-SV40 TAg mice with fasudil

Female CEA424-SV40 TAg mice (two months of age, average body weight 20 g) were used for treatment with fasudil. Fasudil was dissolved in sterile PBS and injected i.p. as a single dose of 10 mg/kg per day. Mice received repetitive injections four times a week over a total time period of four weeks.

2.2.8 PET/CT-imaging

In cooperation with Prof. Wängler (Dept. of Clinical Radiology and Nuclear Medicine (Molecular Imaging and Radiochemistry), Medical Faculty Mannheim of University Heidelberg, Mannheim, Germany), PET/CT-imaging was performed as published (Hinsenkamp et al., 2016).

2.2.9 Statistics

For statistics, the software PRISM GraphPad (version 7.0) was used. Results are means ± standard errors (S.E.) from at least three independent experiments. P-values of 0.05 or less were defined as significant. All tests used were two-tailed.

3 Results

3.1 Characterization of Deleted in liver cancer 1 (DLC1)

3.1.1 Expression analysis of DLC1

For analysis of endogenous *DLC1* expression in human cell lines PCR was performed using specific primers for the N- or C-terminus of *DLC1*. The amplified products were loaded on an agarose gel (Fig. 3.1).

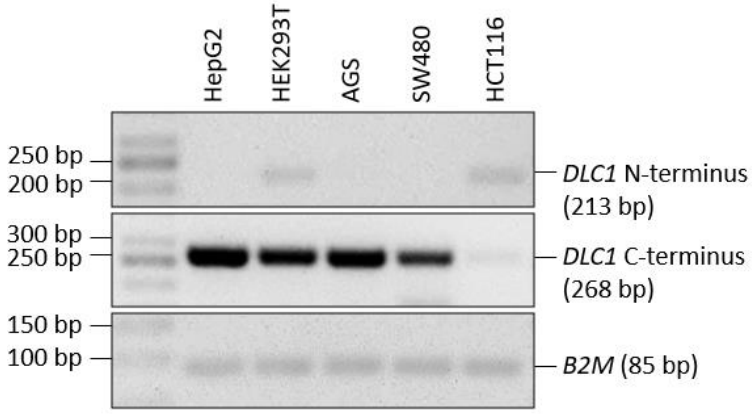

Fig. 3.1: Expression of *DLC1* mRNA variants in human cell lines. Total RNA of all cell lines indicated was isolated, transcribed into cDNA and subjected to PCR for amplification of endogenous N- or C-terminal *DLC1* mRNA. The housekeeper β2-microglobulin (*B2M*) served as control. Amplified products were loaded on an agarose gel (n=1).

The *DLC1* C-terminus was present in all analyzed cell lines showing the lowest expression in HCT116 cells, whereas the *DLC1* N-terminus was only expressed in non-cancer HEK293T cells and HCT116 cells to lesser extent.

To determine endogenous expression of *Dlc1* in WT mouse organs PCR was carried out using mouse specific primers for amplification of N- or C-terminal *Dlc1* mRNA. The amplified products were loaded on an agarose gel (Fig. 3.2).

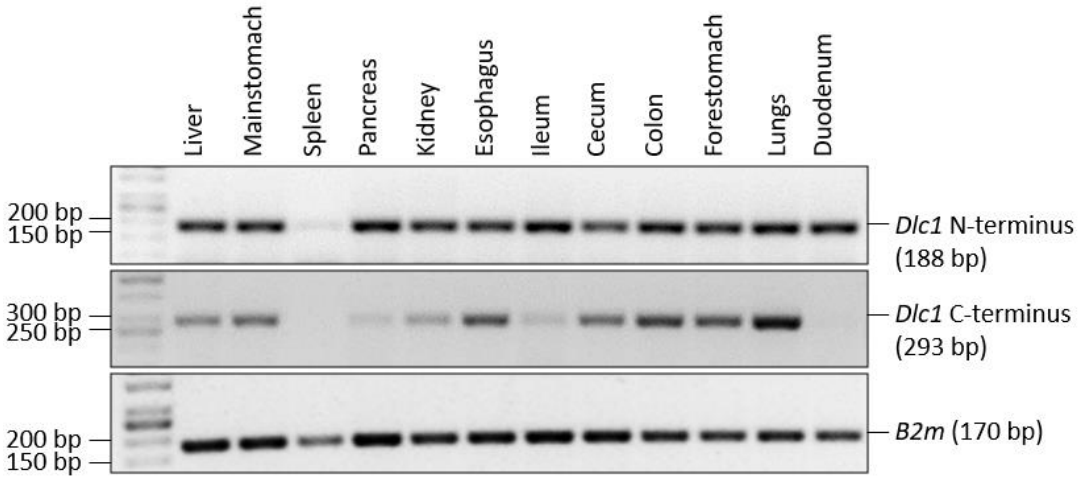

Fig. 3.2: Expression of *Dlc1* mRNA variants in WT mouse organs. Total RNA was isolated of all organs indicated, transcribed into cDNA and subjected to PCR for amplification of endogenous N- or C-terminal *Dlc1* mRNA. The housekeeper β2-microglobulin (*B2m*) served as control. Amplified products were loaded on an agarose gel (n=1).

N-terminal *Dlc1* was expressed ubiquitously in all analyzed organs showing the weakest expression in spleen tissue. Similar results revealed expression analysis of C-terminal *Dlc1*, which was expressed in almost all organs tested, but not in the spleen and duodenum.

Furthermore, N- and C-terminal *DLC1* expression was determined in tumor tissue (TU) and matched normal tissue (NT) of GC patients by PCR. Figure 3.3 shows the amplified products loaded on an agarose gel and quantification of the bands in gel.

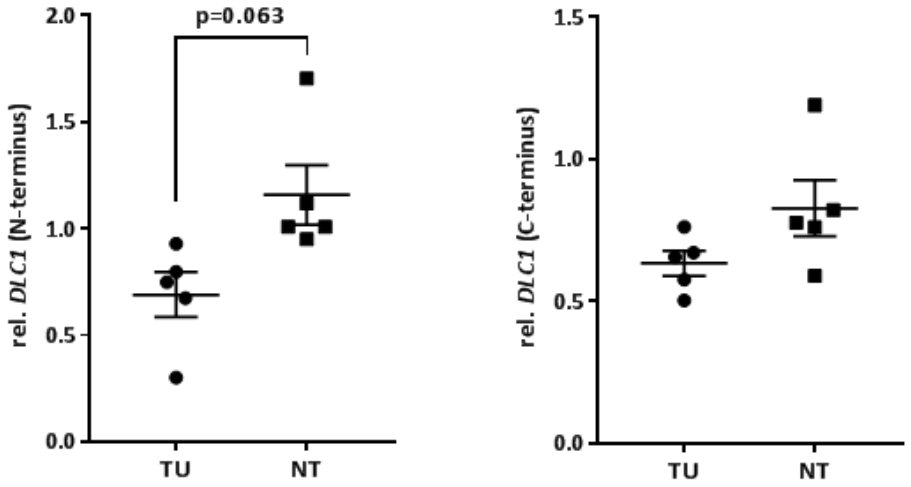

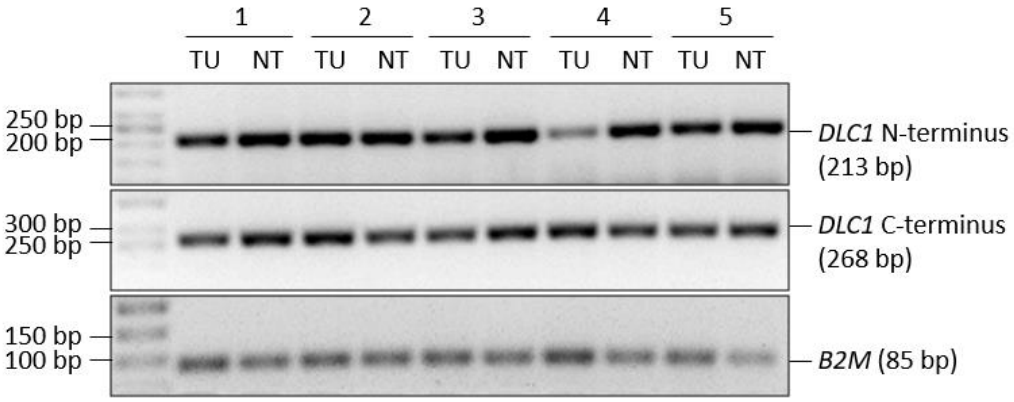

Fig. 3.3: Expression of *DLC1* mRNA variants in tumor tissue (TU) and matched normal tissue (NT) of GC patients. Total RNA of GC patient tissues was isolated, transcribed into cDNA and subjected to PCR for amplification of endogenous N- or C-terminal *DLC1* mRNA. The housekeeper β2-microglobulin (*B2M*) served as control. Agarose gel (lower panel) and quantification of bands in gel (upper panel) is shown; O.D. values were normalized to *B2M* and calculated as -fold ± S.E. (n=5; p=0.063: Wilcoxon matched-pairs signed rank test TU vs. NT).

DLC1 expression was decreased in TU compared with NT. N-terminal *DLC1* expression was reduced by 40% and C-terminal *DLC1* level by 23% in TU compared to NT.

3.1.2 Localization of DLC1

It is known that DLC1 fulfills tumor suppressor functions in epithelial cells (Braun and Olayioye, 2015; Low et al., 2011; Tripathi et al., 2012). To investigate, if DLC1 is also present in other cell types, immunofluorescence co-stainings of formalin-fixed and paraffin embedded mouse and human stomach tissues were performed using antibodies specific for DLC1 and Chromogranin A (Fig. 3.4).

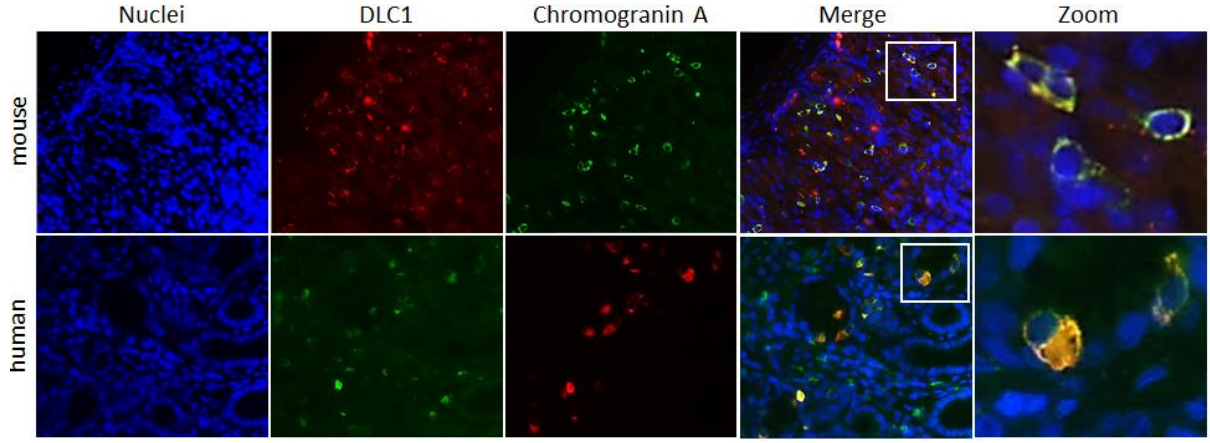

Fig. 3.4: DLC1 is present in mouse and human enterochromaffin-like (ECL) cells. Formalin-fixed and paraffin embedded WT mouse and human stomach tissues were subjected to immunofluorescence co-staining using DLC1 (Thermo Fisher Scientific) and Chromogranin A specific antibodies. Representative pictures of the corpus region are shown. Blue: DAPI/nuclei; for mouse tissue DLC1 was stained in red and Chromogranin A in green; for human tissue DLC1 was stained in green and Chromogranin A in red; n=6 for mouse and n=3 for human tissue; magnification 400x.

Both, mouse and human tissue sections, showed a co-localization of Chromogranin A and DLC1 positive cells visualized by a yellow color in the overlay. Chromogranin A is a marker for enterochromaffin-like (ECL) cells, which are the predominant enteroendocrine cell subtype in the corpus and secrete histamine (Hakanson et al., 1998; Hakanson et al., 1995; Li et al., 2014). These findings indicate that DLC1 is present in human and mouse ECL cells.

3.1.3 The DLC1$^{gt/+}$ mouse model

For further characterization of DLC1 and elucidation of its biological functions, DLC1$^{gt/+}$ mice were kindly provided by Prof. Mowat (Dept. of Biochemistry & Medical Genetics, University of Manitoba, Winnipeg, Canada). A gene trapped embryonic cell line containing an insertion between exon 1 and 2 of isoform 2 transcript was used for generation of a transgenic mouse resulting in a reduced expression of DLC1 isoform 2. Other *Dlc1* transcripts were not affected. Mice were heterozygously gene trapped, because homozygous gene trap leads to embryonic lethality. Heterozygous gene trapped adult mice do not show any physical or behavioral defects and they do not develop any spontaneous tumors. Embryonic cells show an increased RHOA activity, cytoskeletal changes and increased cell migration (Sabbir et al., 2012; Sabbir et al., 2010). Hence, these mice represent an appropriate model for the investigation of the role of DLC1 as a tumor suppressor and inhibitor of RHOA in *Helicobacter*-related gastric disease.

3.1.3.1 Confirmation of DLC1 gene trap

For confirmation of a successful gene trap of DLC1$^{gt/+}$ mice, Western Blot analysis was performed. For this purpose, total protein was isolated from liver tissue of WT and DLC1$^{gt/+}$ mice. DLC1 was detected using a C-terminal specific antibody (Fig. 3.5).

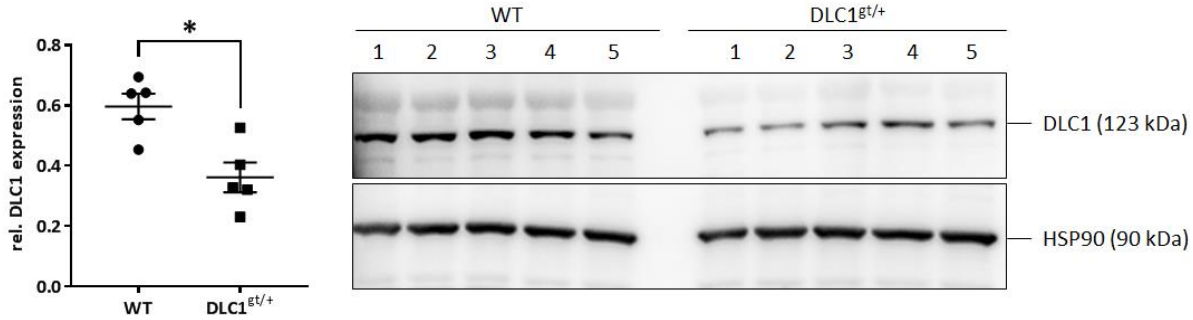

Fig. 3.5: Expression of DLC1 protein is reduced in liver tissue of DLC1$^{gt/+}$ mice compared to WT mice. Total protein was isolated from liver tissue of WT and DLC1$^{gt/+}$ mice using RIPA buffer and subjected to Western Blot analysis. DLC1 was detected by a C-terminal specific antibody. HSP90 served as control. O.D. values of bands in gels were normalized to HSP90 and calculated as -fold ± S.E. (n=5 mice per group; *p<0.05: unpaired t-test WT vs. DLC1$^{gt/+}$). Quantitative analysis (left panel) and gels (right panel) are shown.

The Western Blot analysis revealed a significantly reduced DLC1 level in liver tissue of DLC1$^{gt/+}$ mice compared to WT mice.

For further confirmation of the gene trap, immunofluorescence staining of WT and DLC1$^{gt/+}$ mouse stomach tissue was performed using the identical C-terminal DLC1 specific antibody as for Western Blot analysis (Fig. 3.6).

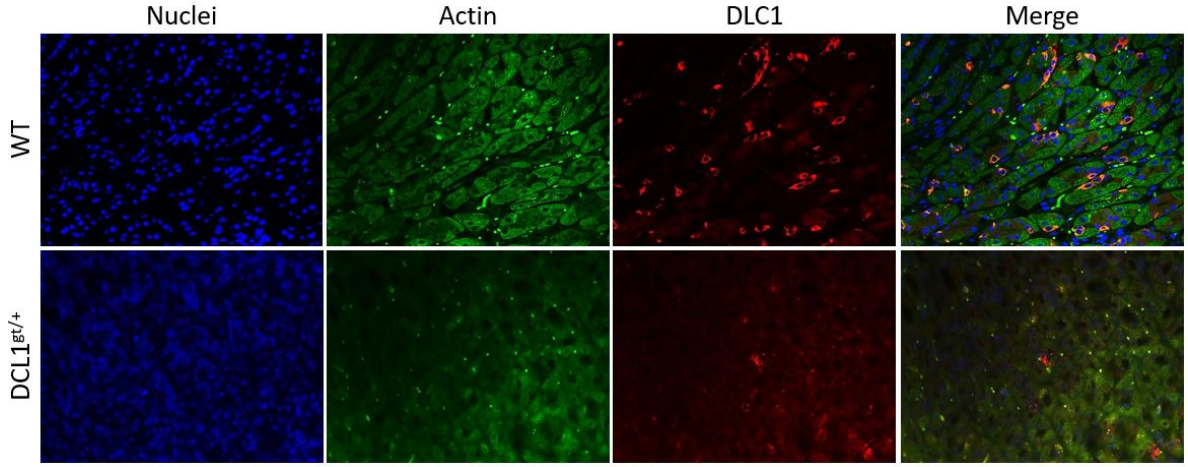

Fig. 3.6: DLC1$^{gt/+}$ mice show less positive gastric immunofluorescent staining of DLC1 compared to WT mice. Paraffin embedded WT and DLC1$^{gt/+}$ mouse stomach tissues were subjected to immunofluorescence staining. Representative pictures of the corpus region are shown. Blue: DAPI/nuclei; green: actin; red: DLC1; n=6; magnification 400x.

The immunofluorescence staining demonstrated a reduced gastric DLC1 expression in DLC1$^{gt/+}$ mice compared to WT mice.

In addition, WT and DLC1$^{gt/+}$ mouse stomach tissues were subjected to immunohistochemical staining using the C-terminal DLC1 specific antibody. The results are shown in Figure 3.7.

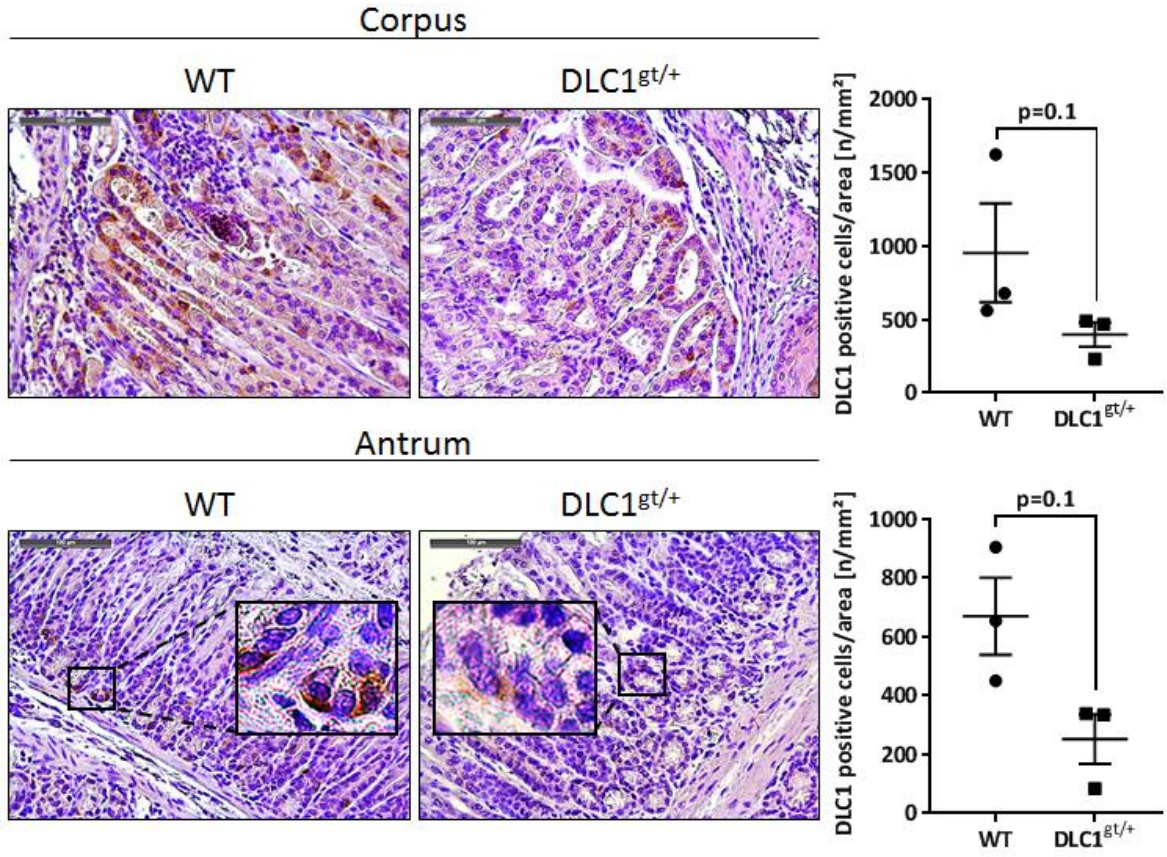

Fig. 3.7: DLC1$^{gt/+}$ mice show less positive gastric immunohistochemical staining of DLC1 compared with WT mice. Paraffin embedded WT and DLC1$^{gt/+}$ mouse stomach tissues were subjected to immunohistochemical staining using a C-terminal DLC1 specific antibody. Representative pictures of the corpus and antrum region are shown. Three pictures per individual were analyzed and positive cells of five anatomical structures per picture were quantified as means ± S.E. (n=3 mice per group; p=0.1: Mann Whitney *U* test WT vs. DLC1$^{gt/+}$; magnification 200x).

Figure 3.7 illustrates a reduction of the amount of DLC1 positive cells in the corpus and antrum by 60% in DLC1$^{gt/+}$ mice compared to WT mice. Parietal cells of the corpus showed unspecific staining.

In summary, section 3.1.3.1 verifies a successful heterozygous gene trap. The C-terminal DLC1 specific antibody still detects the remaining *DLC1* transcripts resulting in a reduced DLC1 detection in DLC1$^{gt/+}$ mice compared with WT mice.

3.1.3.2 Microscopic analysis

The DLC1 mutant mice were bred for up to one year. After this time, the stomach was removed, fixed in formalin, embedded in paraffin and subjected to Hematoxylin/Eosin (H&E) staining for microscopic analysis. Representative pictures are shown in Figure 3.8.

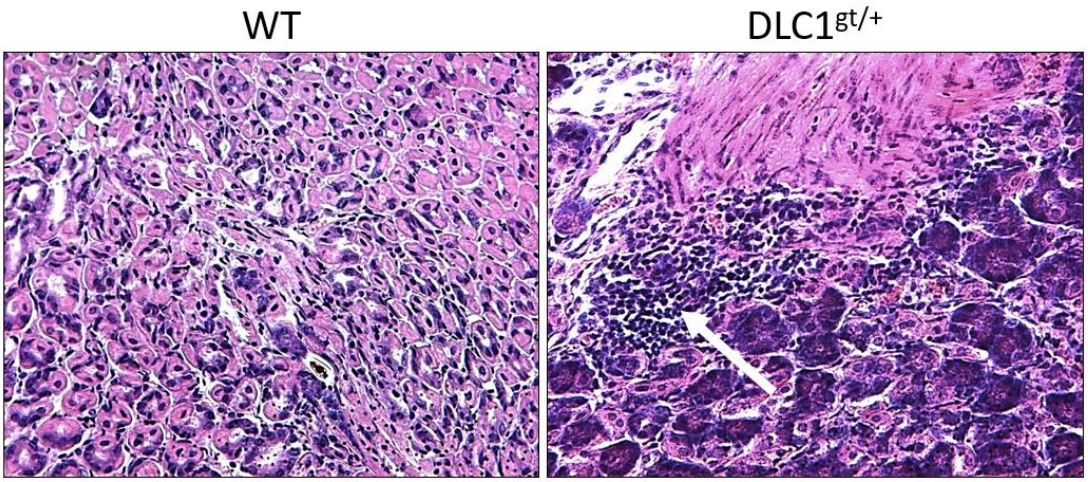

Fig. 3.8: DLC1$^{gt/+}$ mice show an increased infiltration of inflammatory cells in the stomach. Paraffin embedded WT and DLC1$^{gt/+}$ mouse stomach tissues were subjected to H&E staining. The white arrow indicates increased inflammatory cell infiltration. Representative pictures of the corpus region are shown; magnification 400x.

The microscopic analysis revealed an increased infiltration of inflammatory cells in the corpus region of DLC1$^{gt/+}$ stomachs compared to WT mice. Statistical analysis will be subject of an upcoming project in the author's group.

3.1.3.3 Immunohistochemical analysis

Since DLC1$^{gt/+}$ mice showed an increased inflammatory infiltration, the inflammatory cells were characterized in more detail by immunohistochemical staining using the F4/80 antibody, which is a characteristic surface marker for macrophages. Macrophages play a key role during immune response by eliminating pathogens via phagocytosis and regulating adaptive immunity (Wilson and Crabtree, 2007). In addition, differences in cell proliferation between DLC1$^{gt/+}$ and WT mice were analyzed by Ki67 staining (Fig. 3.9).

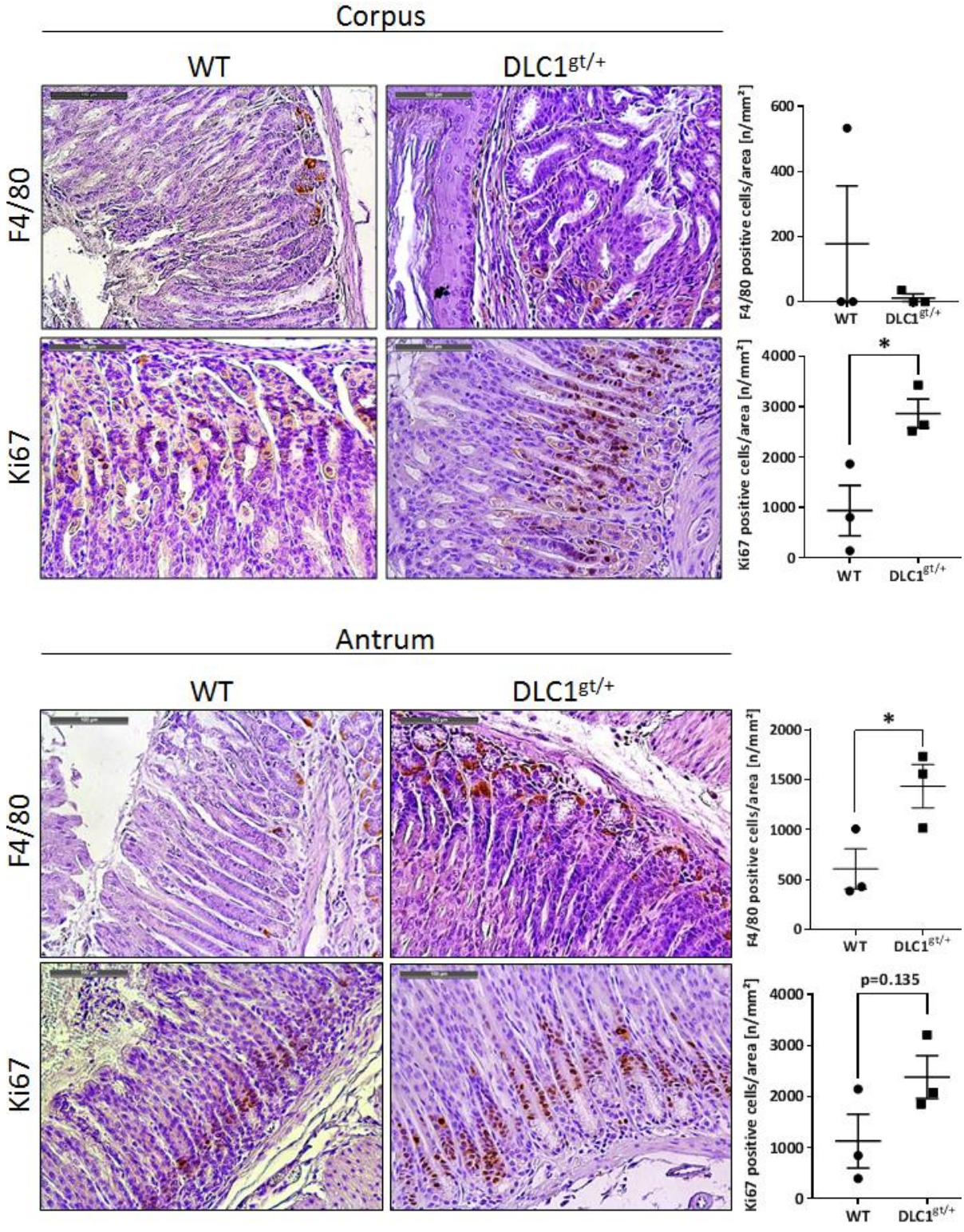

Fig. 3.9: DLC1$^{gt/+}$ mice show increased cell proliferation and infiltration of macrophages in gastric tissue compared with WT mice. Paraffin embedded WT and DLC1$^{gt/+}$ mouse stomach tissues were subjected to F4/80 and Ki67 immunohistochemical staining. Representative pictures of the corpus and antrum region are shown. Three to five pictures per individual were analyzed and positive cells of five anatomical structures per picture were quantified as means ± S.E. (n=3 mice per group; *p<0.05: unpaired t-test WT vs. DLC1$^{gt/+}$; magnification 200x).

There was nearly no macrophage staining of the corpus, but F4/80 staining of the antrum revealed a significantly increased infiltration in DLC1$^{gt/+}$ mice compared to WT mice. The Ki67 staining was three times stronger in the corpus of DLC1$^{gt/+}$ mice in comparison to WT mice. Antral staining of Ki67 was increased 2-fold in DLC1$^{gt/+}$ compared with WT mice. Parietal cells of the corpus showed unspecific staining.

3.1.3.4 Analysis of the immune cell profile

For further analysis and characterization of the inflammatory infiltration and, thus, the immune response in DLC1$^{gt/+}$ mice, RT-qPCR was performed using primers for different markers of immune cells and cytokines. Table 3.1 specifies the chosen markers and figure 3.10 shows the results of RT-qPCR. Corresponding melting curves are presented by figure 7.1 (appendices).

Table 3.1: Overview of the genes encoding markers for immune cells and cytokines analyzed by RT-qPCR in WT and DLC1$^{gt/+}$ mice.

Immune cell marker/cytokine	Gene	Producing cell type/function	reference
CD4	*Cd4*	Surface marker of T_h cells.	(Buchholz et al., 2016; Famili et al., 2017)
CD8	*Cd8*	Surface marker of T_c cells.	(Famili et al., 2017)
FOXP3	*Foxp3*	Specific transcription factor for T_{reg} cells. FOXP3 binds RORγt to inhibit T_h17 and enforce T_{reg} development.	(Fasching et al., 2017; Li et al., 2015)
GATA3	*Gata3*	T cell specific transcription factor.	(Famili et al., 2017)
RORγt	*Rorc*	Specific transcription factor for T_h17 cells.	(Fasching et al., 2017)
iNOS	*iNOS*	Specific marker of M1 macrophages. M1 macrophages act cytotoxic and pro-inflammatory and secrete IFNγ.	(Eapen et al., 2017)
ARG1	*Arg1*	Specific marker of M2 macrophages. M2 macrophages act anti-inflammatory, and secrete IL-4, -10 and -13.	(Aras and Zaidi, 2017; Caux et al., 2016; Eapen et al., 2017)
IFNγ	*Ifng*	Cytokine produced by T_h1 cells; recruits macrophages and natural killer cells.	(Parkin and Cohen, 2001; Wilson and Crabtree, 2007)

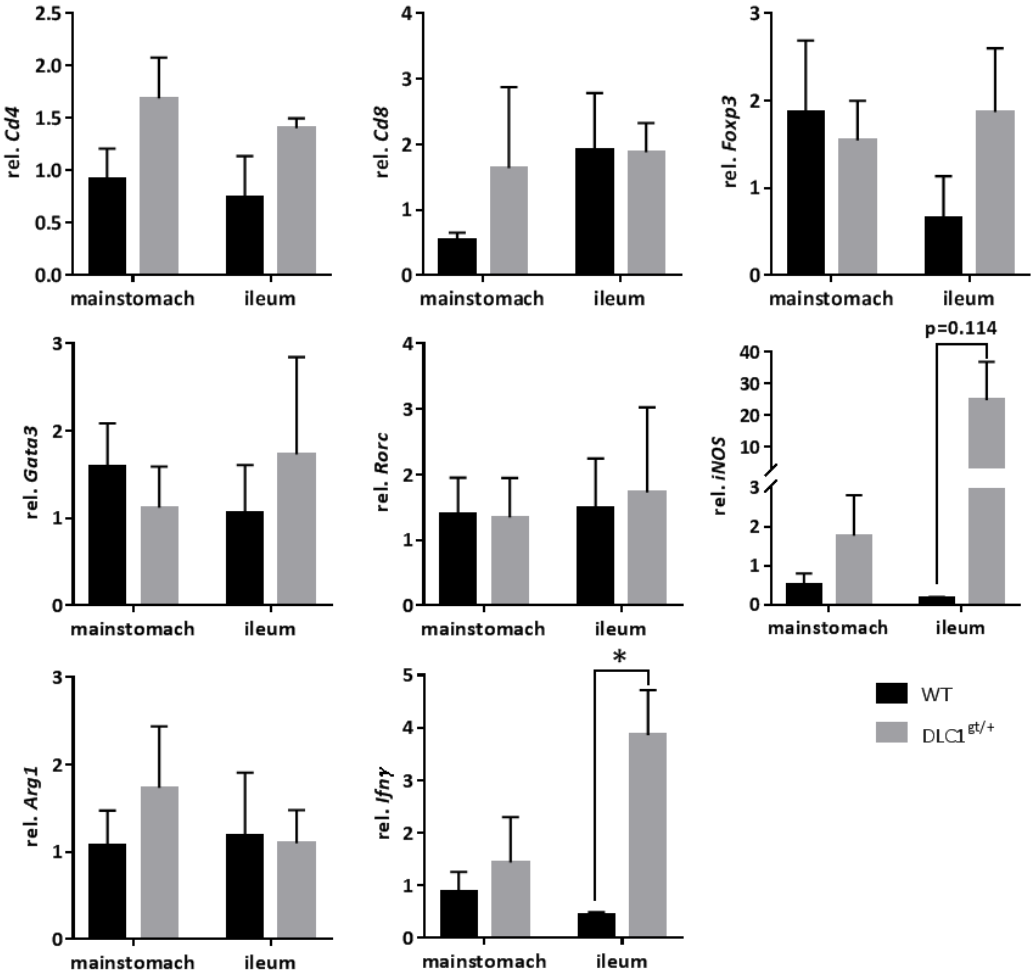

Fig. 3.10: Expression of surface markers of immune cells and cytokines in DLC1$^{gt/+}$ mice compared with WT mice. Total RNA was extracted from the mainstomach and ileum of WT and DLC1$^{gt/+}$ mice and subjected to RT-qPCR analysis after reverse transcription. CT-values were normalized to β2-microglobulin (*β2m*) and calculated as -fold ± S.E. (n=3 mice per group; *p<0.05: unpaired t-test WT vs. DLC1$^{gt/+}$).

DLC1$^{gt/+}$ mice showed a 2-fold increased gastric and ileal *Cd4* expression compared to WT mice. *Cd8* expression was elevated 3-fold in mainstomachs of DLC1$^{gt/+}$ mice but showed no ileal difference. There was a decrease of gastric *Foxp3* expression by 17% in DLC1$^{gt/+}$, whereas ileal *Foxp3* level was increased 3-fold in DLC1$^{gt/+}$ mice in comparison to WT mice. Expression of *Gata3* was reduced to 70% in DLC1$^{gt/+}$ mainstomachs, but elevated 1.6-fold in DLC1$^{gt/+}$ ileum compared with WT mice. *Rorc* showed no difference between DLC1$^{gt/+}$ and WT mice, but gastric *iNOS* was increased 3-fold and ileal *iNOS* level was 100-times elevated in DLC1$^{gt/+}$ mice in comparison to WT mice. Expression of *Arg1* was increased 1.6-fold in the mainstomach of DLC1$^{gt/+}$ mice compared with WT mice but showed no ileal difference. Furthermore, there was 1.6-fold elevated gastric *Ifnγ* expression and significantly increased

expression of *Ifnγ* in the ileum of DLC1$^{gt/+}$ mice compared with ileal *Ifnγ* level of WT mice (9-fold).

3.1.3.5 Analysis of the hormone profile

Since DLC1 was present in neuroendocrine ECL cells (see 3.1.2), the hormone profile of DLC1$^{gt/+}$ mice was analyzed in detail by performing expression analysis of diverse gastric hormones and proteins involved in hormone balance and gastric acid secretion via RT-qPCR. Table 3.2 specifies the analyzed proteins, figure 3.11 shows the results of the RT-qPCR. Corresponding melting curves are presented by figure 7.2 (appendices).

Table 3.2: Overview of proteins involved in hormone balance and gastric acid secretion analyzed by RT-qPCR in WT and DLC1$^{gt/+}$ mice.

Protein/hormone	Gene	Producing cell type/function	reference
Adiponectin	*Adipoq*	Produced by adipocytes.	(Mueller et al., 2003)
Chromogranin A	*Chga*	Produced by histamine-secreting enterochromaffin-like (ECL) cells; precursor to a series of peptides.	(Al-Risi et al., 2017; Hakanson et al., 1998; Li et al., 2014)
Ghrelin	*Ghrl*	Produced by oxyntic glands; increases acid secretion.	(Blaser and Atherton, 2004)
Histidine decarboxylase	*Hdc*	Produced by ECL cells; key enzyme in histamine synthesis; histamine modulates gastric acid secretion.	(Mueller et al., 2003)
H^+K^+-ATPase	*Atp4*	Expressed by acid secreting parietal cells.	(Malfertheiner, 2011)
Intrinsic factor	*Gif*	Produced by parietal cells; important for vitamin B_{12} absorption.	(Shum et al., 1971)
Pepsinogen C	*Pgc*	Produced by chief cells; proenzyme of pepsin; marker for atrophic changes.	(Cho et al., 2017)
Somatostatin	*Sst*	Produced by D cells; suppresses gastrin secretion.	(Blaser and Atherton, 2004; Malfertheiner, 2011)
Tryptophan hydroxylase	*Tph1*	Localized in ECL cells; involved in serotonin synthesis.	(Gershon, 2013)

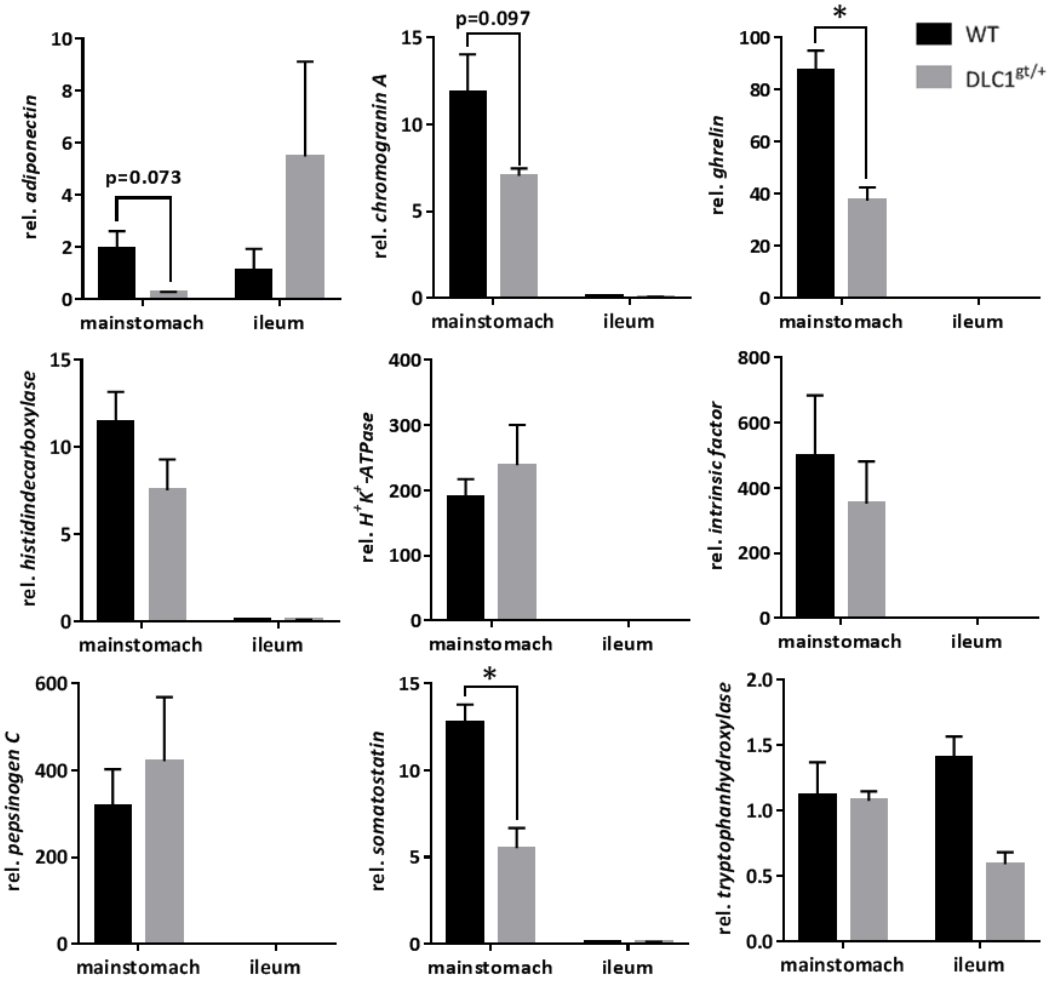

Fig. 3.11: Expression of proteins involved in hormone balance and gastric acid secretion in DLC1$^{gt/+}$ mice compared with WT mice. Total RNA was extracted from the mainstomach and ileum of WT and DLC1$^{gt/+}$ mice and subjected to RT-qPCR analysis after reverse transcription. CT-values were normalized to β2-microglobulin (*β2m*) and calculated as -fold ± S.E. (n=3 mice per group; *p<0.05: unpaired t-test WT vs. DLC1$^{gt/+}$).

The gastric *adiponectin* level was decreased to 13% in DLC1$^{gt/+}$ mice, whereas it showed a 5-fold increased expression level in the ileum of DLC1$^{gt/+}$ mice compared to WT mice. *Chromogranin A* expression was reduced by 40% in the mainstomach of DLC1$^{gt/+}$ mice. Gastric *ghrelin* and *somatostatin* level was significantly decreased by 60% in DLC1$^{gt/+}$ mice compared with WT mice. Expression of *histidine decarboxylase* and *intrinsic factor* was reduced by 30% in the mainstomach of DLC1$^{gt/+}$ mice, whereas the gastric level of *H$^+$K$^+$-ATPase* and *pepsinogen C* was elevated by 25%. Gastric *tryptophan hydroxylase* level showed no difference, but ileal expression was reduced by 40% in DLC1$^{gt/+}$ mice.

The findings from characterization of DLC1 suggest a ubiquitous expression of the tumor suppressor in all organs and a downregulation in tumors. Besides its localization in epithelial cells, DLC1 is additionally expressed by neuroendocrine cells thereby showing an involvement in hormonal balance and gastric acid secretion. Furthermore, microscopic analysis of H&E stained DLC1$^{gt/+}$ mice stomachs and RT-qPCR data suggest a role of DLC1 in the regulation of the immune response.

3.2 Antagonism between DLC1 and CagA

3.2.1 Interaction analysis of DLC1 and CagA

Hitkova et al. showed that CAV1 recruits DLC1 in case of *H. pylori*-infection to potentiate the tumor suppressor functions (Hitkova et al., 2013). Different DLC1 and CagA constructs were used for investigation of a direct interaction between DLC1 and the *Helicobacter* toxin CagA as well as the identification of interaction domains. The DLC1 constructs include the human full length DLC1.1 and truncated DLC1.4 without SAM domain. For CagA, deletion series of defined sections of the *cagA* gene were used including the full length wild type CagA, two C-terminal constructs (CagA_838-1216 and CagA_1029-1216) and one N-terminal mutant (CagA_1-877). The constructs CagA_1029-1216 and CagA_1-877 did not contain any EPIYA motifs and multimerization domains. DLC1 constructs contain a FLAG tag and CagA mutants were GFP-fused. All constructs used were verified by Western Blot analysis and immunofluorescence microscopy and are represented by figure 3.12.

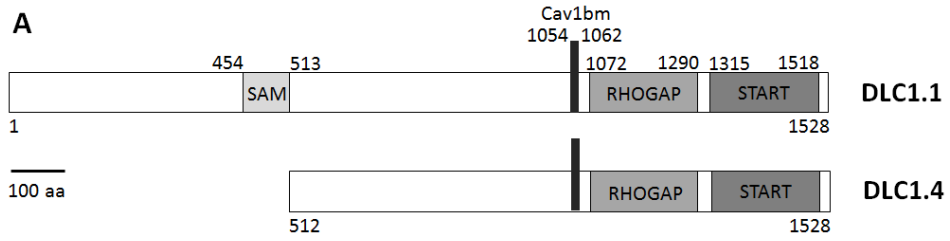

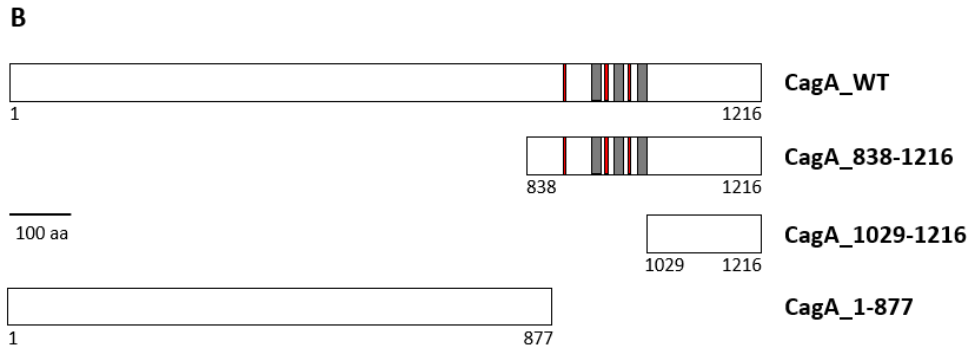

Fig. 3.12: DLC1 and CagA constructs used for interaction analyses of the two proteins. A: DLC1 constructs used in this study. SAM: sterile α motif; RHOGAP: catalytic domain for inhibition of RHO; START: StAR-related lipid-transfer domain; Cav1bm: CAV1 binding motif. **B:** CagA constructs used in this study. Red: EPIYA motif; grey: multimerization domain. All schemes drawn to scale.

3.2.1.1 Co-immunoprecipitation

For analysis of an interaction between DLC1 and CagA, Co-immunoprecipitations (CoIPs) were performed. To this end, HEK293T cells were transiently transfected with CagA_WT, CagA_838-1216 (CT) or CagA_1-877 (NT) in combination with the DLC1 constructs. Immunoprecipitation was performed via DLC1 and CagA specific antibodies and precipitates were subjected to Western Blot analysis by use of the same antibodies in a reciprocal manner. Total cell lysates of transfected cells served as controls for successful transfection (Input). Figure 3.13 shows the CoIP experiment for the investigation of a complex formation between CagA_WT and DLC1.

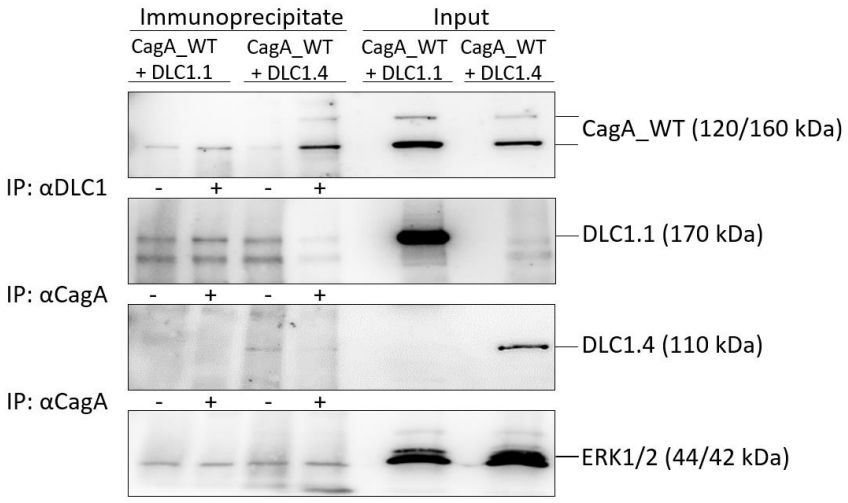

Fig. 3.13: CagA_WT interacts with both DLC1 isoforms. HEK293T cells were transiently transfected with CagA_WT in combination with DLC1.1 or DLC1.4, respectively. Cytosolic lysates were prepared by hypotonic lysis (Input). For immunoprecipitation (IP) CagA- and DLC1-specific antibodies were used, for immunoblot the same antibodies were used in a reciprocal manner.

The CoIP for CagA_WT and DLC1 suggests an interaction between CagA_WT and both DLC1 isoforms, represented by CagA protein in the DLC1.1 and DLC1.4 immunoprecipitates. Interaction between CagA_WT and DLC1.4 seems stronger compared with DLC1.1. Only low amounts of DLC1.4 were co-immunoprecipitated. The bands of the DLC1.1 immunoblot may be unspecific products, although transfection was successful as represented by the input control. This can be explained by conformational changes of DLC1.1 due to complex formation.

Figure 3.14 shows the CoIP experiment for investigation of a complex formation between CagA_1-877 (NT) and DLC1.

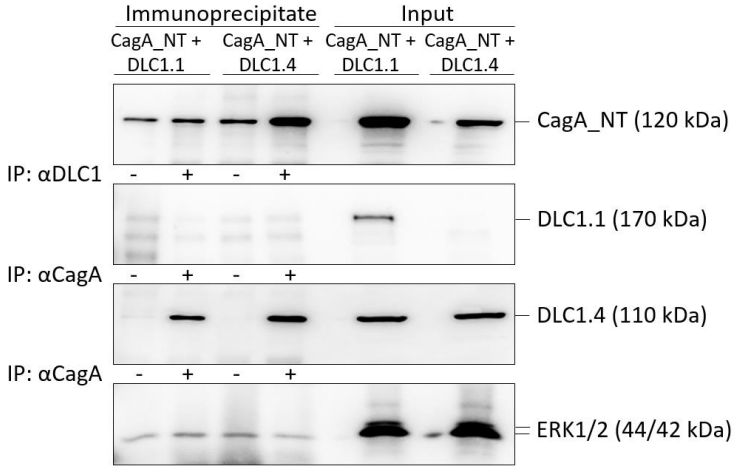

Fig. 3.14: CagA_1-877 interacts with both DLC1 isoforms. HEK293T cells were transiently transfected with CagA_1-877 (NT) in combination with DLC1.1 or DLC1.4, respectively. Cytosolic lysates were prepared by hypotonic lysis (Input). For immunoprecipitation (IP) CagA- and DLC1-specific antibodies were used, for immunoblot the same antibodies were used in a reciprocal manner.

The CoIP for analysis of a complex formation between CagA_1-877 and DLC1 suggests an interaction between CagA_1-877 and both DLC1 isoforms, represented by CagA_1-877 protein in DLC1.1 and DLC1.4 immunoprecipitates. Interaction between the N-terminal CagA construct and DLC1.4 seems stronger compared to the interaction with DLC1.1. Co-immunoprecipitated DLC1.4 confirmed an interaction between CagA_1-877 and DLC1.4.

There was also a band for the DLC1.1 immunoprecipitate in case of DLC1.4 detection, which can be explained by a putative proteolysis of the DLC1.1 protein. The DLC1.1 immunoblot shows successful transfection by the input controls, but bands suggesting a complex formation with CagA_1-877 were unspecific possibly due to conformational changes. There was a general problem of unspecific precipitates.

Furthermore, CoIP experiments were performed for the analysis of an interaction between CagA_838-1216 (CT) and DLC1 (Fig. 3.15).

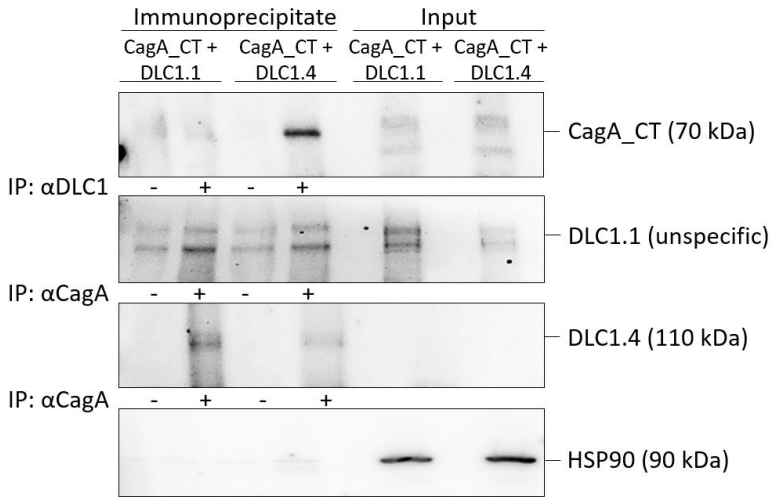

Fig. 3.15: CagA_838-1216 interacts mainly with DLC1.4. HEK293T cells were transiently transfected with CagA_838-1216 (CT) in combination with DLC1.1 or DLC1.4, respectively. Cytosolic lysates were prepared by hypotonic lysis (Input). For immunoprecipitation (IP) CagA- and DLC1-specific antibodies were used, for immunoblot (IB) the same antibodies were used in a reciprocal manner.

Figure 3.15 shows an interaction between CagA_838-1216 and DLC1.4 represented by co-immunoprecipitated DLC1.4 using CagA-specific antibody for CagA_838-1216 and co-immunoprecipitated CagA_838-1216 using the DLC1.4-specific antibody. Once more, a band for the DLC1.1 immunoprecipitate was observed in case of DLC1.4 detection, which can be explained by a proteolysis of DLC1.1. The DLC1.1 immunoblot revealed unspecific bands.

3.2.1.2 Proximity ligation assay

Due to poor reproducibility of the CoIP experiments, proximity ligation assay (PLA) was performed for each CagA/DLC1 construct combination shown by figure 3.16. To this end, HEK293T cells were transiently transfected with one of the CagA constructs in combination with DLC1.1 or DLC1.4, respectively. Overexpressed DLC1 was detected by DLC1 specific antibodies and CagA was detected by GFP fusion. Oligonucleotide-labeled secondary antibodies generated a red fluorescent signal only if CagA and DLC1 were in close proximity, indicating a complex formation.

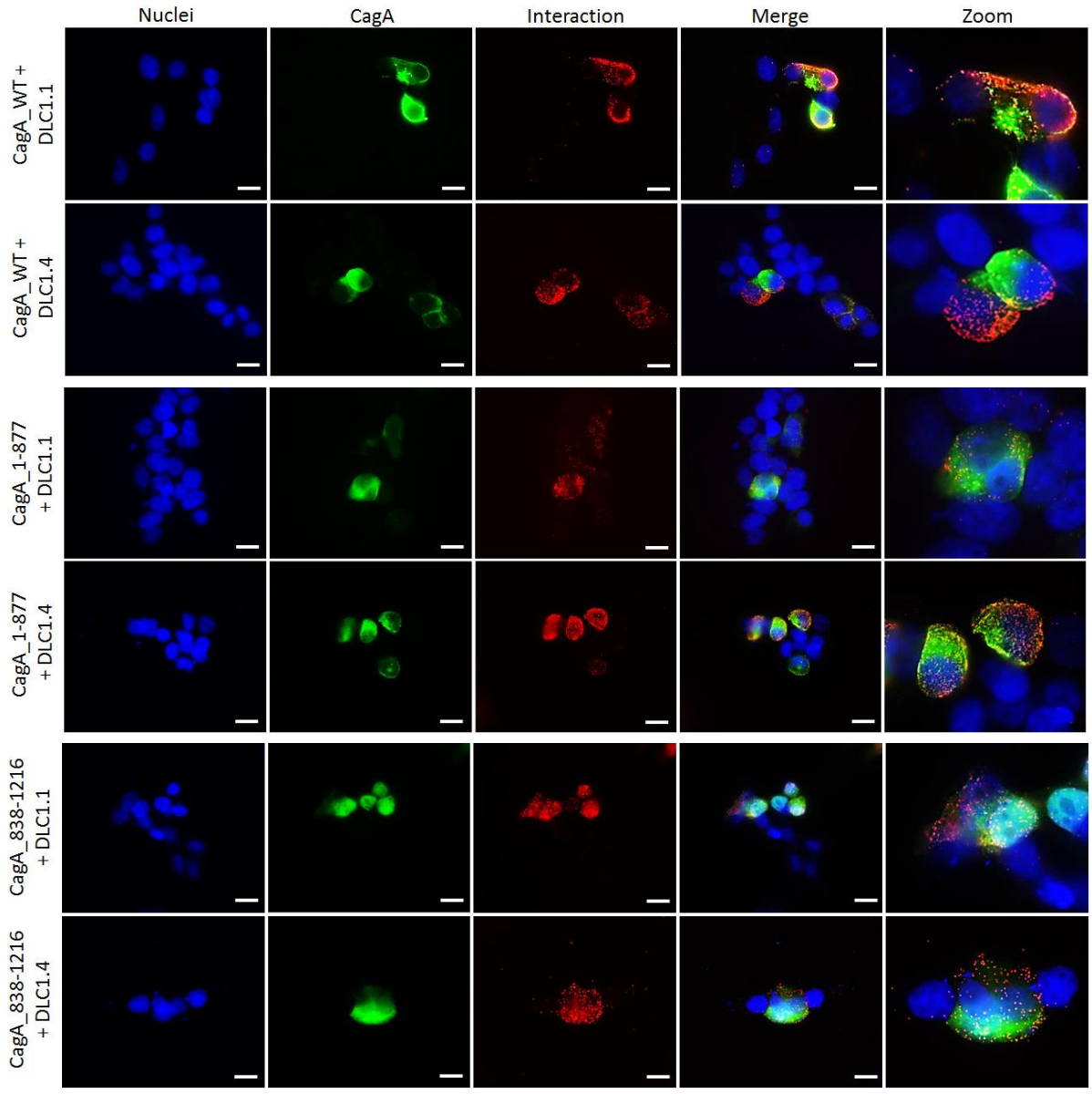

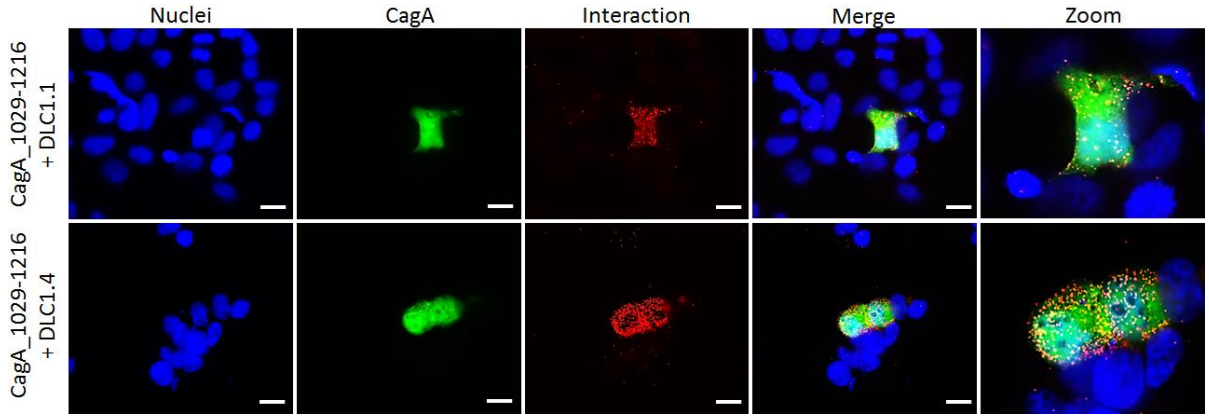

Fig. 3.16: All tested CagA constructs interact with both DLC1 isoforms. HEK293T cells were transiently transfected with CagA_WT, CagA_1-877, CagA_838-1216 or CagA_1029-1216 in combination with DLC1.1 or DLC1.4, respectively. Proximity ligation assay (PLA) was performed. Representative pictures are shown. Blue: DAPI/nuclei; green: CagA (GFP); red dots: interaction; n=3; scale bar=10 µm.

PLA results revealed an interaction between all CagA constructs tested and both DLC1 isoforms visualized by red fluorescent spots exclusively in the area of CagA positive cells.

Summarized, the interaction studies suggest a complex formation between CagA and DLC1. Both, the N-terminus and C-terminus of CagA seem to be important for this interaction. CoIP experiments indicate a stronger interaction between CagA and DLC1.4 compared with DLC1.1.

3.2.1.3 Transcriptional regulation of DLC1 by CagA

DLC1 is a tumor suppressor frequently downregulated or even lost in many human cancer entities. This can be due to genetic or epigenetic mechanisms (Durkin et al., 2007; Ko and Ping Yam, 2014). Hitkova et al. showed that the tumor suppressor CAV1 was transcriptionally downregulated by *H. pylori* (Hitkova et al., 2013). The promoter of both DLC1 isoforms were cloned into the luciferase reporter plasmid pGL3 (pGL3_*DLC1.1p* and pGL3_*DLC1.4p*) to investigate if this holds true for DLC1. Thus, luciferase activity was under control of the *DLC1* promoter (*DLC1p*). *DLC1* promoter activity was analyzed by luciferase activity assay. For this purpose, cells were transiently transfected with or without CagA in combination with one of the *DLC1p* reporter plasmids. Figure 3.17 shows the results of the luciferase activity assays in HEK293T, AGS and NCI-N87 cells.

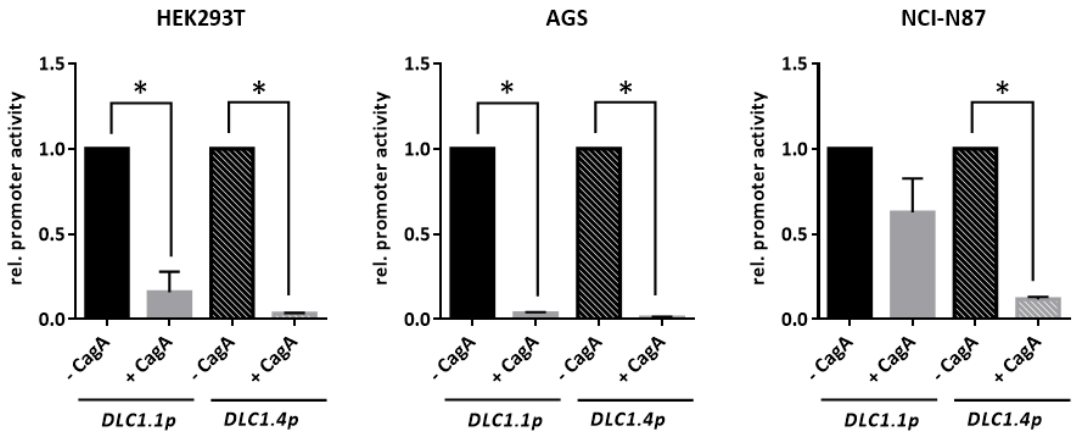

Fig. 3.17: CagA inhibits promoter activity of both DLC1 isoforms. HEK293T, AGS and NCI-N87 cells were transiently transfected with or without CagA in addition to the *DLC1p* reporter plasmids (pGL3_*DLC1.1p* or pGL3_*DLC1.4p*). Luciferase activity was measured by luciferase assay, normalized to protein concentration and calculated as -fold ± S.E. (n=3 per cell line; *p<0.05: one sample t-test -CagA vs. +CagA).

The luciferase activity assays revealed a significant inhibition of *DLC1* promoter activity by CagA. For HEK293T cells, there was a decrease in the activity of both *DLC1* promoters by up to 97% in case of CagA transfection. For AGS cells, both *DLC1* promoters were inhibited by CagA up to 1% of activity. NCI-N87 cells showed still 62% of *DLC1.1* promoter activity for CagA transfection, but *DLC1.4* promoter activity was significantly inhibited to 12% by CagA.

These results demonstrate an efficient inhibition of DLC1 by *H. pylori* CagA on a transcriptional level.

3.2.2 Influence of DLC1 and CagA on cell morphology

Since DLC1 interacts with components of the focal adhesions (Blaser and Atherton, 2004), and CagA is responsible for the formation of actin stress fibers (“hummingbird phenotype”) (Braun and Olayioye, 2015), the cell morphologies of DLC1 and CagA transfected cells were analyzed in detail. For this purpose, AGS and HEK293T cells were transiently transfected with CagA or a combination of CagA and DLC1.1 and subjected to immunofluorescence staining (Fig. 3.18).

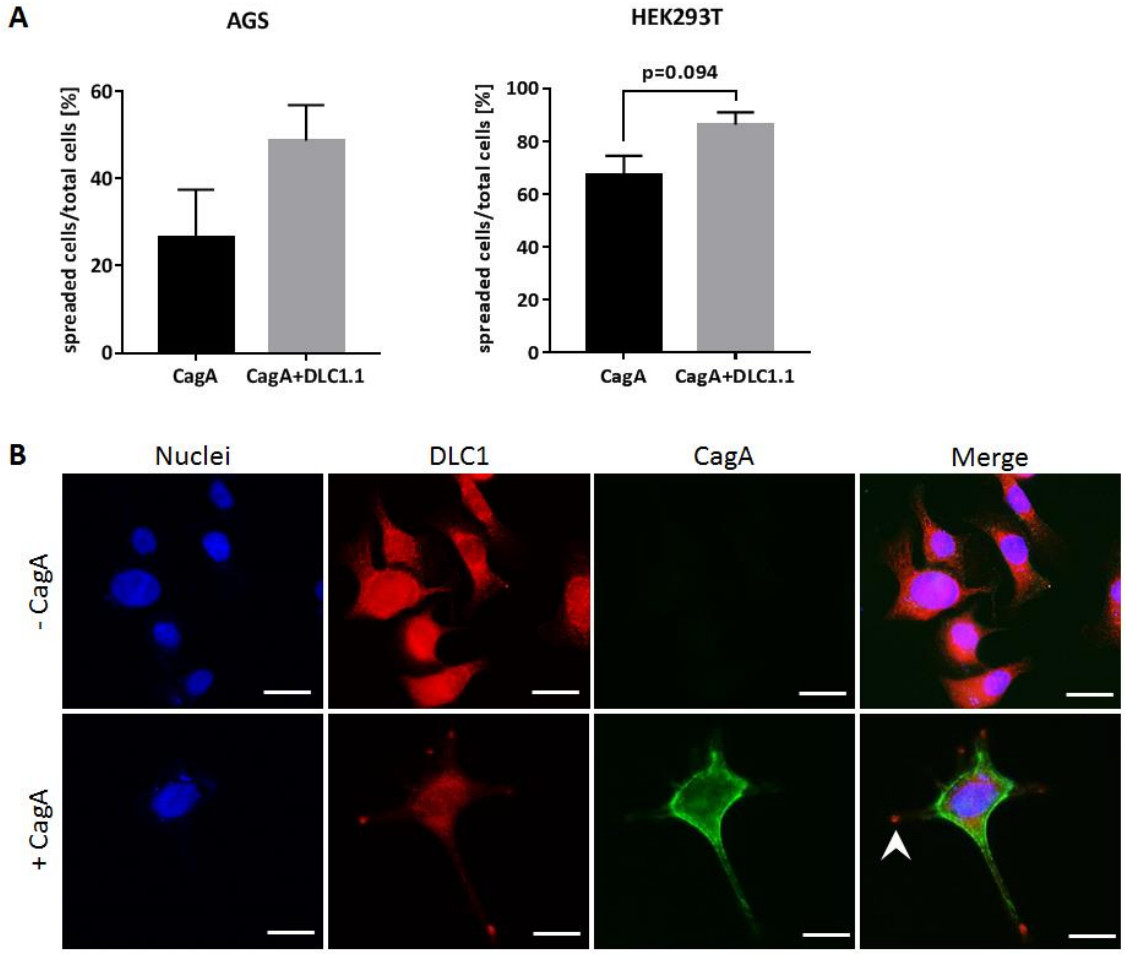

Fig. 3.18: DLC1.1 is responsible for cell spreading and is localized to focal adhesions, whereas CagA promotes cell elongation. A: AGS and HEK293T cells were transiently transfected with CagA or a combination of CagA with DLC1.1 and subjected to immunofluorescence staining. The number of spread cells was counted, normalized to the number of total cells and calculated as means ± S.E. (n=3 per cell line, p=0.094: unpaired t-test CagA vs. CagA+DLC1.1). **B:** Representative pictures of immunofluorescence staining of DLC1.1 and CagA transfected AGS cells. Blue: DAPI/nuclei; red: DLC1; green: CagA (GFP); white arrow indicates focal adhesions; scale bar=10 µm.

Figure 3.18 A indicates increased cell spreading of AGS and HEK293T cells in the presence of DLC1. The spread cell morphology of DLC1 overexpressing AGS cells is illustrated by figure 3.18 B. In the presence of CagA, the cells showed an elongated morphology. These findings have already been shown during another project within the authors group (Hitkova, 2013). The cytoplasm was CagA positive and DLC1 was additionally accumulated at the focal adhesions.

These findings suggest that CagA and DLC1 are responsible for antagonizing cell morphologies. CagA evokes a needle-like cell shape and DLC1 promotes cell spreading by focal adhesion localization.

3.2.3 Functional antagonism between DLC1 and CagA

Section 3.2.1 showed that DLC1 and CagA interact by complex formation. Luciferase activity assays were performed for a detailed assessment of the functions both proteins fulfill by this interaction.

3.2.3.1 Effect of DLC1 and CagA on cell proliferation

For investigation of the effect of DLC1 and CagA on the cell proliferation, cells were transiently transfected with an empty vector (EV), CagA, DLC1.1 or a combination of CagA and DLC1.1 in addition to pGL3_*SRE*. The pGL3_*SRE* plasmid is a luciferase reporter plasmid containing serum response elements (*SRE*). The c-Fos promoter element *SRE* is known to be stimulated by growth factors and subsequent mitogen-activated protein kinase (MAPK) signaling to regulate cell proliferation (Vickers et al., 2004). Furthermore, *SRE* has been identified as a target of *H. pylori* CagA (Hirata et al., 2002). Hence, this luciferase activity assay was used to elucidate the role of DLC1 and CagA concerning cell proliferation. Results are shown by figure 3.19.

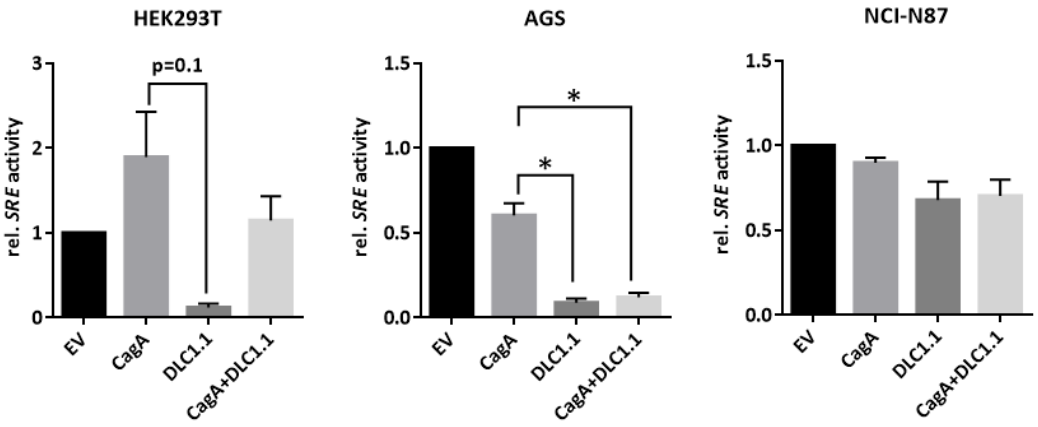

Fig. 3.19: Impact of CagA and DLC1 on the activation of the c-Fos promoter as a surrogate read-out for cell proliferation. HEK293T, AGS and NCI-N87 cells were transiently transfected with empty vector (EV), CagA, DLC1.1 or a combination of CagA and DLC1.1 in addition to the *SRE* luciferase reporter plasmid (pGL3_*SRE*). Luciferase activity was measured by luciferase assay, normalized to protein concentration and calculated as -fold ± S.E. (n=3 per cell line; HEK293T: p=0.1, Mann-Whitney *U* test CagA vs. DLC1.1; AGS: *p<0.05, unpaired t-test CagA vs. DLC1.1/CagA+DLC1.1; NCI-N87: n.s.).

This luciferase activity assay revealed an increased *SRE* activity upon CagA transfection in comparison to DLC1.1, which inhibited *SRE* activity. SRE activity was reduced by DLC1.1 compared with CagA transfection for HEK293T (to 6%) and AGS (to 10%) cells. In AGS cells, DLC1.1 efficiently inhibited CagA-mediated *SRE* activation. For NCI-N87 cells, *SRE* activity was marginally reduced by DLC1.1 compared with CagA. In general, CagA-mediated *SRE* activity in AGS and NCI-N87 cells was lower in contrast to HEK293T cells.

3.2.3.2 Effect of DLC1 and CagA on the cellular stress response and hypoxia

H. pylori-infection is known to evoke oxidative stress by the synthesis of reactive oxygen species (ROS) (Wilson and Crabtree, 2007). For this reason, the effect of DLC1 and CagA on the cellular stress response and hypoxia was investigated. To this end, cells were transiently transfected with an empty vector (EV), CagA, DLC1.1 or a combination of CagA and DLC1.1 in addition to pGL3_*HRE*. The pGL3_*HRE* plasmid is a stress sensitive luciferase reporter plasmid containing the promoter of the high-mobility group box (HMGB) protein 2 and a hypoxia responsive element (*HRE*). The results are shown by figure 3.20.

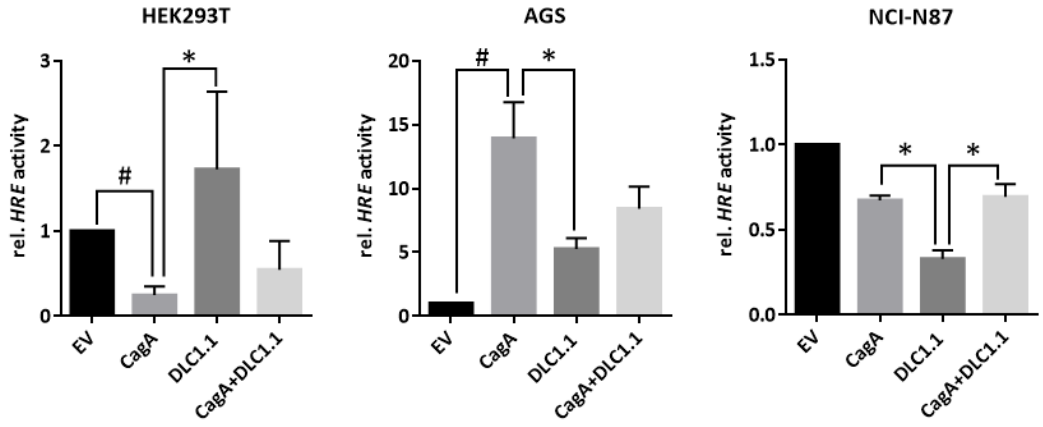

Fig. 3.20: Impact of CagA and DLC1 on the activation of the stress-responsive *HMGB2* promoter as a surrogate read-out for hypoxia. HEK293T, AGS and NCI-N87 cells were transiently transfected with empty vector (EV), CagA, DLC1.1 or a combination of CagA and DLC1.1 in addition to the *HRE* luciferase reporter plasmid (pGL3_*HRE*). Luciferase activity was measured by luciferase assay, normalized to protein concentration and calculated as -fold ± S.E. (n=3 per cell line; *p<0.05: unpaired t-test; #p<0.05: one sample t-test EV vs. CagA).

HRE activity was reduced to 24% by CagA compared with EV and increased 7-fold by DLC1.1 in comparison to CagA in HEK293T cells, whereas the effect was reciprocal in AGS and NCI-N87 cells. AGS and NCI-N87 cells showed a significant downregulation of *HRE* activity in DLC1.1 transfected cells compared with CagA transfection. Despite the fact that CagA was no strong activator of *HRE* in NCI-N87 cells, there was a significant restoration of DLC1-mediated *HRE* inhibition by CagA in NCI-N87 cells.

FACS analysis was performed to further investigate the role of DLC1 and CagA in the production of ROS. To this end, HEK293T cells were transiently transfected with an empty vector (EV), CagA, DLC1.1 or DLC1.4 and stained using the Cellular Reactive Oxygen Species Detection Assay Kit according to the manufacturer's instructions. Figure 3.21 shows the results of the FACS analysis.

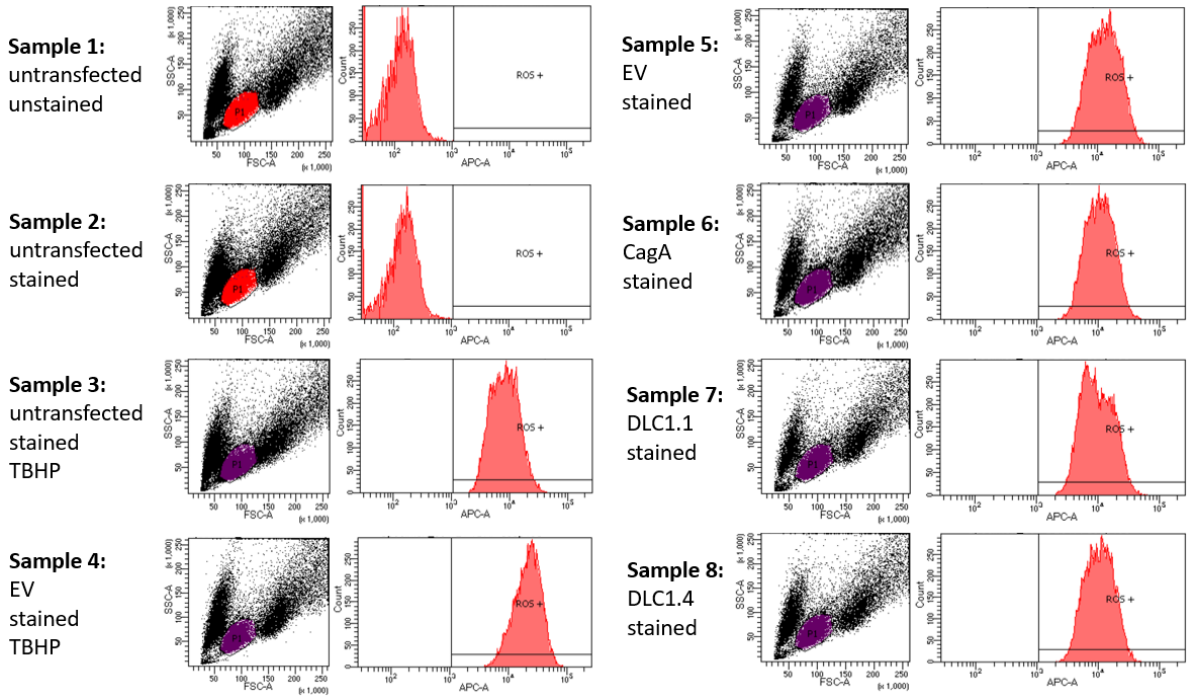

Fig. 3.21: Impact of CagA and DLC1 on reactive oxygen species (ROS) generation. HEK293T cells were transiently transfected with empty vector (EV), CagA, DLC1.1 or DLC1.4 and stained for FACS analysis using the Cellular Reactive Oxygen Species Detection Assay Kit (Deep Red Fluorescence). TBHP: tert-Butyl hydrogen peroxide (positive control); n=1.

The FACS analysis revealed positivity for ROS independent of transfection. Thus, all transfected cells were positive for ROS production.

In addition, Western Blot analysis of total cell lysates of CagA and/or DLC1.1 transfected and $CoCl_2$ treated AGS cells was performed to investigate the expression of the hypoxia-inducible factor 1α (HIF1α) (Fig. 3.22).

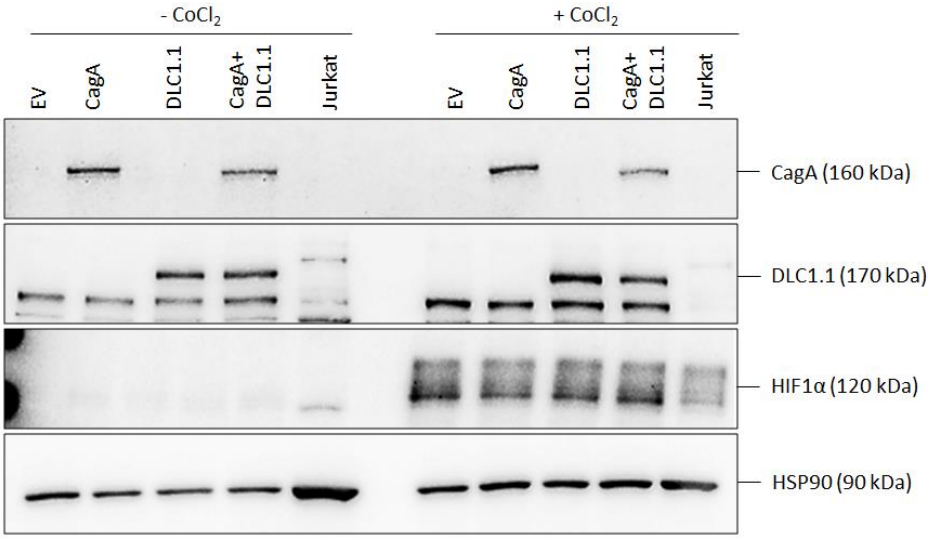

Fig. 3.22: Both, CagA and DLC1 have no effect on HIF1α signaling. AGS cells were transiently transfected with empty vector (EV), CagA, DLC1.1 or DLC1.4 and treated with 0.1mM $CoCl_2$ for 4h. Total cell lysates were subjected to Western Blot analysis for detection of HIF1α. Untransfected but $CoCl_2$ treated Jurkat cells served as positive control (n=1).

The Western Blot analysis revealed a stabilization of HIF1α by $CoCl_2$ treatment, but no difference in HIF1α expression upon CagA and DLC1 transfection.

Further Western Blot analysis was performed to show the impact of DLC1 and CagA on NFκB signaling. For this purpose, AGS cells were transiently transfected with CagA or DLC1, stimulated with LPS (derived from *E. coli*) for different time periods (0 min, 15 min, 30 min, 60 min). Total protein lysates were subjected to Western Blot analysis for (P)-NFκB detection (Fig. 3.23).

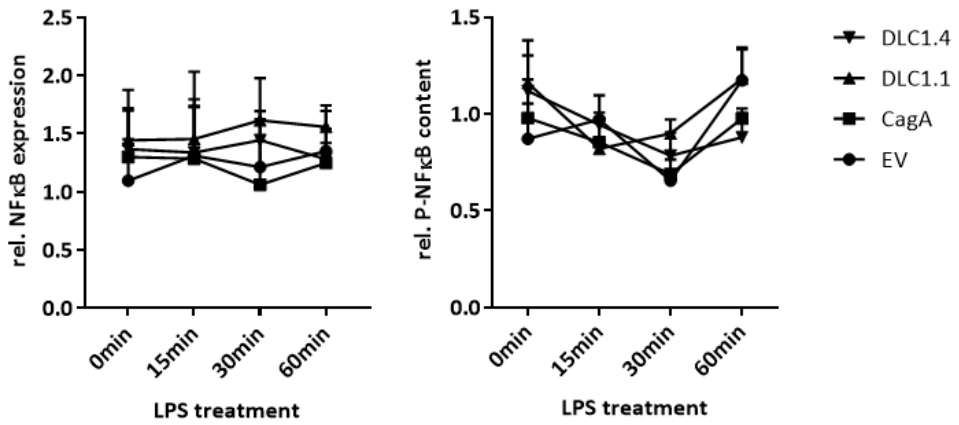

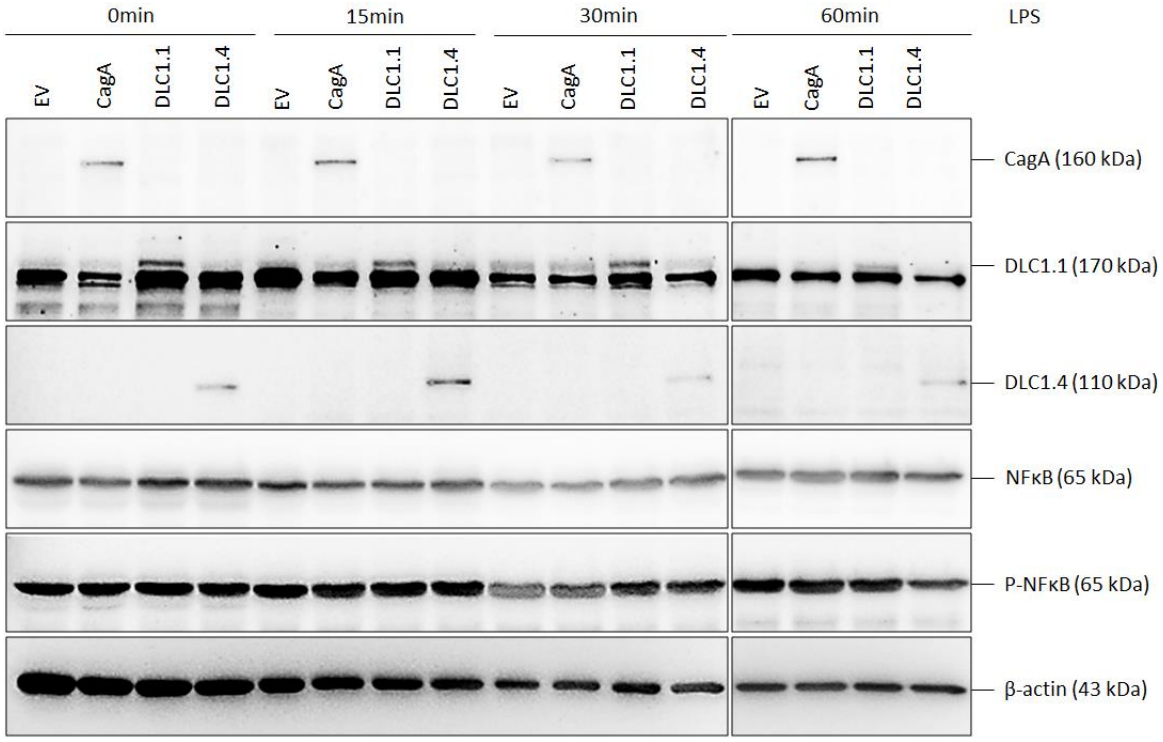

Fig. 3.23: Both, CagA and DLC1 have no effect on NFκB signaling. AGS cells were transiently transfected with empty vector (EV), CagA, DLC1.1 or DLC1.4 and treated with 1µg/ml LPS for 0min, 15min, 30min and 60min. Total cell lysates were subjected to Western Blot analysis. Representative gels are shown (lower panel). NFκB and P- NFκB bands in gels were quantified and O.D. values were normalized to β-actin and calculated as -fold ± S.E. (upper panel) (n=3, ordinary one-way ANOVA n.s.).

Figure 3.23 shows no effect of CagA or DLC1 on NFκB signaling, although successful transfection was verified.

3.2.3.3 Impact of DLC1 and CagA on RHOA activity

It is reported in the literature that CagA activates and DLC1 inhibits RHOA (Braun and Olayioye, 2015; De Falco et al., 2015; Yamahashi and Hatakeyama, 2013). Luciferase activity and pulldown assays were performed to investigate the interdependency between the two proteins concerning RHOA activity and to verify, if DLC1 inhibits CagA-mediated G-protein-coupled RHOA activation. For luciferase activity assay, cells were transfected with an empty vector (EV), CagA, DLC1.1, DLC1.4 or a combination of CagA and both DLC1 isoforms in addition to the RHOA specific p*SRE*.L luciferase reporter plasmid. This reporter plasmid contains mutated *SRE*, which is deficient for the c-Fos ternary complex-binding site. This leads to a specific response to active RHOA compared with wild type *SRE* (Wells et al., 2001).

Due to this fact, p*SRE*.L was used as an appropriate system to detect RHOA activity. Specificity for active RHOA was furthermore verified by control plasmids. To this end, a RHOA activating and a RHOA inhibiting plasmid co-transfected with DLC1 or CagA, respectively, in addition to p*SRE*.L was used. The RHOA activating plasmid contained the constitutively active form of the α subunit of the heterotrimeric G-protein α13 (G13qL). The plasmid showing RHO inhibiting effects contained the *Clostridium botulinum* C3 toxin (C3T), which is specific for RHO, but not for RAC1 and CDC42 GTPases (Saito et al., 2010; Williams, 2011). CagA-mediated activation of mutated *SRE* was abolished by C3T and DLC1-mediated inhibition of mutated *SRE* was repealed by co-transfection with G13qL confirming specificity of p*SRE*.L for active RHOA (Fig. 7.3 appendices). Figure 3.24 shows the results of the p*SRE*.L luciferase activity assay.

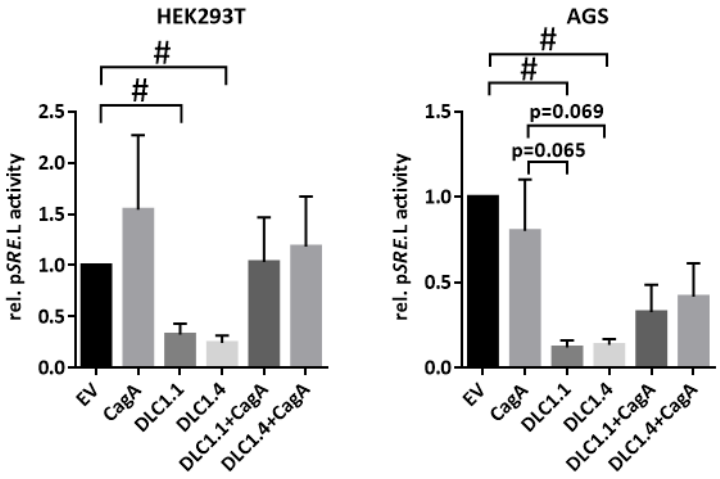

Fig. 3.24: DLC1 inhibits RHO-driven *SRE*, which is deficient for c-Fos ternary complex-binding site. HEK293T and AGS cells were transiently transfected with empty vector (EV), CagA, DLC1.1, DLC1.4 or a combination of CagA and DLC1.1/DLC1.4 in addition to p*SRE*.L luciferase reporter plasmid. Luciferase activity was measured by luciferase assay, normalized to protein concentration and calculated as -fold ± S.E. (n=3 for HEK293T; n=4 for AGS; $^{\#}p<0.05$: one sample t-test; p=0.065: unpaired t-test CagA vs. DLC1.1; p=0.069: unpaired t-test CagA vs. DLC1.4).

The luciferase activity assay revealed a weak activation of mutated *SRE* by CagA for HEK293T cells and a significant inhibition of mutated *SRE* by both DLC1 isoforms compared with EV. There was no inhibition of CagA-mediated activation of mutated *SRE* by DLC1 monitored. CagA was no strong activator of mutated *SRE* in AGS cells, but mutated *SRE* was efficiently inhibited by DLC1 in contrast to EV and CagA transfection.

RHOA pulldown assay was performed to further investigate the effect of CagA and DLC1 on RHOA activity. RHOA specificity was successfully verified by C3T and G13qL controls also for RHOA pulldown. C3T efficiently inhibited CagA- and G13qL-mediated RHOA activation (Fig. 7.4 appendices). To assess inhibition of CagA-mediated RHOA activity by DLC1, tsA201 cells were transiently transfected with an empty vector (EV), CagA, DLC1 and a combination of CagA with DLC1. Active RHOA was precipitated by GST-pulldown. Total cell lysates served as input controls of transfection efficiency and detection of total RHOA level (Fig. 3.25).

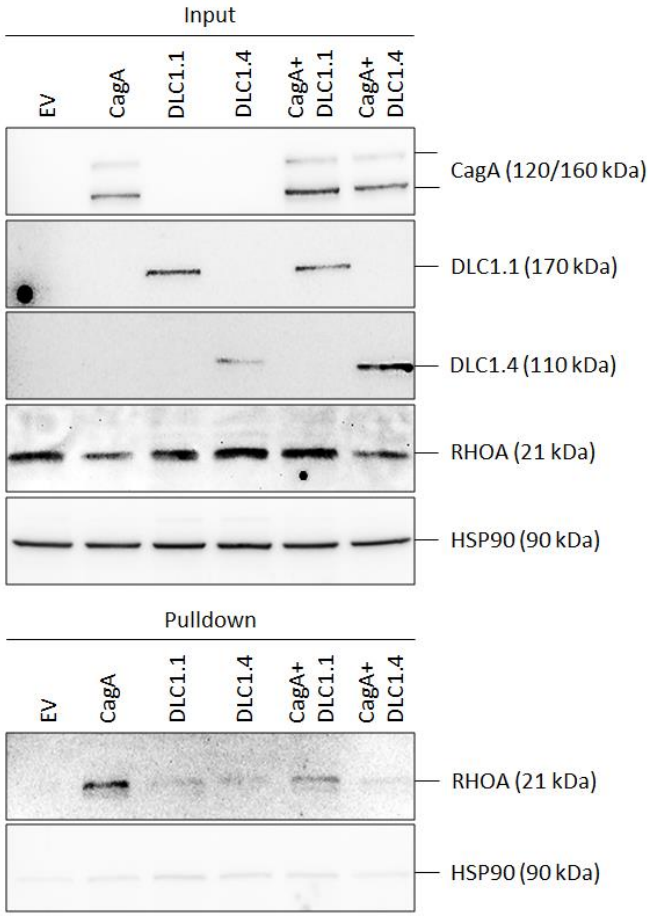

Fig. 3.25: DLC1 inhibits CagA-mediated G-protein coupled RHOA activation. TsA201 cells were transiently transfected with empty vector (EV), CagA, DLC1.1, DLC1.4 or a combination of CagA and DLC1.1/DLC1.4. GST-pulldown assay was performed for the analysis of RHOA activity. Total cell lysates (Input) were subjected to Western Blot for verification of transfection efficiency and detection of total RHOA amount (n=1). Data jointly produced with the group of Prof. Wieland (Dept. of Experimental Pharmacology, Medical Faculty Mannheim of University Heidelberg).

Figure 3.25 shows a strong G-protein coupled activation of RHOA for CagA transfection, which was efficiently inhibited by both DLC1 isoforms. Input controls revealed a successful transfection and a consistent level of total RHOA.

In summary, the experiments to assess a functional antagonism between DLC1 and CagA revealed antagonizing functions of the two proteins concerning cell proliferation, hypoxic stress response and RHOA activity.

3.3 Verification of *Helicobacter spec.*

Different *Helicobacter* strains are available for an infection of DLC1$^{gt/+}$ mice to study the role of DLC1 in *H. pylori*-related gastric disease *in vivo* and to perform *in vitro* assays thereby replacing CagA by live bacteria. The bacteria strains were verified by genotyping and immunofluorescence staining (Fig. 3.26) before performing infection studies. The G27 strain is a cell-adapted wild type *H. pylori* strain, which expresses functional VacA and CagA and is able to inject CagA successfully into the host cell (Covacci et al., 1993; Xiang et al., 1995). This strain is suitable to analyze CagA-specific effects in cell culture due to the efficient translocation of CagA into cultivated cells (El-Etr et al., 2004; Segal et al., 1999). The SS1 strain is a mouse-adapted *H. pylori* strain, which expresses functionally active CagA, but is not able to bring the toxin into the host cell (Lee et al., 1997; Van Doorn et al., 1999). Due to its genetic predisposition, the SS1 strain is suitable for long term infection of mice. *H. pylori* SS1 has been shown to induce an active chronic gastritis paralleled by atrophic changes in C57BL/6 and BALB/c wild type mice after eight months of infection (Krueger et al., 2011; Lee et al., 1997). *H. felis* is isolated from cat and does not express CagA or VacA (Mohammadi et al., 1996). Nevertheless, *H. felis* is able to evoke gastric disease patterns such as MALT lymphoma (Gossmann et al., 2016).

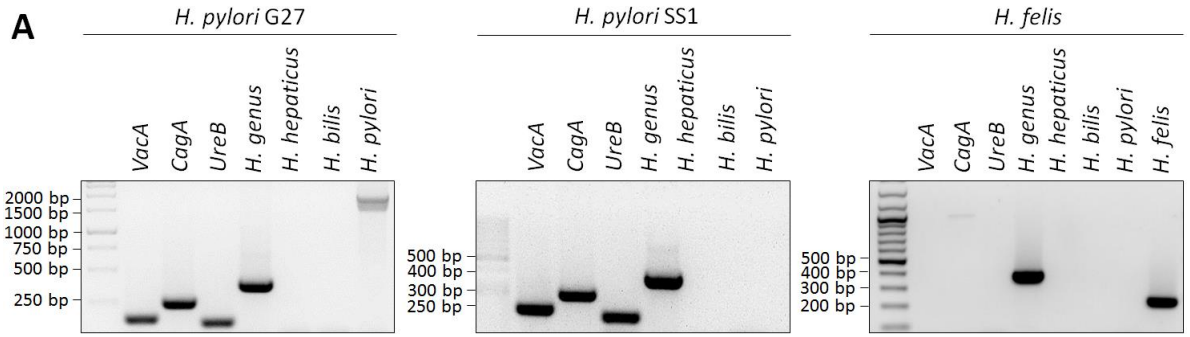

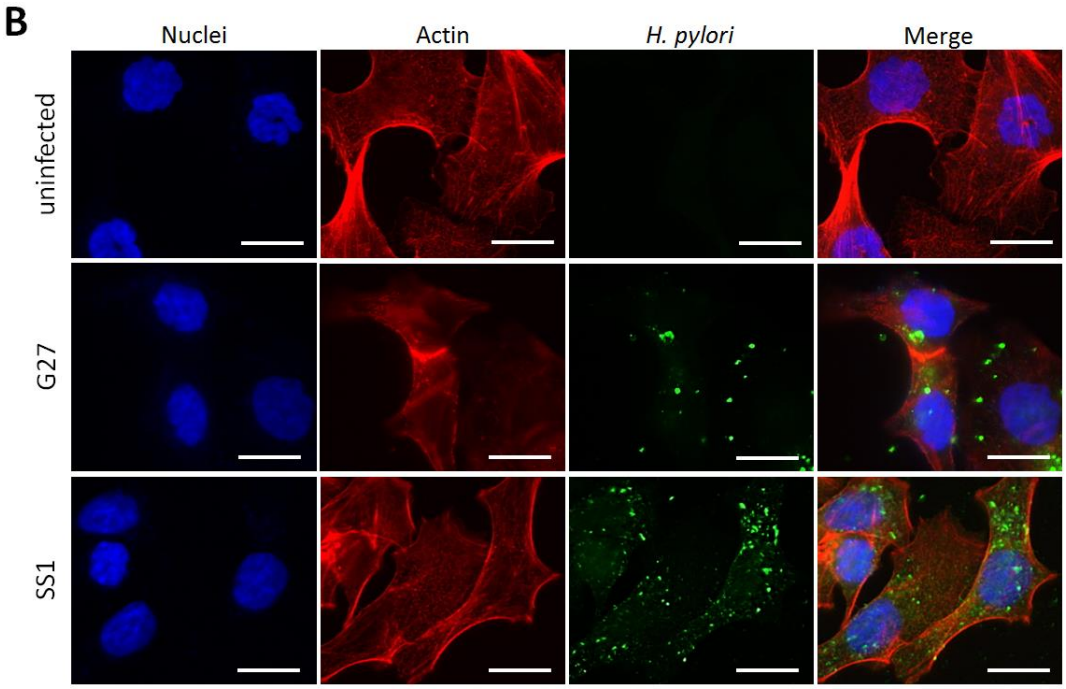

Fig. 3.26: Verification of *Helicobacter spec*. A: Genotyping of *Helicobacter spec*. Genomic DNA isolated from *H. pylori* G27, *H. pylori* SS1 and *H. felis* was subjected to PCR analysis. Amplified products were loaded on agarose gels. *VacA*: 164bp; *CagA*: 257bp; *UreB*: 144bp; *H. genus*: 382bp; *H. hepaticus*: 705bp; *H. bilis*: 435bp; *H. pylori*: 992-1548bp; *H. felis*: 241bp. **B:** AGS cells were infected with *H. pylori* G27 or SS1, respectively, and subjected to immunofluorescence staining using a *H. pylori* specific antibody. Blue: DAPI/nuclei; red: actin; green: *H. pylori*; scale bar: 10µm.

Figure 3.26 shows the successful verification of all tested *Helicobacter* strains. Figure 3.26 A demonstrates that G27 and SS1 express all toxins (CagA, VacA and UreB) in contrast to *H. felis*. There is a band for *H. genus* for each bacterial strain. A primer pair specific for *H. felis* verifies it as the cat-derived strain. Immunofluorescence staining of infected gastric cancer cells revealed a successful infection with *H. pylori* G27 and SS1 when compared with uninfected AGS cells (Fig. 3.26 B). Since it was not possible to generate appropriate amounts of bacteria, no *in vivo* infection or further *in vitro* studies to replace CagA by living bacteria were performed.

3.4 Therapy of a preclinical model for GC with an inhibitor of the RHO/ROCK-pathway

DLC1 is supposed to be a novel drug target and biomarker for treatment and diagnosis of GC due to its tumor suppressive functions and its downregulation in tumor tissue. There are

different potential therapeutic strategies including restoration of DLC1 expression by epigenetic approaches or inhibition of the oncogenic RHO/ROCK-pathway, which represents a therapeutic intervention in the DLC1-mediated pathway (Popescu and Goodison, 2014). In this study*, in vivo* inhibition of ROCK was performed using the small molecule inhibitor fasudil, which has not been shown so far for GC (Liao et al., 2007; Miyamoto et al., 2014; Zhang et al., 2009).

As a preclinical model for human GC, CEA424-SV40 TAg mice were used for *in vivo* therapy with fasudil. These transgenic mice express the oncogene large T-antigen (TAg) from the Simian Virus 40 (SV40) under control of the promoter of the human carcinoembryonic antigen (CEA). The animals develop highly proliferative gastric tumors specifically in the lower part of the stomach (pylorus) within 4 weeks of age (Thompson et al., 2000).

3.4.1 Expression of RHOA and ROCK1/2 *in vitro*

Expression and activity of the RHO-pathway components were analyzed *in vitro* first. For this purpose, endogenous levels of *RHOA*, *ROCK1* and *ROCK2* were determined by PCR in AGS, MKN45 and HEK293T cells (Fig. 3.27).

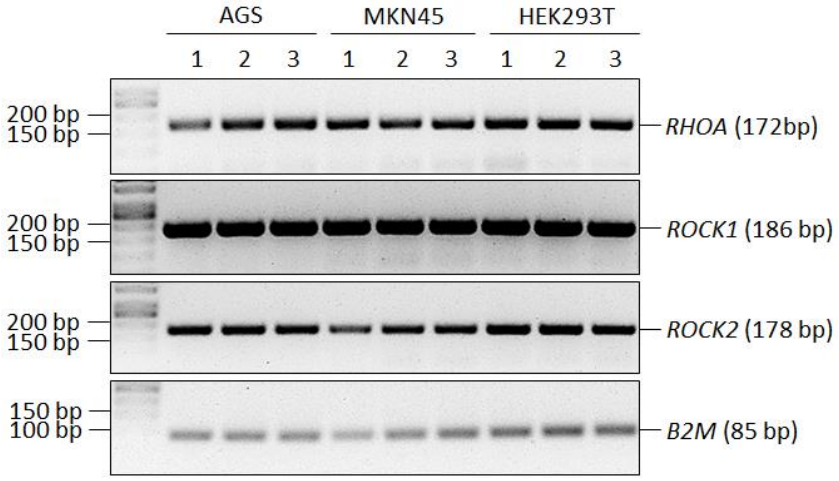

Fig. 3.27: Expression of *RHOA* and *ROCK1/2* in human transformed and GC cell lines. Total RNA of AGS, MKN45 and HEK293T cells was isolated, transcribed into cDNA and subjected to PCR for amplification of endogenous *RHOA*, *ROCK1* and *ROCK2* mRNA. The housekeeper β2-microglobulin (*B2M*) served as control. Amplified products were loaded on an agarose gel (n=3 per cell line).

The PCR results revealed a steady-state expression of *RHOA*, *ROCK1* and *ROCK2* on the RNA level in all cell lines tested.

Pulldown assays were performed to determine RHOA activity by use of recombinant GST-rhotekin for binding of active GTP-bound RHOA in AGS, MKN45 and HEK293T cells (Fig. 3.28).

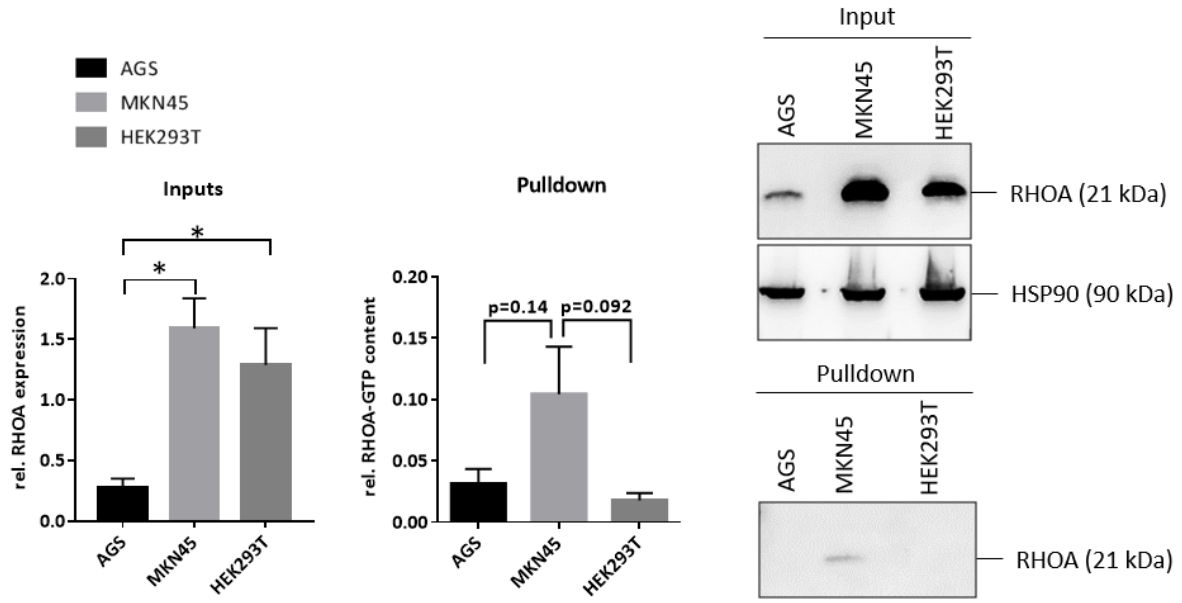

Fig. 3.28: Content of active RHOA in human transformed and GC cell lines. Total cell lysates of AGS, MKN45 and HEK293T cells were subjected to GST-pulldown. Recombinant rhotekin-GDS protein was used as a bait to precipitate active GTP-bound RHOA. Active (Pulldown) and total (Input) RHOA levels were analyzed by performing Western Blot using a RHOA specific antibody. O.D. values from bands in gels were normalized to HSP90 and calculated as -fold ± S.E. (n=3 per cell line, input: *p<0.05: ordinary one-way ANOVA AGS vs. MKN45/HEK293T; pulldown: p=0.14, unpaired t-test AGS vs. MKN45; p=0.092 unpaired t-test HEK293T vs. MKN45). Quantitative analysis (left panel) and representative gels (right panel) are shown.

AGS cells showed the lowest amount of total RHOA protein compared with MKN45 and HEK293T cells (Input). There was low RHOA activity detectable only in MKN45 cells compared with AGS and HEK293T (pulldown).

For the analysis of the *in vitro* efficacy of fasudil, AGS, MKN45 and HEK293T cells were treated with 50µM fasudil or PBS for 30h before subjecting total cell lysates to Western Blot analysis (Fig. 3.29).

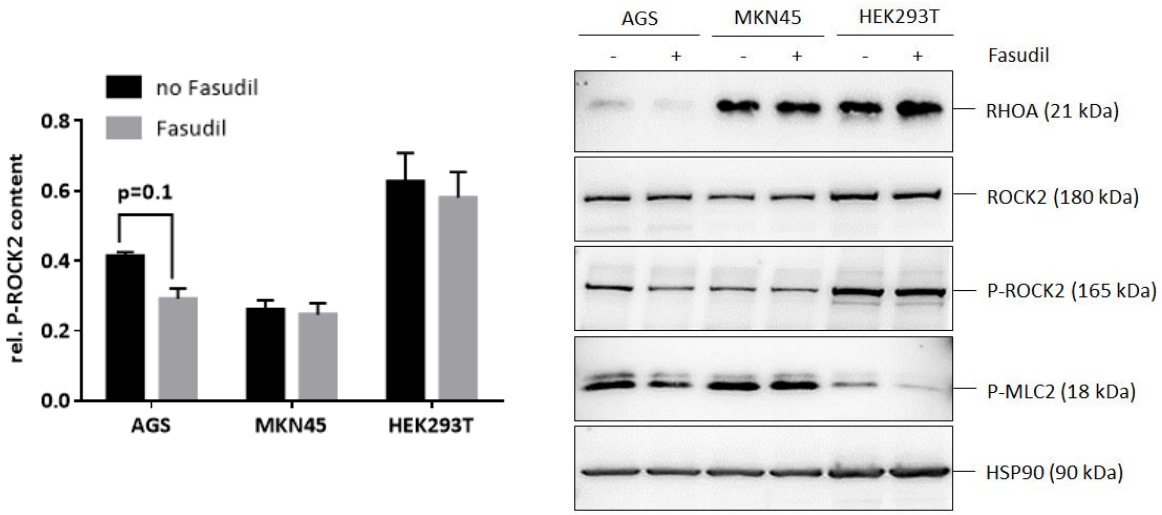

Fig. 3.29: Fasudil decreases P-ROCK2 level in human GC cells. Human transformed and GC cells were treated with vehicle (PBS, no fasudil) or 50µM fasudil for 30 hours. Total cell lysates of treated cells were subjected to Western Blot analysis using specific antibodies for RHOA, (P)-ROCK2 and P-MLC2. O.D. values from P-ROCK2 bands in gels were normalized to HSP90 and calculated as -fold ± S.E. (n=3 per cell line, p=0.01: Mann Whitney *U* test no fasudil vs. fasudil). Quantitative analysis (left panel) and representative gels (right panel) are shown.

The Western Blot analysis confirmed the steady-state expression of RHOA and ROCK2 on a protein level in all cell lines tested. AGS showed the lowest level of total RHOA protein. Fasudil treatment of AGS cells resulted in a reduced level of phosphorylated ROCK2 by 30% compared with vehicle control. Also phosphorylated MLC2 protein tends to be decreased in AGS and HEK293T cells.

3.4.2 Effect of fasudil on cell viability

To elucidate the effect of fasudil on cancer cell viability *in vitro*, SW480, AGS and MKN45 cells were grown to confluency and treated with PBS or increasing concentrations of fasudil for 48h followed by MTT assay (Fig. 3.30).

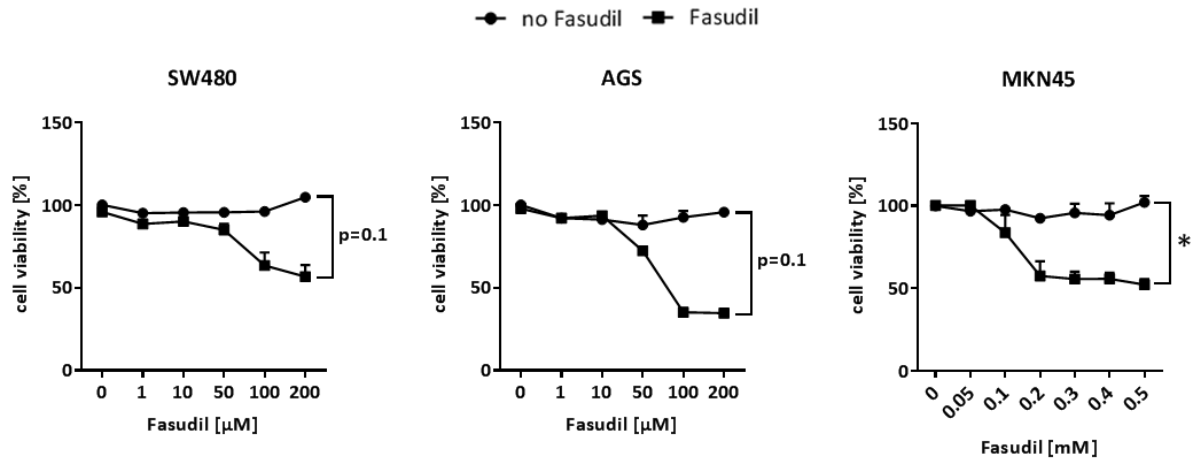

Fig. 3.30: Fasudil promotes cell death of human CRC and GC cell lines. Cells were treated with vehicle (PBS, no fasudil) or increasing fasudil concentrations for 48 hours. Cell viability was measured by colorimetric MTT assay. O.D. values were calculated as % ± S.E. (n=3 per cell line, *p<0.05: unpaired t-test no fasudil vs. fasudil; p=0.1: Mann Whitney *U* test no fasudil vs. fasudil).

Fasudil reduced cell viability to 54% at 200µM in SW480 cells, to 36% at 200µM in AGS cells and to 51% at 0.5mM in MKN45 cells.

3.4.3 Expression of RHOA and ROCK1/2 *in vivo*

In order to determine the expression of *RhoA* and *Rock1/2* in mouse tissue, total RNA was isolated from normal gastric tissue (NT) and gastric tumor tissue (TU) of CEA424-SV40 TAg mice and subjected to RT-qPCR analysis (Fig. 3.31).

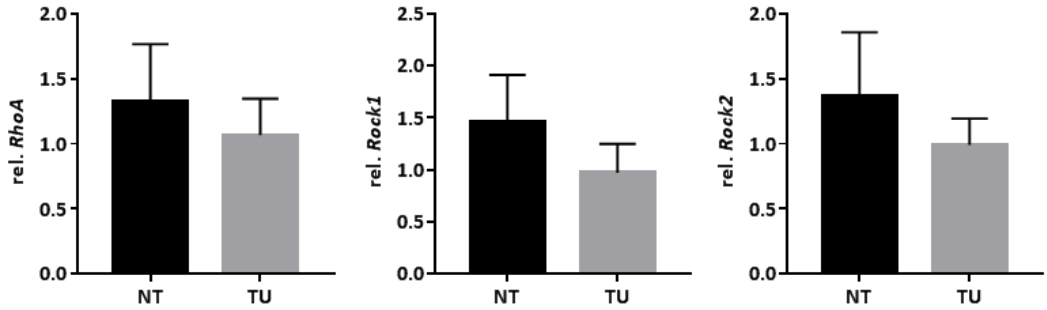

Fig. 3.31: Expression analysis of *RhoA* and *Rock1/2 in vivo*. Total RNA was extracted from normal WT gastric tissue (NT) and gastric tumor tissue of CEA424-SV40 TAg mice (TU) and subjected to RT-qPCR analysis after reverse transcription. CT-values were normalized to β2-microglobulin (*ß2m*) and calculated as -fold ± S.E. (n=5 mice per group, unpaired t-test NT vs. TU n.s.).

RhoA and *Rock1/2* mRNA was present in normal gastric tissue (NT) and gastric tumor tissue (TU) of CEA424-SV40 TAg mice.

Total tissue lysates of normal gastric tissue (NT) and gastric tumor tissue (TU) of CEA424-SV40 TAg mice were isolated and subjected to Western Blot analysis to verify RHOA and (P)-ROCK2 expression *in vivo* on the protein level. RHOA- and (P)-ROCK2 specific antibodies were used for detection (Fig. 3.32).

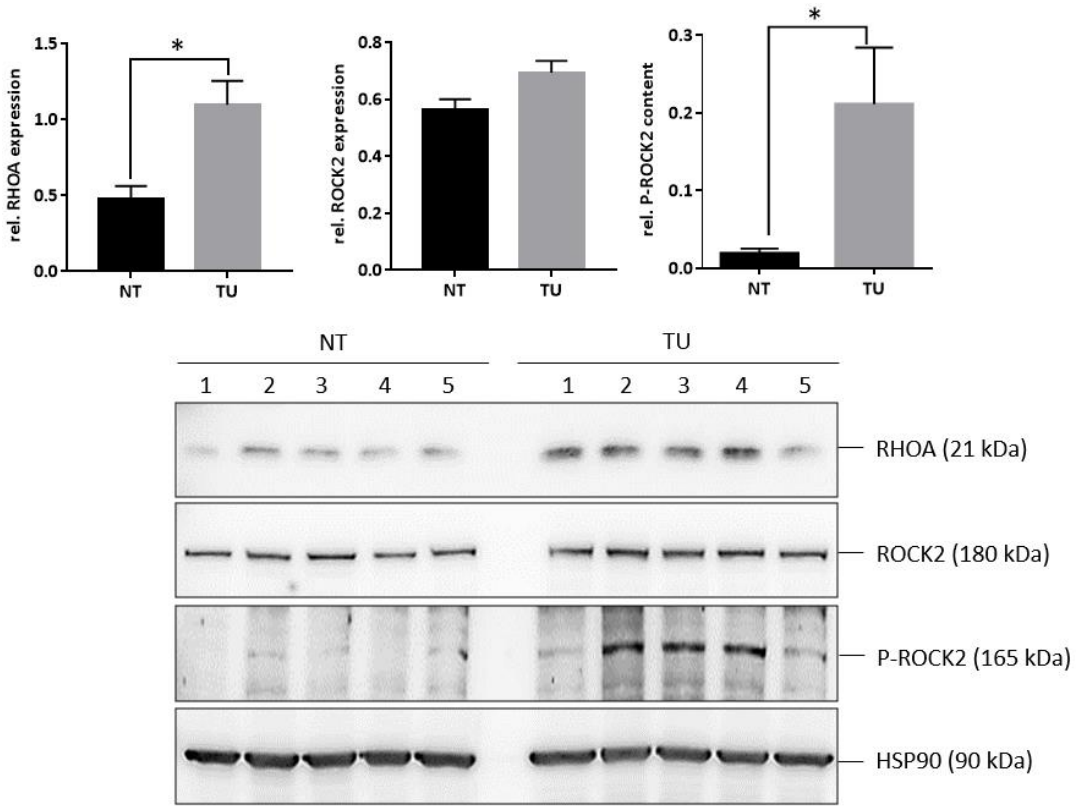

Fig. 3.32: Total RHOA and P-ROCK2 protein level is elevated in GC tissue. Total tissue lysates from normal WT (NT) and gastric tumor tissue of CEA424-SV40 TAg mice (TU) were subjected to Western Blot using RHOA and (P)-ROCK2 specific antibodies. O.D. values of bands in gels were normalized to HSP90 and calculated as -fold ± S.E. (n=5 mice per group, *p<0.05: unpaired t-test NT vs. TU). Quantitative analysis (upper panel) and representative gels (lower panel) are shown.

The Western Blot analysis confirmed expression of total RHOA and ROCK2 protein in stomach tissues of CEA424-SV40 TAg mice. RHOA expression was increased 2-fold in tumor tissue, phosphorylated ROCK2 protein content was elevated 11-fold in gastric tumor tissue compared with normal gastric tissue.

Total tissue lysates from normal gastric tissue (NT) and gastric tumor tissue (TU) of CEA424-SV40 TAg mice were subjected to pulldown assay using recombinant GST-rhotekin for the binding of active GTP-bound RHOA to determine RHOA activity *in vivo* (Fig. 3.33).

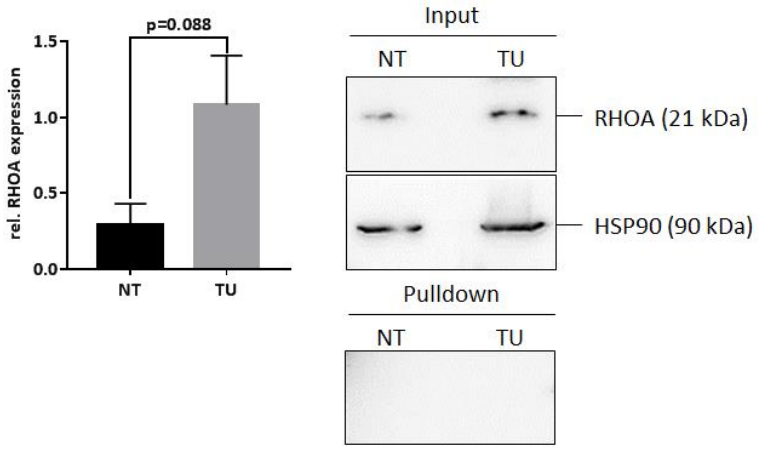

Fig. 3.33: Total but not active RHOA is highly expressed in GC tissue. Total tissue lysates from normal WT (NT) and gastric tumor tissue of CEA424-SV40 TAg mice (TU) were subjected to GST-pulldown. Recombinant rhotekin-GDS protein was used as a bait to precipitate active GTP-bound RHOA. Active (Pulldown) and total (Input) RHOA levels were analyzed by performing Western Blot using a RHOA specific antibody. O.D. values from input bands in gels were normalized to HSP90 and calculated as -fold ± S.E. (n=3 mice per group, p=0.088: unpaired t-test NT vs. TU). Quantitative analysis of inputs (left panel) and representative gels (right panel) are shown.

RHOA pulldown detected no active GTP-bound RHOA in gastric tissue of CEA424-SV40 TAg mice. The input controls revealed a 4-fold increase of total RHOA expression in gastric tumor tissue compared with normal gastric tissue.

The findings indicate an increased level of total RHOA and phosphorylated ROCK2 in gastric tumors of transgenic CEA424-SV40 TAg mice suggesting this pathway as a potential target for ROCK-inhibition. Fasudil furthermore promotes cell death of cancer cells and shows *in vitro* efficacy.

3.4.4 Preclinical efficacy of fasudil in GC of CEA424-SV40 TAg mice

To analyze if fasudil decreases tumor growth *in vivo*, PET/CT imaging was performed in cooperation with the group of Prof. Wängler (Dept. of Clinical Radiology and Nuclear Medicine, Medical Faculty Mannheim of University Heidelberg). To this end, transgenic CEA424-SV40 TAg mice received i.p. injections of fasudil (10 mg/kg) or PBS four times a week over a total time period of four weeks. Mice were deprived of food three hours before they were anesthetized and i.v. injected with [^{18}F]-FDG followed by PET/CT imaging, which is based on the elevated glucose metabolism and proliferation index of the gastric tumor (Almuhaideb et al., 2011; Ihler et al., 2012; Thompson et al., 2000; Vetter et al., 2016). Figure

3.34 shows the overlay images of PET/CT of treated and control mice as well as a quantification of the 3D tumor volume.

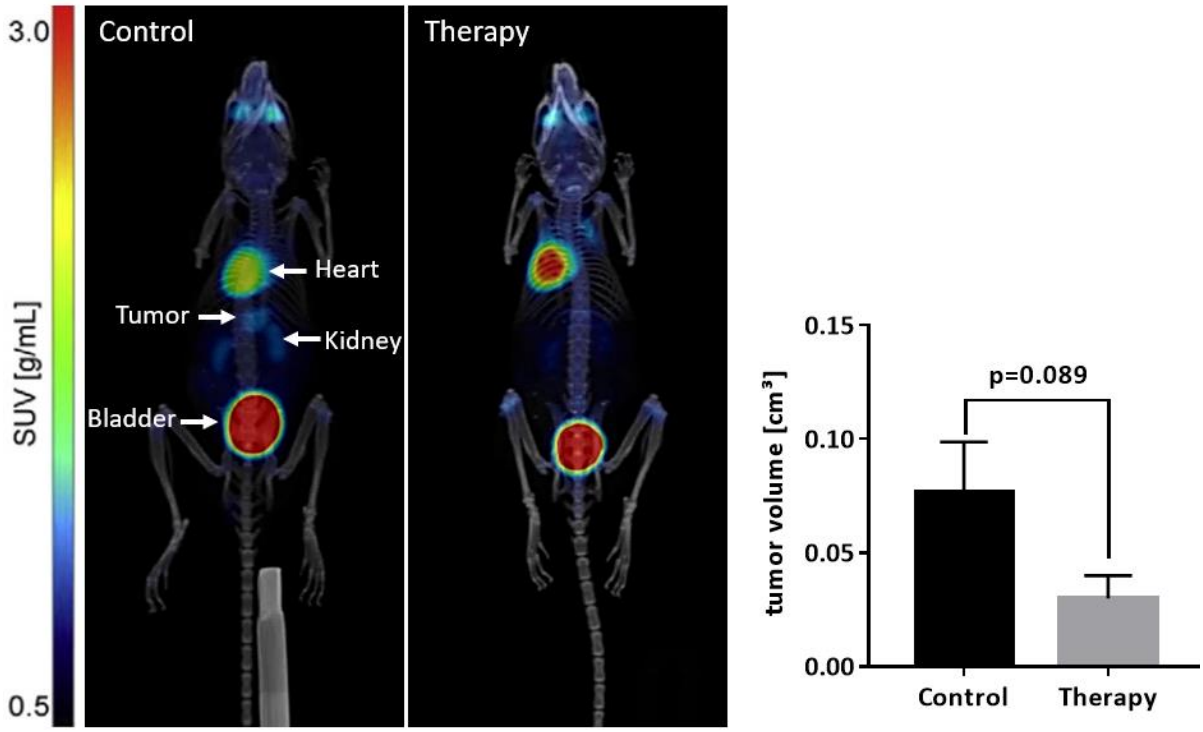

Fig. 3.34: Fasudil treatment decreases tumor volume *in vivo*. CEA424-SV40 TAg mice were injected with fasudil (i.p., 10 mg/kg per day, four times per week) (Therapy) or PBS (Control) for four weeks. The mice were analyzed by 3D PET/CT *in situ* imaging. Signal intensity due to [^{18}F]-FDG uptake is represented by a graded color code with a SUV range of 0.5-10. The tumor volumes detected by PET/CT were quantified. Signals from [^{18}F]-FDG uptake values were calculated as means ± S.E. (n=12 mice per group, p=0.089: Mann-Whitney *U* test Control vs. Therapy). Representative pictures of PET/CT imaging (left panel) and quantification of the tumor volume (right panel) are shown. Data jointly produced with the group of Prof. Wängler (Dept. of Clinical Radiology and Nuclear Medicine, Medical Faculty Mannheim of University Heidelberg).

PET/CT imaging revealed a signal below the heart and between the kidneys for vehicle treated mice, but not for fasudil treated mice, demonstrating the tumor localization. The heart and bladder showed strong signals, which can be explained by the high glucose metabolism of the heart and the clearance of fasudil by the urinary tract system. A quantitative analysis of the 3D tumor volume revealed a decreased tumor volume of treated mice compared with PBS controls by 60%.

After PET/CT imaging, the mice were sacrificed, liver tissues were snap-frozen for protein isolation and stomach tissues were embedded in paraffin for H&E staining as well as

immunohistochemical analysis. Tumor areas were measured on H&E stained stomach sections (Fig. 3.35 A) and immunohistochemical Ki67 staining on paraffin embedded stomach tissue was performed to analyze the effect of fasudil on cell proliferation (Fig. 3.35 B).

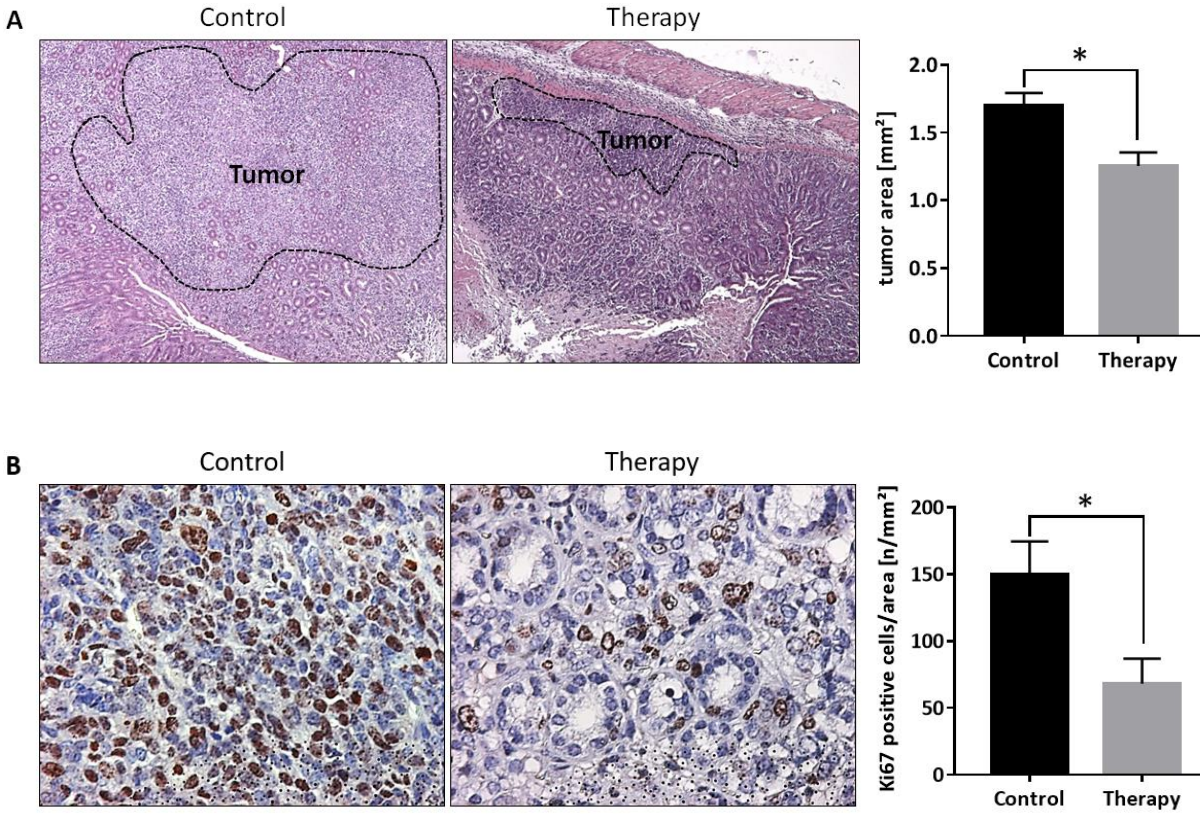

Fig. 3.35: Fasudil treatment decreases the tumor area and proliferation *in vivo*. A: Paraffin embedded stomach tissues of PBS (Control) and fasudil (Therapy) treated CEA424-SV40 TAg mice were subjected to H&E staining. Tumor areas (indicated by dotted lines) were calculated as means ± S.E. (n=23 mice per group, *p<0.05: Mann-Whitney *U* test Control vs. Therapy). Representative pictures (left panel) and quantification (right panel) are shown. **B:** Paraffin embedded stomach tissues of fasudil (Therapy) and PBS (Control) treated CEA424-SV40 TAg mice were subjected to immunohistochemical Ki67 staining. The amount of Ki67 positive cells was calculated as means ± S.E. (n=4 mice per group, *p<0.05: unpaired t-test Control vs. Therapy). Representative pictures (left panel) and quantification (right panel) are shown.

Figure 3.35 A shows a significantly decreased 2D tumor area by 26% of fasudil treated mice compared with PBS controls. Staining of the nuclear proliferation marker Ki67 revealed significantly decreased amounts of Ki67-positive cells to 45% by fasudil treatment in comparison to vehicle controls.

This data demonstrated for the first time that fasudil treatment lowers growth of GC *in vivo*.

3.4.5 Effect of fasudil on RHO-pathway signaling in GC

Immunofluorescence staining was performed on paraffin embedded stomach sections of fasudil treated mice and PBS controls to assess the effect of fasudil on RHOA *in situ* (Fig. 3.36).

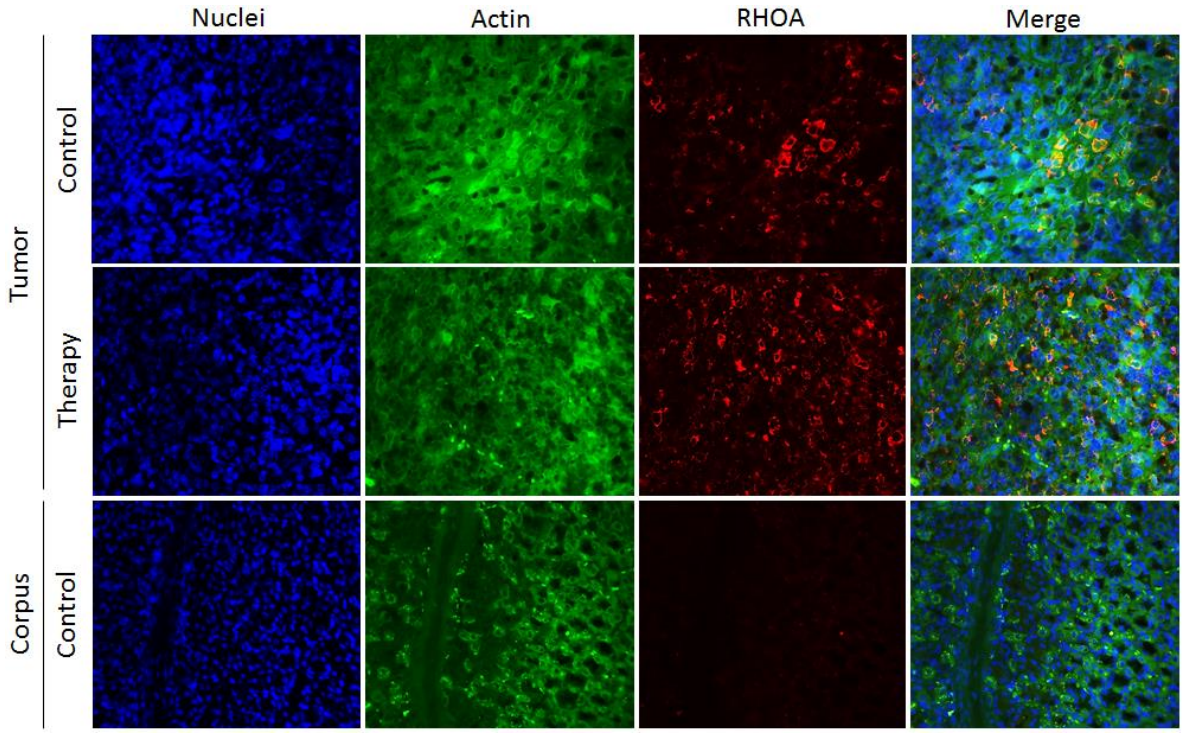

Fig. 3.36: Fasudil does not affect total RHOA expression *in situ*. A: Paraffin embedded stomach tissues of fasudil (Therapy) and PBS (Control) treated CEA424-SV40 TAg mice were subjected to RHOA immunofluorescence staining. Gastric tumor tissue (pylorus) was compared with normal gastric tissue (corpus) of PBS treated mice. Blue: DAPI/nuclei; green: actin; red: RHOA; magnification 400x. n=3 mice per group, representative pictures are shown.

RHOA was present in fasudil treated mice and in PBS controls, but not in normal gastric tissue of the same transgenic mice, which received PBS injection. Immunofluorescence staining of the downstream targets of the RHOA-pathway p38 and ERK 1/2 using phosphorylation-specific antibodies revealed a decreased staining in tumor regions by fasudil treatment (Fig. 7.6 and 7.7 appendices).

Snap-frozen liver tissues of treated and control mice were subjected to immunoprecipitation (IP) of phosphorylated ROCK2 protein to analyze the effect of fasudil treatment on the RHOA-pathway *in vivo* (Fig. 3.37).

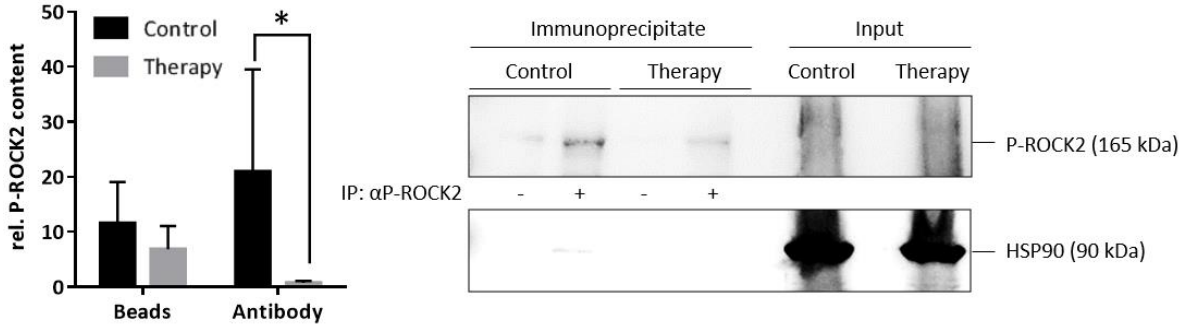

Fig. 3.37: Fasudil lowers RHOA-pathway activity *in vivo*. Total liver tissue lysates of fasudil (Therapy) and PBS (Control) treated CEA424-SV40 TAg mice were subjected to immunoprecipitation (IP) using a P-ROCK2 specific antibody followed by Western Blot analysis using the same antibody. O.D. values from bands in gels were normalized to HSP90 and calculated as -fold ± S.E. (n=8 mice per group, *p<0.05: Mann-Whitney *U* test Control vs. Therapy). Quantitative analysis of the immunoprecipitates (left panel) and representative gels (right panel) are shown.

Immunoprecipitation revealed a significantly decreased level by 97% of phosphorylated ROCK2 protein in fasudil treated transgenic mice compared with control mice.

In summary, these results show an efficient inhibition of RHOA downstream target proteins by fasudil treatment *in vivo*.

4 Discussion

Recruitment of DLC1 to the tumor suppressor CAV1 in case of *H. pylori* infection was first identified during another project within the author's group (Hitkova et al., 2013). These findings necessitated a detailed analysis of the role of DLC1 in *Helicobacter*-related gastric disease, as done by this thesis.

4.1 Characterization of DLC1

Characterization of DLC1 was enabled by use of the DLC1$^{gt/+}$ mouse model. The effects of DLC1 on the immune response was examined after successful verification of the gene trap by Western Blot (Fig. 3.5), immunofluorescence (Fig. 3.6) and immunohistochemical staining (Fig. 3.7).

DLC1$^{gt/+}$ mice showed increased gastric infiltration of immune cells (Fig. 3.8). Immunohistochemical F4/80 staining (Fig. 3.9) identified the infiltrate as macrophages, which were further analyzed by RT-qPCR (Fig. 3.10). According to the binary polarization model, macrophages differentiate into two subsets, namely M1 and M2 macrophages. T_h1 cells activate M1 polarization via IFNγ secretion. M2 polarization is initiated by T_h2 cells via IL-4, IL-5 and IL-13 secretion (Gordon, 2003). M1 macrophages eliminate microorganisms and tumor cells by secretion of pro-inflammatory cytokines and ROS through iNOS, whereas M2 macrophages produce anti-inflammatory cytokines and promote angiogenesis, tumor progression and metastasis. This suggests a categorization of M1 as "good" and M2 as "bad" macrophages, but evidence raises that this classical M1/M2 polarization concept is insufficient and fails to explain the complexity of macrophage activation (Aras and Zaidi, 2017; Caux et al., 2016; Quiding-Jarbrink et al., 2010). DLC1$^{gt/+}$ mice showed elevated gastric (3-fold) and ileal (100-fold) *iNOS* levels compared to WT mice. According to the classical M1/M2 polarization model, this implicates that DLC1 is dispensable to eliminate pathogens and tumor cells. But M1 polarization also indicates increased inflammation, which can initiate pre-neoplastic changes. In addition, Quiding-Jarbrink et al. showed that iNOS promotes the development of GC through production of reactive nitrogen species, thereby inducing DNA damage, impairing DNA repair and evoking *p53* mutations (Quiding-Jarbrink et

al., 2010). Transferring these findings to the DLC1$^{gt/+}$ mouse model, this is in line with the tumor suppressive role of DLC1. Markedly increased ileal *iNOS* levels compared to gastric *iNOS* expression is consistent with the findings of Hamano et al., who was able to detect ileal iNOS on a protein level, but no expression in the stomachs of BALB/c mice (Hamano et al., 2007). It is not surprising that *Ifng* levels are conform to *iNOS* expression patterns in DLC1$^{gt/+}$ mice, because IFNγ activates M1 macrophages. A genetic profile of M2 macrophages revealed an upregulation of the *Arg1* gene, suggesting *Arg1* as a hallmark of the M2 population (Aras and Zaidi, 2017; Caux et al., 2016). DLC1$^{gt/+}$ mice exhibited elevated gastric *Arg1* levels, which indicate a protective role of DLC1 in tumor progression and metastasis and suggest an enhanced risk for GC due to DLC1 deficiency for these mice. Furthermore, it has been shown that infiltration of tumor-associated macrophages positively correlates with Ki67 levels indicating increased cell proliferation (Caux et al., 2016). This was confirmed for DLC1$^{gt/+}$ mice, which showed elevated gastric F4/80 staining and M1/M2 polarization paralleled by an increased number of Ki67 positive gastric cells (Fig. 3.9). An increased cell proliferation is positively correlated to the incidence of DNA mutations thereby contributing to the development of pre-neoplastic changes (Preston-Martin et al., 1990).

Besides macrophages, T cells are further putative candidates for the inflammatory gastric infiltrate of DLC1$^{gt/+}$ mice. Quantitative gene expression analysis of DLC1$^{gt/+}$ mice revealed increased levels of the T cell co-receptors *cd4* and *cd8* (Fig. 3.10). There are different sublineages of CD4$^+$ T_h cells, namely T_h1, T_h2, T_h17 and T_{reg} (Buchholz et al., 2016). The characteristic upregulation of *Ifng* expression in DLC1$^{gt/+}$ mice argues for a predominant T_h1 phenotype of the gene trap mice, because T_h1 cells are known to secrete IFNγ for activation of macrophages, thereby inhibiting T_h2 differentiation (Parkin and Cohen, 2001). Additionally, suppressed *Gata3* levels argue for a T_h1 phenotype, which is true for the mainstomach tissue of the DLC1$^{gt/+}$ mice (Wilson and Crabtree, 2007). It is further known, that GATA3 positively correlates with DLC1 expression, explaining low gastric *Gata3* levels in DLC1 deficient mice (Dydensborg et al., 2009). T_h17 differentiation and, thus, protection against microbial invaders, seems to be independent of DLC1, because there were no changes in *Rorc* levels for DLC1$^{gt/+}$ mice compared with WT mice. Expression of the transcription factor FOXP3 is known to be responsible for T_{reg} differentiation, which plays an important role in the maintenance of immunologic balance. In DLC1$^{gt/+}$ mice, there was a

marginally decreased gastric *Foxp3* level, whereas expression was increased 3-fold in ileal tissues. A high T_{reg} level in tumor infiltrates positively correlates with a poor prognosis (Kim and Cantor, 2014). This suggests that DLC1 is crucial for the survival of the transgenic mice concerning the lower GI tract but not the stomach. Elevated *cd8* levels in transgenic mice represent increased T_c cell expression (Famili et al., 2017). T_c cells cause apoptosis of tumor cells (Kim and Cantor, 2014). Thus, enhanced *cd8* levels in DLC1$^{gt/+}$ mice are contradictory to the function of DLC1 as tumor suppressor. Nonetheless, a loss or mutation of *p53* results in an impaired T_c response and, consequently, in uncontrolled tumor growth (Braun and Iwakuma, 2016). With respect to the elevated *iNOS* levels of DLC1$^{gt/+}$ mice, which can cause *p53* mutations, this leads to an increased risk for cancer development for these mice. Nevertheless, this hypothesis needs to be validated by *p53* expression analyses. A statistically significant number of cases is furthermore necessary to intensify the hypotheses.

Summarized, DLC1$^{gt/+}$ mice showed increased gastric inflammatory infiltration and alterations in the immune response compared to WT mice. These findings suggest a protective role of DLC1 in inflammation and cancer progression of the GI tract.

It was not possible to generate appropriate amounts of *Helicobacter* bacteria for infection studies of DLC1$^{gt/+}$ mice. The mouse-adapted *H. pylori* strain SS1 is suitable for examination of the role of DLC1 in *Helicobacter*-related gastric disease *in vivo*. Macrophage polarization has been attributed a crucial role to the development of *H. pylori*-associated GC. *Helicobacter*-related atrophic gastritis is associated with an increased iNOS expression and, thus, enhanced M1 polarization in patients and SS1-infected mice. (Quiding-Jarbrink et al., 2010). Quiding-Jarbrink et al. furthermore postulated a rather important role of iNOS for the development of gastric disease than for protection during *H. pylori* infection. Concerning T cells, *H. pylori* has been shown to provoke a predominant T_h1 response thereby enforcing gastric inflammation (Blaser and Atherton, 2004; Carbo et al., 2013). Enhanced FOXP3 expression and, consequently, induction of T_{regs} ensures persistent survival of the bacteria and prevents a damaging inflammation (Wilson and Crabtree, 2007). Infection with *Helicobacter* furthermore enforces DNA damage and inhibits DNA repair (Obst et al., 2000; Yao et al., 2006). Hence, infection of DLC1$^{gt/+}$ mice with *Helicobacter* could result in cumulative effects of the molecular events suggesting the DLC1 gene trap mice as an

appropriate model for investigation of the role of DLC1 as a tumor suppressor in *Helicobacter*-related gastric disease.

The gastric co-localization of DLC1 and Chromogranin A (Fig. 3.4) gave first evidence for a localization of DLC1 to ECL cells. ECL cells represent one of the main endocrine cell populations of the acid-producing part of the stomach. Due to this fact, the role of DLC1 in homeostasis of gastric hormones and acid secretion was analyzed in detail by RT-qPCR (Fig. 3.11). DLC1$^{gt/+}$ mice showed a decreased gastric expression level of *chromogranin A* compared with WT mice. Chromogranin A is produced by ECL cells. The secretory activity of ECL cells is triggered by gastrin followed by the activation of the histamine-producing enzyme histidine decarboxylase, which in turn stimulates acid-producing parietal cells. Activation of these molecular events stimulates gastric acid secretion and is supposed to result in a multistep process including hypertrophy, diffuse hyperplasia and dysplasia towards neoplasia, if triggered over a long time period (Hakanson et al., 1998; Hakanson et al., 1995; Li et al., 2014; Mueller et al., 2003). A reduced *chromogranin A* level consequently argues for a decrease in gastric acid production. This leads to the conclusion that deficiency of DLC1 protects against cancer progression by inhibiting gastric acid secretion, which is inconsistent with the known tumor-suppressive functions of DLC1. It is known from the literature that the correlation between gastric acid secretion and disease outcome is even more complicated. Both, reduced and increased gastric acid secretion, results in different disease patterns dependent on the distribution of the gastritis. Whereas a corpus-predominant gastritis is characterized by a reduced gastric acid secretion and causes GC, an antrum-predominant gastritis shows increased gastric acid production and results in the development of DU (Malfertheiner, 2011). Transferring this hypothesis to the findings above, this suggests an increased risk for GC by DLC1 deficiency through inhibition of gastric acid production. This is supported by decreased gastric levels of *histidine decarboxylase*, *intrinsic factor*, *ghrelin* and increased gastric *pepsinogen C* in DLC1$^{gt/+}$ mice. Decreased *histidine decarboxylase* levels imply reduced histamine levels and, consequently, a low gastric acid secretion (Calam, 1999; Hakanson et al., 1998). The intrinsic factor is produced by acid-secreting parietal cells and plays a crucial role in the binding of vitamin B_{12} (Shum et al., 1971). Low vitamin B_{12} levels are proposed to increase the risk for GC and decreased expression of *intrinsic factor* indicates a reduced activity of acid-secreting parietal cells

(Miranti et al., 2017). Low *ghrelin* levels imply a reduced acid secretion thereby also enhancing the risk for GC (Blaser and Atherton, 2004). Elevated *pepsinogen C* expression is related to atrophic changes leading to the development of GC (Cho et al., 2017). These findings are contradictory to increased gastric *H^+K^+-ATPase* and decreased *somatostatin* expression in DLC1$^{gt/+}$ mice. H^+K^+-ATPase is expressed by acid-secreting parietal cells and somatostatin suppresses gastrin, which indicates elevated acid production in case of low somatostatin levels and, hence, rather the development of DU than GC (Malfertheiner, 2011). Nevertheless, the molecular events evoking decreased gastric acid secretion thereby provoking GC in DLC1$^{gt/+}$ mice are predominant over the events suggesting DU development for the gene trap mice. Furthermore, the mice showed a corpus-predominant inflammation (Fig. 3.8), which also gives evidence for an increased risk for GC. However, a statistical significance is not accomplished since the number of cases is insufficient. In addition, tryptophan hydroxylase is localized to ECL cells and involved in serotonin production (Gershon, 2013). The role of serotonin concerning cancer development is concentration-dependent. On the one hand, serotonin acts growth stimulating in cancers but on the other hand it can also inhibit tumor growth if present at low doses (Sarrouilhe et al., 2015). Due to this fact, it is difficult to discuss the *serotonin* level in DLC1$^{gt/+}$ mice. However, there was no difference between WT and gene trap mice in gastric expression of *tryptophan hydroxylase* suggesting a dispensable role for DLC1. Adiponectin is a product of adipocytes, which are one of the largest endocrine cell subtypes. The functions of adiponectin are not well understood, but adipocytes also secrete the adipokine leptin. Leptin plays a crucial role in the regulation of immunity and inflammation. Increased *leptin* levels are associated with elevated inflammation (Mueller et al., 2003). *Adiponectin* expression was downregulated in the mainstomach but upregulated in the ileum of DLC1$^{gt/+}$ mice, suggesting a tissue-dependent role of this hormone. As adiponectin is a marker for adipocytes, this implies an increased ileal *leptin* level and elevated inflammation of the lower GI tract caused by DLC1 gene trap.

These results demonstrate a crucial role of DLC1 in the homeostasis of gastric acid *in vivo*, thereby giving evidence that DLC1 fulfills a protective role in the development of GC.

H. pylori is suggested to inhibit ghrelin secretion (Blaser and Atherton, 2004; Weigt and Malfertheiner, 2009) and *histidine decarboxylase* expression (Calam, 1999) leading to a

decreased gastric acid secretion, which facilitates bacterial colonization of the stomach. Furthermore, the bacteria suppress somatostatin production resulting in hypergastrinemia. Since gastrin is a growth factor for *H. pylori*, suppressed somatostatin levels enforce the bacterial growth (Blaser and Atherton, 2004; Calam, 1999; Malfertheiner, 2011; Weigt and Malfertheiner, 2009). These findings are in line with the expression patterns in DLC1$^{gt/+}$ mice, suggesting a potential cumulative effect by performing infection studies with *Helicobacter*. Cag PAI gene products are further known to downregulate *H^+K^+-ATPase* expression (Malfertheiner, 2011), which could probably not be reached by an infection of the mice with the SS1 strain, because these bacteria are not able to bring functionally active CagA into the host cell (Lee et al., 1997; Van Doorn et al., 1999). Furthermore, *H. pylori* causes increased gastric leptin levels (Blaser and Atherton, 2004), which was not observed for DLC1$^{gt/+}$ mice. However, an upregulation of adiponectin is associated with immunity to *Helicobacter* in an animal model (Blaser and Atherton, 2004), suggesting increased gastric susceptibility of DLC1$^{gt/+}$ mice to the bacteria.

Nevertheless, the molecular changes of DLC1$^{gt/+}$ mice discussed so far are not sufficient for evoking spontaneous development of GC *in vivo*. Infection of these mice with *Helicobacter* can end up in the progression of gastric malignancies, but for establishment of a reliable mouse model for genetically driven GC, additional accelerating molecular events are needed. To this end, further knock-out (KO) or transgene (tg) mouse strains showing a loss or overexpression of certain host genes are available. Homozygous CAV1-KO mice are deficient for the tumor suppressor CAV1, which plays a central role in cell transport processes and represents a control platform for signal transduction thereby inhibiting small GTPases (Cohen et al., 2004; Zaas et al., 2005). The loss of CAV1 results in hyperproliferation and hyperplasia of the GI tract (Burgermeister et al., 2011; Cohen et al., 2004). Infection of these mice with *H. pylori* evokes active chronic gastritis (Hitkova et al., 2013). Transgene HK-IL1β mice overexpress human *Il1β* under control of the murine *H^+K^+-ATPase* promoter and develop a spontaneous gastritis within 18 months, which progresses to carcinoma by *H. felis*-infection (Tu et al., 2008). Cross breeding of the two mouse lines (HK-IL1β x CAV1-KO) also with DLC1$^{gt/+}$ mice (HK-IL1β x CAV1-KO x DLC1$^{gt/+}$) has been already conducted, expecting an acceleration of the molecular events. Histopathological analysis of these mice will be subject of an upcoming project. If spontaneous progression of GC fails, *Helicobacter*-infection is

proposed to promote tumorigenesis and to enable the analysis of *Helicobacter*-driven GC progression in more detail.

4.2 Interaction between DLC1 and CagA

It is known from the literature that host cell responses are modified by both, the C- and the N-terminus of the CagA protein. Besides signaling motifs of the C-terminus, the N-terminus contains an inhibitory domain to reduce host cell responses thereby promoting cancer formation (Pelz et al., 2011). CoIP experiments gave first evidence for an interaction between DLC1 and CagA on a protein level (Fig. 3.13, Fig. 3.14, Fig. 3.15), which was confirmed by PLA (Fig. 3.16). An interaction was manifested for all DLC1 (DLC1.1 and DLC1.4) and CagA (CagA_WT, CagA_838-1216, CagA_1029-1216 and CagA_1-877) constructs used. Thus, the N- and the C-terminus of CagA are essential for an interaction with DLC1. To identify specific interaction domains, further DLC1 and CagA plasmids containing defined sections of the corresponding genes are necessary to clarify involved protein-protein interaction domains. Nevertheless, CoIP experiments suggest a stronger interaction between CagA and DLC1.4 rather than DLC1.1. This is in agreement with previously published data, which showed that CagA-proficient *H. pylori* bacteria promote the recruitment of DLC1.4 to CAV1 in human gastric epithelial cells suggesting DLC1.4 as the *Helicobacter*-interacting isoform (Hitkova et al., 2013).

As described in 3.2.1.3, DLC1 and CagA interactions are not limited to the protein level and were also observed on the DNA level. CagA efficiently inhibited promoter activities of both DLC1 isoforms in human transformed and GC cell lines (Fig. 3.17). Only CagA-mediated *DLC1.1p* repression in NCI-N87 cells was not significant. In contrast to transformed HEK293T cells and primary tumor cells (AGS), NCI-N87 cells are derived from a metastatic site. Hence, the findings in NCI-N87 cells indicate a stronger interaction for CagA and DLC1.4 than for DLC1.1 during metastasis, suggesting once more DLC1.4 as the oncogenic *Helicobacter*-interacting DLC1 isoform. Nonetheless, the transcriptional repression mechanism of DLC1 by CagA needs to be clarified. *In silico* screens can help to identify putative binding elements of the *DLC1* promoter. Previous data demonstrated an activation of SREBP1 by *Helicobacter*-infection resulting in inhibition of the *CAV1* promoter (Hitkova, 2013). To validate if this

holds true for DLC1, performing chromatin-immunoprecipitation (ChIP) of transiently transfected ± CagA cells is proposed to elucidate a putative CagA-dependent binding between active SREBP1 and the *DLC1* promoter. Furthermore, Hitkova et al. showed DLC1.1 expression in non-cancer cell lines in contrast to DLC1.4, which was only expressed in cancer cells (Hitkova et al., 2013). These findings were confirmed by DLC1 expression analyses using N-terminal specific primers representing human DLC1.1 and DLC1.3 expression and C-terminal specific primers demonstrating human DLC1.1, DLC1.2 and DLC1.4 expression (Fig. 3.1). Furthermore, it is known that DLC1 is ubiquitously expressed in normal tissue and frequently downregulated or even lost in many human cancer entities including GC. This was confirmed by method as illustrated in figures 3.2 and 3.3. Silencing of DLC1 is caused by mutations or epigenetic inactivation (Durkin et al., 2007; Ko and Ping Yam, 2014; Popescu and Goodison, 2014; Sabbir et al., 2016; Sabbir et al., 2010). This study suggests that transcriptional DLC1 downregulation by CagA could also contribute to DLC1 silencing.

For the first time, these findings demonstrate a complex formation of the CagA and DLC1 proteins. Transcriptional downregulation of DLC1 by CagA constitutes DLC1 as an early molecular marker before the transition of inflammation to cancer in *Helicobacter*-infected patients.

4.3 Antagonism between DLC1 and CagA

CagA is known to promote the formation of needle-like cell elongations (“hummingbird phenotype”) by activation of the RHO/ROCK/MLC-pathway (Barras and Widmann, 2014; Moese et al., 2004; Segal et al., 1999; Wessler et al., 2011). The characteristic “hummingbird phenotype” was also observed in CagA-transfected GC cells in this study confirming the findings from the literature (Fig. 3.18 B). The CagA-mediated morphological changes and, hence, disruption of the intercellular barriers (Amieva et al., 2003) cause damage to the gastric mucosa, which allows *H. pylori* access to nutrients and facilitates persistence of the bacteria (Blaser and Atherton, 2004; De Falco et al., 2015). By inducing a spindle-like cell shape, CagA further enforces cell migration and invasive growth similar to Epithelial-Mesenchymal-Transition (EMT) (Jie et al., 2017; Wessler et al., 2011). In contrast to the oncogenic CagA-mediated cell morphologies, DLC1 is known to be localized to focal

adhesions thereby promoting cell spreading (Barras and Widmann, 2014; Ravi et al., 2015). This was confirmed by Figure 3.18 and indicates an increased adhesion of DLC1-positive cells. Although the molecular mechanism of the observed phenotype was not analyzed by this investigation, cell spreading might be explained by interaction of DLC1 with components of the focal adhesions such as FAK, talins and tensins thereby regulating assembly and disassembly of the focal adhesions (Cao et al., 2012; Li et al., 2011; Yam et al., 2006). DLC1 can further be sequestered in the cytoplasm, which was also observed in this study. However, localization to focal adhesions is suggested to be essential for the full tumor suppressive function of DLC1 (Barras and Widmann, 2014). In contrast to RAC and CDC42, which are essential for membrane ruffling and formation of filopodia, RHOA is involved in the actin rearrangement and assembly of focal adhesions (Wessler et al., 2011). With respect to the RHOA-inhibiting function of DLC1 it is not surprising that DLC1 accumulates at the focal adhesions.

In summary, this data demonstrates antagonizing cell morphologies evoked by CagA and DLC1, respectively. CagA promotes a spindle-like cell shape thereby enforcing oncogenic processes. In contrast, DLC1 is localized to focal adhesions, which enables full tumor suppressive RHOA-inhibiting function and promotes cell adhesion.

Besides the analysis of the antagonizing cell morphologies mediated by DLC1 and CagA, studies on a putative functional antagonism of the two proteins were performed. Immunohistochemical analysis of $DLC1^{gt/+}$ mice already revealed an anti-proliferative effect of DLC1 (Fig. 3.9) attributing a protective role against pre-neoplastic changes to DLC1. In contrast, *H. pylori* CagA is known to fulfill oncogenic functions and to promote tumorigenesis. To obtain detailed data of the effect of the two proteins on cell proliferation, luciferase reporter assays were performed using a reporter plasmid containing the proliferation-regulating *SRE*s (Vickers et al., 2004) (Fig. 3.19). The analyses revealed that CagA is a strong activator of *SRE* only in human transformed non-cancer cells (HEK293T), suggesting that the pro-proliferative effect of CagA is an initial process in cancer development and plays a minor role in primary tumors (AGS) or metastasis (NCI-N87), respectively. This is in line with findings of Wang et al., which also demonstrate that CagA promotes proliferation of human transformed cells (Wang et al., 2017). Nevertheless, *SRE* activity was significantly elevated by CagA transfection compared with DLC1.1, also in human

GC cells (AGS). Merely in AGS cells DLC1.1 markedly inhibited the CagA-mediated cell proliferation, suggesting an antagonism of the two proteins concerning cell proliferation in GC. The strong inhibition of *SRE* activity by DLC1.1 in HEK293T and AGS cells, but not in NCI-N87 cells, indicates that the anti-proliferative function of DLC1 has been overcome in metastasis.

Summarized, the pro-proliferative effect of CagA is suggested to be an initial process in the development of GC, whereas DLC1 fulfills an anti-proliferative function also in initial stages of gastric disease.

The functional antagonism was further studied regarding the functions of DLC1 and CagA in the stress response of the host cell during *Helicobacter*-infection. An infection with pathogens, including gram-negative bacteria such as *H. pylori*, evokes oxidative stress by the production of reactive oxygen species (ROS). *H. pylori*-related oxidative burst potentiates tumorigenesis, increases apoptosis and causes DNA damage. There are different sources of ROS during an infection. Pro-inflammatory cytokines are induced by infection and recruit host phagocytes to the site of inflammation, which release ROS actively, whereas *H. pylori* itself also produces ROS (Ding et al., 2007; Fang, 2011; Spooner and Yilmaz, 2011). Thus, it is not clear, whether ROS act to eliminate pathogens, host cells or even both. In infected cells, ROS regulate the active secretion of high-mobility group box (HMGB) proteins, which act as damage-associated molecular patterns (DAMPs) extracellularly (Kang et al., 2013; Tang et al., 2011). HMGB proteins are known to bind to cell surface receptors such as TLR4. This triggers downstream signaling pathways including NFκB, which results in the induction of early response genes modulating the immune response and carcinogenic processes (Bekhbat et al., 2017; Sokolova and Naumann, 2017). HMGB proteins further function as DNA chaperones in a redox-sensitive manner repairing oxidative DNA damage in the nucleus (Kang et al., 2013; Tang et al., 2011; Yanai et al., 2012). Furthermore, Küchler et al. showed anti-microbial activity of HMGB2 against commensal and pathogenic bacteria in the human intestinal tract (Küchler et al., 2013). ROS have further been postulated to act as hypoxia signaling molecules. These cause the stabilization and translocation of the transcription factor hypoxia-inducible factor 1α (HIF1α) into the nucleus, where it binds to hypoxia responsive elements (*HRE*s) to activate a wide range of target genes. This results in the modulation of diverse cellular processes including cell proliferation, apoptosis,

differentiation, angiogenesis and inflammation. *HRE*s are enhancers, which are located to the coding regions of oxygen-responsive genes (Biddlestone et al., 2015; Hamanaka and Chandel, 2009; Javan and Shahbazi, 2017).

For investigation of the involvement of DLC1 and CagA in the signaling pathways mentioned above, luciferase reporter activity assays were performed using the pGL3_*HRE* reporter plasmid (Fig. 3.20). This stress responsive plasmid contains the *HMGB2* promoter and the enhancer *HRE*. In non-cancer HEK293T cells, CagA efficiently inhibited *HRE* activity compared to EV transfection. This suggests, with regard to the anti-microbial activity of HMGB2, that CagA inhibits the host's anti-microbial defense against *H. pylori* to ensure colonization and persistence of the bacteria. In contrast, DLC1.1 significantly increased *HRE* activity compared with CagA. This leads to the conclusion that DLC1.1 promotes the anti-microbial defense to eliminate the bacteria and to minimize the oncogenic effects of CagA. This further demonstrates antagonizing functions of the two proteins in initial steps of infection. Nevertheless, abolishment of CagA-mediated inhibition of the anti-microbial response by DLC1.1 was not observed. The effect of CagA and DLC1.1 on *HRE* activity was reversed in GC AGS cells and metastasis-derived NCI-N87 cells compared to non-cancer HEK293T cells. In AGS but not NCI-N87 cells, CagA was a strong activator of *HRE*. However, in both cancer cell lines, CagA transfection resulted in significantly increased *HRE* activity over DLC1.1 transfection. Inflammation and cancer are metabolically costly processes characterized by an increased use of oxygen. Hence, hypoxia is a hallmark of solid tumors and cancer is characterized by an imbalance in the production of ROS and antioxidants (Acharya et al., 2010; Javan and Shahbazi, 2017; Sokolova and Naumann, 2017). Transferring this to the findings from the luciferase activity assays, CagA seems to promote the imbalance in ROS production during carcinogenesis to cause damage to the host cell, whereas DLC1.1 counteracts. Merely in NCI-N87 cells, CagA was able to abolish DLC1.1-mediated *HRE*-inhibition, verifying a powerful oncogenic role of CagA in metastasis. Thus, the effect of CagA and DLC1 on *HRE* activity was strongly dependent on the cell line used, suggesting stage-dependent, but always antagonizing functions of the two proteins during tumorigenesis. This data further demonstrates a stage-dependent role of ROS in gastric disease. Due to the fact that ROS derive from different sources and it still needs to be elucidated if ROS act to eliminate pathogens or the host cells, the luciferase activity assays leave room for various

interpretation possibilities. Thus, further analyses concerning CagA/DLC1-mediated ROS generation and stress induction were conducted to support and strengthen the findings from luciferase activity assays. FACS analyses showed *per se* ROS induction by transfection (Fig. 3.21). Hence, it was not possible to make a clear statement on the effect of CagA or DLC1 on the ROS production. To further investigate the role of CagA and DLC1 in the hypoxic response, the effect of the two proteins on the mediator of the hypoxic response HIF1α was analyzed in AGS cells by Western Blot (Fig. 3.22). To induce ROS and to stabilize HIF1α, which is unstable and proteasomally degraded under normoxia, cells were additionally treated with $CoCl_2$ (Javan and Shahbazi, 2017; Kotake-Nara and Saida, 2007). This experiment was not able to shed light on the role of DLC1 and CagA in hypoxic response as well, because HIF1α level did not change by DLC1 or CagA transfection. Nonetheless, a crosstalk between HIFs and NFκB attracts increasing attention in these days (Bonello et al., 2007; Sokolova and Naumann, 2017). Thus, the effect of CagA and DLC1 on NFκB signaling was examined by Western Blot analyses (Fig. 3.23). To enhance this effect, TLR4-positive AGS cells were additionally treated with *E. coli*-derived LPS, because LPS of *H. pylori* is not recognized by TLR4 (Salama et al., 2013; Su et al., 2003). Furthermore, *E. coli*-derived LPS has been shown to form a heterocomplex with HMGB proteins, which binds to TLR4 and thereby triggers the synthesis of mitochondrial ROS and NFκB signaling (Kang et al., 2013; Sokolova and Naumann, 2017). Tripathi et al. showed that DLC1 suppresses the activity of NFκB in prostate cells in a GAP and α-catenin dependent manner. They demonstrated an inhibition of NFκB signaling by suppression of the RHO-pathway and an accumulation and nuclear translocation of HIF1α when DLC1 is silenced (Tripathi et al., 2012). DLC1-mediated inhibition of active NFκB was not confirmed by this study. CagA transfection did not change the level of phosphorylated NFκB as well. This is not in line with findings from the literature, which showed that CagA is required for the activation of NFκB (Lamb et al., 2009). In contrast, other studies demonstrated that CagA is dispensable for a direct NFκB activation (Sokolova and Naumann, 2017).

Summarized, these findings suggest an antagonizing mode of action of DLC1 and CagA concerning cellular hypoxic stress response. The functions of the two proteins change from initial to advanced steps in carcinogenesis. Whereas CagA seems to inhibit the host's anti-microbial defense, DLC1 intends to eliminate the pathogens in the initial phase. During

carcinogenesis, CagA enforces ROS production and benefits from ROS imbalance in GC to damage the host cells. This is in contrast to DLC1, which inhibits ROS generation to minimize the oncogenic effects of CagA. Nevertheless, these findings require confirmation and the specific function of DLC1 and CagA in stress response and hypoxia needs to be clarified. To this end, multiplex analyses (e.g. protein microarrays) are suggested to elucidate the involved pathways. In this context, Tripathi et al. gave first evidence for a crucial role of the cytoskeleton and DLC1's interaction with components of the focal adhesions (Tripathi et al., 2012).

Although CagA-mediated RHOA activation and DLC1-mediated inhibition of RHOA are well established, inhibition of CagA-mediated G-protein coupled RHOA activation by DLC1 still needs to be verified (Braun and Olayioye, 2015; De Falco et al., 2015; Yamahashi and Hatakeyama, 2013). To this end, luciferase activity assays were performed using the p*SRE*.L plasmid, which contains mutant *SRE* and is therefore suitable to monitor RHOA activity (Wells et al., 2001) (Fig. 3.24). DLC1-mediated RHOA inhibition was confirmed for HEK293T and AGS cells. CagA was no strong activator of mutated *SRE* and inhibition of CagA-mediated RHOA activation by DLC1 was not clearly verified, neither for HEK293T, nor for AGS cells. In contrast, GST-pulldown assay revealed a strong activation of RHOA by CagA, suppression of RHOA activity by DLC1 and inhibition of CagA-mediated G-protein-coupled RHOA activation by both DLC1 isoforms (Fig. 3.25). Inhibition of the CagA-mediated RHOA activation was stronger by DLC1.4 compared to DLC1.1. This is in agreement with the interaction studies (see 3.2.1), which suggest a stronger interaction between CagA and DLC1.4 compared with DLC1.1, confirming DLC1.4 as the *Helicobacter*-interacting isoform as already mentioned (Hitkova et al., 2013).

In summary, DLC1 and CagA act antagonizing concerning RHOA activation. Inhibition of CagA-mediated G-protein-coupled RHOA activation by DLC1 has been shown for the first time by this thesis. This suggests a new risk stratification of *Helicobacter*-infected GC patients according their *RHOA* mutations into the genomically stable subtype of GC and establishes new options for cancer treatment and response prediction.

4.4 Therapy of a preclinical model for GC with an inhibitor of the RHO/ROCK-pathway

Besides restoration of DLC1 expression by epigenetic approaches, inhibition of the RHO/ROCK-pathway represents a potential therapeutic strategy for treatment of GC, since *RHOA* was identified as the major oncogenic driver mutation of diffuse GC (Cancer Genome Atlas Research, 2014; Kakiuchi et al., 2014; Popescu and Goodison, 2014; Wang et al., 2014). RHOA activates several downstream effectors such as the RHO-associated protein kinases ROCK1/2. ROCK 1 and 2 share highly related functional domains and distribution patterns are similar throughout adult tissues. ROCK1/2 phosphorylates a series of downstream proteins including MLC2, which regulates cell processes such as contractility, migration and growth thereby attributing the ROCK-pathway a key role in cancer (Julian and Olson, 2014). For this study, the ROCK inhibitor fasudil [1-(5-isoquinoline sulfonyl)-homopiperazine) was used for *in vivo* therapy of a preclinical model for GC. Fasudil is already in use for treatment of hypertension, cerebral vasospasm or atherosclerosis. Furthermore, anti-tumor efficacy of fasudil has been shown in rodent xenograft studies for breast, myeloma, lung, melanoma, glioblastoma and head-and-neck cancer (Deng et al., 2010; Julian and Olson, 2014; Miyamoto et al., 2012; Xia et al., 2015; Ying et al., 2006).

The transgenic CEA424-SV40 TAg mouse model of GC was used for therapy. These mice express the oncogene SV40 large T-antigen of the Simian Virus as a transgene under control of the human CEA promoter, which is particularly active in the pylorus of the stomach (Thompson et al., 2000). Transgenic mice develop highly proliferative tumors within 4 weeks of age, which are characterized by upregulated stem cell and neuroendocrine gene signatures (Ihler et al., 2012; Vetter et al., 2016). Due to the anatomical localization of the tumor, its diffuse histomorphology, the high proliferation index and its genetic characteristics, these transgenic mice were suggested to be an appropriate preclinical model for human diffuse GC.

Presence of the drug target proteins RHOA and ROCK1/2 was validated on mRNA and protein levels *in vitro* (Fig. 3.27 and 3.29) and *in vivo* (Fig. 3.31, Fig. 3.32, Fig. 3.36). For *in vitro* experiments human GC cell lines (AGS and MKN45) and HEK293T cells were used. The HEK293T cells had been transformed by the same viral oncogene SV40 large T-antigen that

was overexpressed by the transgenic mice used for fasudil therapy and, thus, were defined as an appropriate *in vitro* model for ROCK1/2 inhibition (Thakur et al., 2012). It is suggested that there is a gain of function (GOF) of RHO-signaling in human GC cell lines (Lin et al., 2007; Pan et al., 2004), which means that RHO is bound to GTP and, thus, constitutively active resulting in malignant cell phenotypes. *In vitro* studies demonstrated that this GOF can be abolished by inhibition of ROCK1/2 (Liu et al., 2004; Sun et al., 2007; Xu et al., 2012). Figure 3.28 showed only weak RHOA activity for MKN45 cells. However, there is no evidence in the literature concerning RHOA function *in vivo*. The results of this thesis suggest a GOF of RHOA for the preclinical model of human GC used for therapy. Although it was not possible to detect active RHOA, total protein levels of RHOA and its phosphorylated downstream effector ROCK1/2 were increased in gastric tumor tissue compared to normal tissue. Significantly elevated levels of active phosphorylated ROCK1/2 protein in tumor tissue (Fig. 3.32, Fig. 3.33) as a surrogate marker argue for a GOF of RHOA similar to oncogenic *KRAS* mutations, which are responsible for the development of CRC (Lemieux et al., 2015). Problems in detecting active RHOA may be of experimental nature, because RHOA is known to have more than one substrate such as rhotekin (Heasman and Ridley, 2008). Nevertheless, further studies on other mouse models and human samples are needed to elucidate whether increased GTPase activity or the increase in total RHOA protein amounts are responsible for activation of the downstream ROCK1/2 signaling pathway.

Decreased levels of phosphorylated ROCK2 and MLC2 protein in fasudil treated GC cells and reduced cell viability by fasudil treatment of CRC and GC cells demonstrated *in vitro* efficacy of the ROCK1/2 inhibitor (Fig. 3.29, Fig. 3.30). MALDI-MS imaging was performed in cooperation with Prof. Hopf (Center for Applied Research in Biomedical Mass Spectrometry and Institute of Medical Technology of Heidelberg University and Mannheim University of Applied Sciences, Mannheim, Germany) and verified the presence of the drug in the gastric tumor of transgenic mice (data not shown, Hinsenkamp et al., 2016). Preclinical efficacy of fasudil was assessed by PET/CT imaging in cooperation with Prof. Wängler (Dept. of Clinical Radiology and Nuclear Medicine, Medical Faculty Mannheim of University Heidelberg) in living transgenic mice. Uptake of [^{18}F]-FDG due to high metabolic activity of the tumor was determined in the anatomical area corresponding to the pylorus of the stomach. Tumor volume, tumor area and staining of the proliferation marker Ki67 were significantly reduced

in treated mice compared with control animals (Fig. 3.34, Fig. 3.35). Furthermore, phosphorylation of ROCK2 was decreased in treated mice compared with vehicle controls (Fig. 3.37). Since fasudil acts downstream of RHOA, total protein amounts of the small GTPase, but not of its downstream targets P-p38 and P-ERK1/2 were unaffected by fasudil treatment (Fig. 3.36, Fig. 7.6, Fig. 7.7). These findings demonstrate inhibited GC growth *in vivo* by inhibition of the RHO/ROCK-pathway.

Summarized, this data proposes inhibition of the RHO/ROCK-pathway as a potential therapy strategy for human GC.

5 Conclusion

This thesis demonstrates a protective role of DLC1 in inflammation and cancer progression of the GI tract by regulating the immune response and gastric acid homeostasis. *Helicobacter*-infection is known to potentiate the risk for GC and represents an initial event in tumorigenesis before the onset of neoplastic changes. Transcriptional downregulation of DLC1 by the *Helicobacte*r toxin CagA proposes DLC1 as an early diagnostic marker for human *Helicobacter*-related gastric disease. DLC1 showed antagonizing functions compared to CagA by complex formation *in vitro*. DLC1 herewith neutralized the oncogenic effects of CagA and acted anti-proliferative, promoted cell adhesion and antagonized CagA's hypoxic stress modulation (Fig. 5.1). Due to the oppositional effects of the two proteins on the regulation of the major oncogenic driver of human GC RHOA, *Helicobacter*-associated GC may be assigned to the genomically stable subtype. This represents a novel risk stratification for *Helicobacter*-infected GC patients according their *RHOA* mutation characteristics. Efficient tumor growth reduction by inhibition of the RHO/ROCK-pathway furthermore represents a potential therapy strategy of GC and constitutes DLC1 as a future druggable target in human GC.

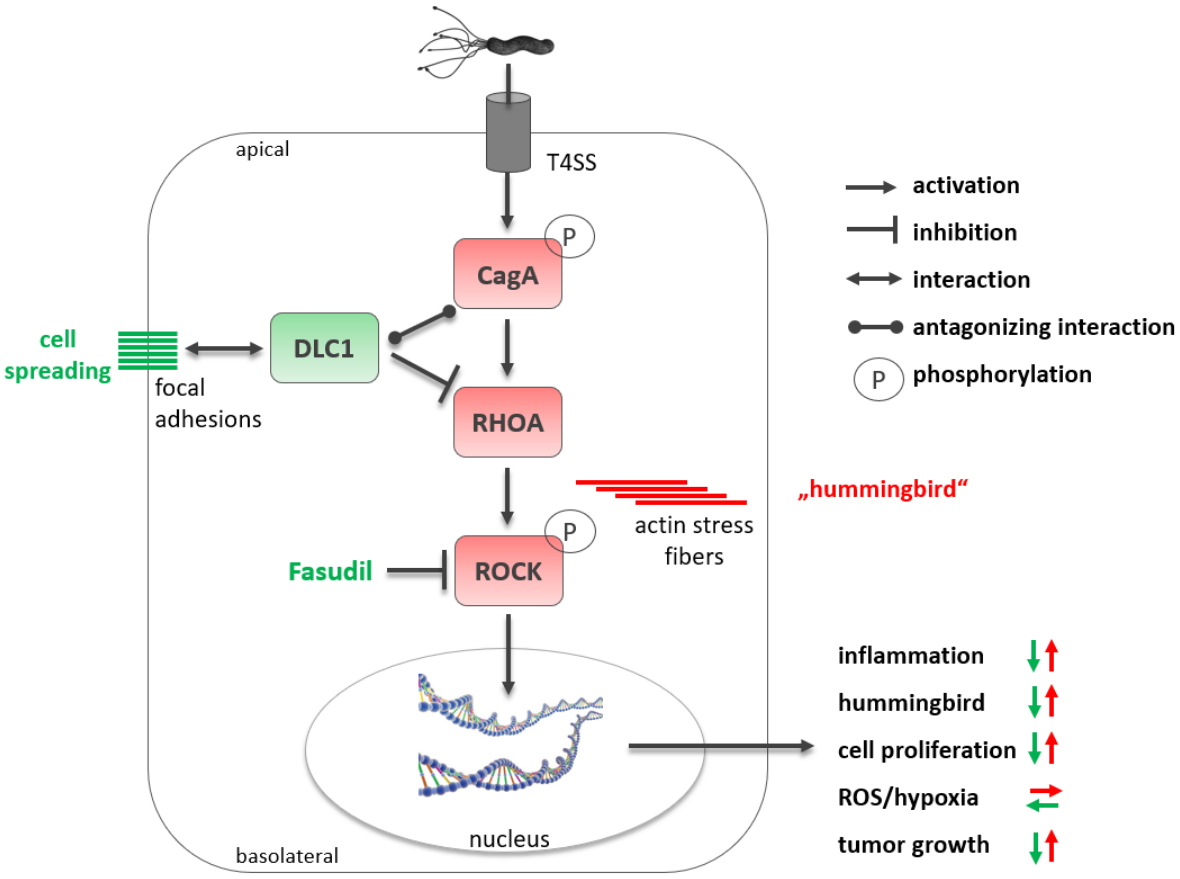

Fig. 5.1: Simplified signaling model of the antagonizing pro- and anti-tumor components CagA and DLC1. After translocation of the *Helicobacter* toxin CagA via a Type IV Secretion System (T4SS) into the host gastric epithelial cell, a pro-tumor pathway is triggered. CagA activates the RHO/ROCK-pathway leading to a deregulation of epithelial polarity (“hummingbird” phenotype). CagA increases cell proliferation, inflammation and modulates cellular hypoxic stress response towards tumorigenesis. In contrast, DLC1 negatively regulates RHOA and directly interacts with CagA thereby antagonizing the pro-oncogenic effects of CagA. DLC1 interacts with components of the focal adhesions, which are responsible for the maintenance of cell adhesion. Fasudil reduced tumor growth by inhibiting ROCK downstream of DLC1. Green: anti-tumor; red: pro-tumor.

6 References

Acharya, A., Das, I., Chandhok, D., and Saha, T. (2010). Redox regulation in cancer: a double-edged sword with therapeutic potential. Oxid Med Cell Longev *3*, 23-34.

Al-Risi, E.S., Al-Essry, F.S., and Mula-Abed, W.S. (2017). Chromogranin A as a Biochemical Marker for Neuroendocrine Tumors: A Single Center Experience at Royal Hospital, Oman. Oman Med J *32*, 365-370.

Almuhaideb, A., Papathanasiou, N., and Bomanji, J. (2011). 18F-FDG PET/CT imaging in oncology. Ann Saudi Med *31*, 3-13.

Amieva, M.R., Vogelmann, R., Covacci, A., Tompkins, L.S., Nelson, W.J., and Falkow, S. (2003). Disruption of the epithelial apical-junctional complex by *Helicobacter pylori* CagA. Science *300*, 1430-1434.

Aras, S., and Zaidi, M.R. (2017). TAMeless traitors: macrophages in cancer progression and metastasis. Br J Cancer *117*, 1583-1591.

Barras, D., and Widmann, C. (2014). GAP-independent functions of DLC1 in metastasis. Cancer metastasis reviews *33*, 87-100.

Bekhbat, M., Rowson, S.A., and Neigh, G.N. (2017). Checks and balances: The glucocorticoid receptor and NFkB in good times and bad. Front Neuroendocrinol *46*, 15-31.

Biddlestone, J., Bandarra, D., and Rocha, S. (2015). The role of hypoxia in inflammatory disease (review). Int J Mol Med *35*, 859-869.

Blaser, M.J., and Atherton, J.C. (2004). *Helicobacter pylori* persistence: biology and disease. Journal of Clinical Investigation *113*, 321-333.

Bonello, S., Zahringer, C., BelAiba, R.S., Djordjevic, T., Hess, J., Michiels, C., Kietzmann, T., and Gorlach, A. (2007). Reactive oxygen species activate the HIF-1alpha promoter via a functional NFkappaB site. Arterioscler Thromb Vasc Biol *27*, 755-761.

Bosetti, C., Bertuccio, P., Malvezzi, M., Levi, F., Chatenoud, L., Negri, E., and La Vecchia, C. (2013). Cancer mortality in Europe, 2005-2009, and an overview of trends since 1980. Ann Oncol *24*, 2657-2671.

Braun, A.C., and Olayioye, M.A. (2015). Rho regulation: DLC proteins in space and time. Cellular signalling *27*, 1643-1651.

Braun, M.W., and Iwakuma, T. (2016). Regulation of cytotoxic T-cell responses by p53 in cancer. Transl Cancer Res *5*, 692-697.

Buchholz, V.R., Schumacher, T.N., and Busch, D.H. (2016). T Cell Fate at the Single-Cell Level. Annu Rev Immunol *34*, 65-92.

Burgermeister, E., Friedrich, T., Hitkova, I., Regel, I., Einwachter, H., Zimmermann, W., Rocken, C., Perren, A., Wright, M.B., Schmid, R.M.*, et al.* (2011). The Ras inhibitors caveolin-1 and docking protein 1 activate peroxisome proliferator-activated receptor gamma through spatial relocalization at helix 7 of its ligand-binding domain. Molecular and cellular biology *31*, 3497-3510.

Calam, J. (1999). *Helicobacter pylori* modulation of gastric acid. Yale J Biol Med *72*, 195-202.

Cancer Genome Atlas Research, N. (2014). Comprehensive molecular characterization of gastric adenocarcinoma. Nature *513*, 202-209.

Cao, X., Voss, C., Zhao, B., Kaneko, T., and Li, S.S. (2012). Differential regulation of the activity of deleted in liver cancer 1 (DLC1) by tensins controls cell migration and transformation. Proceedings of the National Academy of Sciences of the United States of America *109*, 1455-1460.

Carbo, A., Bassaganya-Riera, J., Pedragosa, M., Viladomiu, M., Marathe, M., Eubank, S., Wendelsdorf, K., Bisset, K., Hoops, S., Deng, X.*, et al.* (2013). Predictive computational modeling of the mucosal immune responses during *Helicobacter pylori* infection. PloS one *8*, e73365.

Catalano, V., Labianca, R., Beretta, G.D., Gatta, G., de Braud, F., and Van Cutsem, E. (2009). Gastric cancer. Crit Rev Oncol Hematol *71*, 127-164.

Caux, C., Ramos, R.N., Prendergast, G.C., Bendriss-Vermare, N., and Menetrier-Caux, C. (2016). A Milestone Review on How Macrophages Affect Tumor Growth. Cancer research *76*, 6439-6442.

Cho, J.H., Jeon, S.R., Kim, H.G., Jin, S.Y., and Park, S. (2017). The serum pepsinogen levels for risk assessment of gastric neoplasms: New proposal from a case-control study in Korea. Medicine (Baltimore) *96*, e7603.

Cohen, A.W., Hnasko, R., Schubert, W., and Lisanti, M.P. (2004). Role of caveolae and caveolins in health and disease. Physiol Rev *84*, 1341-1379.

Covacci, A., Censini, S., Bugnoli, M., Petracca, R., Burroni, D., Macchia, G., Massone, A., Papini, E., Xiang, Z., Figura, N.*, et al.* (1993). Molecular characterization of the 128-kDa immunidominant antigen of *Helicobacter pylori* associated with cytotoxicity and duodenal ulcer. Proc Natl Acad Sci *90*, 5791-5795.

Crew, K.D., and Neugut, A.I. (2006). Epidemiology of gastric cancer. World Journal of Gastroenterology *12*, 354-362.

De Falco, M., Lucariello, A., Iaquinto, S., Esposito, V., Guerra, G., and De Luca, A. (2015). Molecular Mechanisms of *Helicobacter pylori* Pathogenesis. Journal of cellular physiology *230*, 1702-1707.

Deng, L., Li, G., Li, R., Liu, Q., He, Q., and Zhang, J. (2010). Rho-kinase inhibitor, fasudil, suppresses glioblastoma cell line progression in vitro and in vivo. Cancer biology & therapy *9*, 875-884.

Ding, S.Z., Minohara, Y., Fan, X.J., Wang, J., Reyes, V.E., Patel, J., Dirden-Kramer, B., Boldogh, I., Ernst, P.B., and Crowe, S.E. (2007). *Helicobacter pylori* infection induces oxidative stress and programmed cell death in human gastric epithelial cells. Infection and immunity *75*, 4030-4039.

Du, X., Qian, X., Papageorge, A., Schetter, A.J., Vass, W.C., Liu, X., Braverman, R., Robles, A.I., and Lowy, D.R. (2012). Functional interaction of tumor suppressor DLC1 and caveolin-1 in cancer cells. Cancer research *72*, 4405-4416.

Durkin, M.E., Yuan, B.Z., Zhou, X., Zimonjic, D.B., Lowy, D.R., Thorgeirsson, S.S., and Popescu, N.C. (2007). DLC-1:a Rho GTPase-activating protein and tumour suppressor. J Cell Mol Med *11*, 1185-1207.

Dydensborg, A.B., Rose, A.A., Wilson, B.J., Grote, D., Paquet, M., Giguere, V., Siegel, P.M., and Bouchard, M. (2009). GATA3 inhibits breast cancer growth and pulmonary breast cancer metastasis. Oncogene *28*, 2634-2642.

Eapen, M.S., Hansbro, P.M., McAlinden, K., Kim, R.Y., Ward, C., Hackett, T.L., Walters, E.H., and Sohal, S.S. (2017). Abnormal M1/M2 macrophage phenotype profiles in the small airway wall and lumen in smokers and chronic obstructive pulmonary disease (COPD). Sci Rep *7*, 13392.

El-Etr, S.H., Mueller, A., Tompkins, L.S., Falkow, S., and Merrell, D.S. (2004). Phosphorylation-independent effects of CagA during interaction between *Helicobacter pylori* and T84 polarized monolayers. J Infect Dis *190*, 1516-1523.

Famili, F., Wiekmeijer, A.S., and Staal, F.J. (2017). The development of T cells from stem cells in mice and humans. Future Sci OA *3*, FSO186.

Fang, F.C. (2011). Antimicrobial actions of reactive oxygen species. mBio *2*, e00141.

Fasching, P., Stradner, M., Graninger, W., Dejaco, C., and Fessler, J. (2017). Therapeutic Potential of Targeting the Th17/Treg Axis in Autoimmune Disorders. Molecules *22*.

Figueiredo, C., Garcia-Gonzalez, M.A., and Machado, J.C. (2013). Molecular pathogenesis of gastric cancer. Helicobacter *18 Suppl 1*, 28-33.

Fox, J.G., Beck, P., Dangler, C.A., Whary, M.T., Wang, T.C., Shi, H.N., and Nagler-Anderson, C. (2000). Concurrent enteric helminth infection modulates inflammation and gastric immune responses and reduces helicobacter-induced gastric atrophy. Nature medicine *6*, 536-542.

Fox, J.G., and Wang, T.C. (2007). Inflammation, atrophy, and gastric cancer. The Journal of clinical investigation *117*, 60-69.

Garattini, S.K., Basile, D., Cattaneo, M., VFanotto, V., Ongaro, E., Bonotto, M., Negri, F.V., Berenato, R., Ermacora, P., Cardellino, G.G*., et al.* (2017). Molecular classification of gastric cancers: Novel insights and possible future applications. World journal of gastrointestinal oncology *9*, 194-208.

Gershon, M.D. (2013). 5-Hydroxytryptamine (serotonin) in the gastrointestinal tract. Curr Opin Endocrinol Diabetes Obes *20*, 14-21.

Gordon, S. (2003). Alternative activation of macrophages. Nat Rev Immunol *3*, 23-35.

Gossmann, J., Stolte, M., Lohoff, M., Yu, P., Moll, R., Finkernagel, F., Garn, H., Brendel, C., Bittner, A., Neubauer, A*., et al.* (2016). A Gain-Of-Function Mutation in the Plcg2 Gene Protects Mice from Helicobacter felis-Induced Gastric MALT Lymphoma. PloS one *11*, e0150411.

Hakanson, R., Chen, D., Lindstrom, E., Norlen, P., Bjorkqvist, M., and Lehto-Axtelius, D. (1998). Physiology of the ECL cells. Yale J Biol Med *71*, 163-171.

Hakanson, R., Ding, X.Q., Norlen, P., and Chen, D. (1995). Circulating pancreastatin is a marker for the enterochromaffin-like cells of the rat stomach. Gastroenterology *108*, 1445-1452.

Hamanaka, R.B., and Chandel, N.S. (2009). Mitochondrial reactive oxygen species regulate hypoxic signaling. Curr Opin Cell Biol *21*, 894-899.

Hamano, N., Inada, T., Iwata, R., Asai, T., and Shingu, K. (2007). The alpha2-adrenergic receptor antagonist yohimbine improves endotoxin-induced inhibition of gastrointestinal motility in mice. Br J Anaesth *98*, 484-490.

Hatakeyama, M. (2004). Oncogenic mechanisms of the *Helicobacter pylori* CagA protein. Nature reviews Cancer *4*, 688-694.

Heasman, S.J., and Ridley, A.J. (2008). Mammalian Rho GTPases: new insights into their functions from in vivo studies. Nat Rev Mol Cell Biol *9*, 690-701.

Hinsenkamp, I., Schulz, S., Roscher, M., Suhr, A.M., Meyer, B., Munteanu, B., Fuchser, J., Schoenberg, S.O., Ebert, M.P., Wängler, B*., et al.* (2016). Inhibition of Rho-Associated Kinase 1/2 Attenuates Tumor Growth in Murine Gastric Cancer. Neoplasia *18*, 500-511.

Hirata, Y., Maeda, S., Mitsuno, Y., Tateishi, K., Yanai, A., Akanuma, M., Yoshida, H., Kawabe, T., Shiratori, Y., and Omata, M. (2002). *Helicobacter pylori* CagA protein activates serum response element-driven transcription independently of tyrosine phosphorylation. Gastroenterology *123*, 1962-1971.

Hitkova, I. (2013). Die Funktion von Caveolin-1 in *Helicobacter pylori*-induzierter Entzündung des Magens. In Lehrstuhl für Mikrobielle Ökologie (Technische Universität München).

Hitkova, I., Yuan, G., Anderl, F., Gerhard, M., Kirchner, T., Reu, S., Rocken, C., Schafer, C., Schmid, R.M., Vogelmann, R.*, et al.* (2013). Caveolin-1 protects B6129 mice against *Helicobacter pylori* gastritis. PLoS pathogens *9*, e1003251.

Howe, H.L., Wu, X., Ries, L.A., Cokkinides, V., Ahmed, F., Jemal, A., Miller, B., Williams, M., Ward, E., Wingo, P.A.*, et al.* (2006). Annual report to the nation on the status of cancer, 1975-2003, featuring cancer among U.S. Hispanic/Latino populations. Cancer *107*, 1711-1742.

IARC Press (2014). World Cancer Report 2014, B.W. Stewart, and P. Kleihues, eds.

Ihler, F., Vetter, E.V., Pan, J., Kammerer, R., Debey-Pascher, S., Schultze, J.L., Zimmermann, W., and Enders, G. (2012). Expression of a neuroendocrine gene signature in gastric tumor cells from CEA 424-SV40 large T antigen-transgenic mice depends on SV40 large T antigen. PloS one *7*, e29846.

Jackson, C., Cunningham, D., Oliveira, J., and Group, E.G.W. (2009). Gastric cancer: ESMO clinical recommendations for diagnosis, treatment and follow-up. Ann Oncol *20 Suppl 4*, 34-36.

Javan, B., and Shahbazi, M. (2017). Hypoxia-inducible tumour-specific promoters as a dual-targeting transcriptional regulation system for cancer gene therapy. Ecancermedicalscience *11*, 751.

Jemal, A., Bray, F., Center, M.M., Ferlay, J., Ward, E., and Forman, D. (2011). Global cancer statistics. CA Cancer J Clin *61*, 69-90.

Jie, X.X., Zhang, X.Y., and Xu, C.J. (2017). Epithelial-to-mesenchymal transition, circulating tumor cells and cancer metastasis: Mechanisms and clinical applications. Oncotarget *8*, 81558-81571.

Julian, L., and Olson, M.F. (2014). Rho-associated coiled-coil containing kinases (ROCK): structure, regulation, and functions. Small GTPases *5*, e29846.

Kakiuchi, M., Nishizawa, T., Ueda, H., Gotoh, K., Tanaka, A., Hayashi, A., Yamamoto, S., Tatsuno, K., Katoh, H., Watanabe, Y.*, et al.* (2014). Recurrent gain-of-function mutations of RHOA in diffuse-type gastric carcinoma. Nature genetics *46*, 583-587.

Kang, R., Zhang, Q., Zeh, H.J., 3rd, Lotze, M.T., and Tang, D. (2013). HMGB1 in cancer: good, bad, or both? Clinical cancer research : an official journal of the American Association for Cancer Research *19*, 4046-4057.

Karimi, P., Islami, F., Anandasabapathy, S., Freedman, N.D., and Kamangar, F. (2014). Gastric cancer: descriptive epidemiology, risk factors, screening, and prevention. Cancer Epidemiol Biomarkers Prev *23*, 700-713.

Kim, H.J., and Cantor, H. (2014). CD4 T-cell subsets and tumor immunity: the helpful and the not-so-helpful. Cancer Immunol Res *2*, 91-98.

Ko, F.C., and Ping Yam, J.W. (2014). Regulation of deleted in liver cancer 1 tumor suppressor by protein-protein interactions and phosphorylation. International journal of cancer *135*, 264-269.

Kotake-Nara, E., and Saida, K. (2007). Characterization of CoCl2-induced reactive oxygen species (ROS): Inductions of neurite outgrowth and endothelin-2/vasoactive intestinal contractor in PC12 cells by CoCl2 are ROS dependent, but those by MnCl2 are not. Neurosci Lett *422*, 223-227.

Krueger, S., Roessner, A., and Kuester, D. (2011). Murine models of *H. pylori*-induced gastritis and gastric adenocarcinoma. Pathol Res Pract *207*, 599-607.

Küchler, R., Schroeder, B.O., Jaeger, S.U., Stange, E.F., and Wehkamp, J. (2013). Antimicrobial Activity of High-Mobility-Group Box 2: a New Function to a Well-Known Protein. Antimicrobial Agents and Chemotherapy *57*, 4782-4793.

Lamb, A., Yang, X.D., Tsang, Y.H., Li, J.D., Higashi, H., Hatakeyama, M., Peek, R.M., Blanke, S.R., and Chen, L.F. (2009). Helicobacter pylori CagA activates NF-kappaB by targeting TAK1 for TRAF6-mediated Lys 63 ubiquitination. EMBO Rep *10*, 1242-1249.

Lee, A., O'Rourke, J., De Ungaria, M., Robertson, B., Daskalopoulos, G., and Dixon, M.F. (1997). A standardized mouse model of *Helicobacter pylori* infection: introducing the sydney strain. Gastroenterology *112*, 1386-1397.

Lemieux, E., Cagnol, S., Beaudry, K., Carrier, J., and Rivard, N. (2015). Oncogenic KRAS signalling promotes the Wnt/beta-catenin pathway through LRP6 in colorectal cancer. Oncogene *34*, 4914-4927.

Li, G., Du, X., Vass, W.C., Papageorge, A.G., Lowy, D.R., and Qian, X. (2011). Full activity of the deleted in liver cancer 1 (DLC1) tumor suppressor depends on an LD-like motif that binds talin and focal adhesion kinase (FAK). Proceedings of the National Academy of Sciences of the United States of America *108*, 17129-17134.

Li, H.J., Johnston, B., Aiello, D., Caffrey, D.R., Giel-Moloney, M., Rindi, G., and Leiter, A.B. (2014). Distinct cellular origins for serotonin-expressing and enterochromaffin-like cells in the gastric corpus. Gastroenterology *146*, 754-764 e753.

Li, Z., Li, D., Tsun, A., and Li, B. (2015). FOXP3+ regulatory T cells and their functional regulation. Cell Mol Immunol *12*, 558-565.

Liao, J.K., Seto, M., and Noma, K. (2007). Rho kinase (ROCK) inhibitors. Journal of cardiovascular pharmacology *50*, 17-24.

Lin, M.T., Lin, B.R., Chang, C.C., Chu, C.Y., Su, H.J., Chen, S.T., Jeng, Y.M., and Kuo, M.L. (2007). IL-6 induces AGS gastric cancer cell invasion via activation of the c-Src/RhoA/ROCK signaling pathway. International journal of cancer *120*, 2600-2608.

Liu, N., Bi, F., Pan, Y., Sun, L., Xue, Y., Shi, Y., Yao, X., Zheng, Y., and Fan, D. (2004). Reversal of the malignant phenotype of gastric cancer cells by inhibition of RhoA expression and activity. Clinical cancer research : an official journal of the American Association for Cancer Research *10*, 6239-6247.

Longley, D.B., Harkin, D.P., and Johnston, P.G. (2003). 5-fluorouracil: mechanisms of action and clinical strategies. Nature reviews Cancer *3*, 330-338.

Low, J.S., Tao, Q., Ng, K.M., Goh, H.K., Shu, X.S., Woo, W.L., Ambinder, R.F., Srivastava, G., Shamay, M., Chan, A.T*., et al.* (2011). A novel isoform of the 8p22 tumor suppressor gene DLC1 suppresses tumor growth and is frequently silenced in multiple common tumors. Oncogene *30*, 1923-1935.

Lukasik, D., Wilczek, E., Wasiutynski, A., and Gornicka, B. (2011). Deleted in liver cancer protein family in human malignancies (Review). Oncol Lett *2*, 763-768.

Malfertheiner, P. (2011). The intriguing relationship of *Helicobacter pylori* infection and acid secretion in peptic ulcer disease and gastric cancer. Dig Dis *29*, 459-464.

Miranti, E.H., Stolzenberg-Solomon, R., Weinstein, S.J., Selhub, J., Mannisto, S., Taylor, P.R., Freedman, N.D., Albanes, D., Abnet, C.C., and Murphy, G. (2017). Low vitamin B12 increases risk of gastric cancer: A prospective study of one-carbon metabolism nutrients and risk of upper gastrointestinal tract cancer. International journal of cancer *141*, 1120-1129.

Miyamoto, C., Maehata, Y., Motohashi, K., Ozawa, S., Ikoma, T., Hidaka, K., Wada-Takahashi, S., Takahashi, S.-S., Yoshino, F., Yoshida, A*., et al.* (2014). Fasudil, a Rho kinase inhibitor, suppresses tumor growth by inducing CXCL14/BRAK in head and neck squamous cell carcinoma. Biomedical Research *35*, 381-388.

Miyamoto, C., Maehata, Y., Ozawa, S., Ikoma, T., Kubota, E., Izukuri, K., Kato, Y., Hata, R.-I., and Lee, M.-C.-i. (2012). Fasudil Suppresses Fibrosarcoma Growth by Stimulating Secretion of the Chemokine CXCL14/BRAK. Journal of Pharmacological Sciences *120*, 241-249.

Moese, S., Selbach, M., Kwok, T., Brinkmann, V., Konig, W., Meyer, T.F., and Backert, S. (2004). *Helicobacter pylori* induces AGS cell motility and elongation via independent signaling pathways. Infection and immunity *72*, 3646-3649.

Mohammadi, M., Redline, R., Nedrud, J., and Czinn, S. (1996). Role of the host in pathogenesis of *Helicobacter*-associated gastritis: *H. felis* infection of inbred and congenic mouse strains. Infection and immunity *64*, 238-245.

Morales-Guerrero, S.E., Mucito-Varela, E., Aguilar-Guitérrez, Lopez-Vidal, Y., and Castillo-Rojas, G. (2013). The Role of CagA Protein Signaling in Gastric Carcinogenesis - CagA Signaling in Gastric Carcinogenesis, G. Mozsik, ed. (Current Topics in Gastritis - 2012).

Moss, S.F., Legon, S., Bishop, A.E., Polak, J.M., and Calam, J. (1992). Effect of *Helicobacter pylori* on gastric somatostatin in duodenal ulcer disease. Lancet *340*, 930-932.

Mueller, A., O'Rourke, J., Chu, P., Kim, C.C., Sutton, P., Lee, A., and Falkow, S. (2003). Protective immunity against *Helicobacter* is characterized by a unique transcriptional signature. Proceedings of the National Academy of Sciences of the United States of America *100*, 12289-12294.

Nagini, S. (2012). Carcinoma of the stomach: A review of epidemiology, pathogenesis, molecular genetics and chemoprevention. World journal of gastrointestinal oncology *4*, 156-169.

Obst, B., Wagner, S., Sewing, K.F., and Beil, W. (2000). *Helicobacter pylori* causes DNA damage in gastric epithelial cells. Carcinogenesis *21*, 1111-1115.

Palframan, S.L., Kwok, T., and Gabriel, K. (2012). Vacuolating cytotoxin A (VacA), a key toxin for *Helicobacter pylori* pathogenesis. Front Cell Infect Microbiol *2*, 1-9.

Pan, Y., Bi, F., Liu, N., Xue, Y., Yao, X., Zheng, Y., and Fan, D. (2004). Expression of seven main Rho family members in gastric carcinoma. Biochemical and biophysical research communications *315*, 686-691.

Parkin, D.M. (2004). International variation. Oncogene *23*, 6329-6340.

Parkin, J., and Cohen, B. (2001). An overview of the immune system. Lancet *357*, 1777-1789.

Pelz, C., Steininger, S., Weiss, C., Coscia, F., and Vogelmann, R. (2011). A novel inhibitory domain of *Helicobacter pylori* protein CagA reduces CagA effects on host cell biology. The Journal of biological chemistry *286*, 8999-9008.

Polk, D.B., and Peek, R.M., Jr. (2010). Helicobacter pylori: gastric cancer and beyond. Nature reviews Cancer *10*, 403-414.

Popescu, N.C., and Goodison, S. (2014). Deleted in liver cancer-1 (DLC1): an emerging metastasis suppressor gene. Mol Diagn Ther *18*, 293-302.

Portal-Celhay, C., and Perez-Perez, G.I. (2006). Immune responses to *Helicobacter pylori* colonization: mechanisms and clinical outcomes. Clin Sci (Lond) *110*, 305-314.

Preston-Martin, S., Pike, M.C., Ross, R.K., Jones, P.A., and Henderson, B.E. (1990). Increased cell division as a cause of human cancer. Cancer research *50*, 7415-7421.

Quiding-Jarbrink, M., Raghavan, S., and Sundquist, M. (2010). Enhanced M1 macrophage polarization in human helicobacter pylori-associated atrophic gastritis and in vaccinated mice. PloS one *5*, e15018.

Ravi, A., Kaushik, S., Ravichandran, A., Pan, C.Q., and Low, B.C. (2015). Epidermal growth factor activates the Rho GTPase-activating protein (GAP) Deleted in Liver Cancer 1 via focal adhesion kinase and protein phosphatase 2A. The Journal of biological chemistry *290*, 4149-4162.

Regel, I., Merkl, L., Friedrich, T., Burgermeister, E., Zimmermann, W., Einwachter, H., Herrmann, K., Langer, R., Rocken, C., Hofheinz, R*., et al.* (2012). Pan-histone deacetylase inhibitor panobinostat sensitizes gastric cancer cells to anthracyclines via induction of CITED2. Gastroenterology *143*, 99-109 e110.

Ren, X.-D., and Schwartz, M.A. (2000). Determination of GTP Loading on Rho. Methods in Enzymology *325*, 264-272.

Sabbir, M.G., Dillon, R., and Mowat, M.R. (2016). Dlc1 interaction with non-muscle myosin heavy chain II-A (Myh9) and Rac1 activation. Biology open *5*, 452-460.

Sabbir, M.G., Prieditis, H., Ravinsky, E., and Mowat, M.R. (2012). The role of Dlc1 isoform 2 in K-Ras2(G12D) induced thymic cancer. PloS one *7*, e40302.

Sabbir, M.G., Wigle, N., Loewen, S., Gu, Y., Buse, C., Hicks, G.G., and Mowat, M.R. (2010). Identification and characterization of Dlc1 isoforms in the mouse and study of the biological function of a single gene trapped isoform. BMC biology *8*, 17.

Saito, Y., Murata-Kamiya, N., Hirayama, T., Ohba, Y., and Hatakeyama, M. (2010). Conversion of *Helicobacter pylori* CagA from senescence inducer to oncogenic driver through polarity-dependent regulation of p21. The Journal of experimental medicine *207*, 2157-2174.

Salama, N.R., Hartung, M.L., and Muller, A. (2013). Life in the human stomach: persistence strategies of the bacterial pathogen *Helicobacter pylori*. Nature reviews Microbiology *11*, 385-399.

Sarrouilhe, D., Clarhaut, J., Defamie, N., and Mesnil, M. (2015). Serotonin and cancer: what is the link? Curr Mol Med *15*, 62-77.

Segal, E.D., Cha, J., Lo, J., Falkow, S., and Tompkins, L.S. (1999). Altered states: involvement of phosphorylated CagA in the induction of host cellular growth changes by *Helicobacter pylori*. Proceedings of the National Academy of Sciences of the United States of America *96*, 14559-14564.

Shum, H.Y., O'Neill, B.J., and Streeter, A.M. (1971). Effect of pH changes on the binding of vitamin B12 by intrinsic factor. Journal of clinical pathology *24*, 239-243.

Siddik, Z.H. (2003). Cisplatin: mode of cytotoxic action and molecular basis of resistance. Oncogene *22*, 7265-7279.

Sokolova, O., and Naumann, M. (2017). NF-kappaB Signaling in Gastric Cancer. Toxins (Basel) *9*.

Spooner, R., and Yilmaz, O. (2011). The role of reactive-oxygen-species in microbial persistence and inflammation. Int J Mol Sci *12*, 334-352.

Strathmann, M.P., and Simon, M.I. (1991). Gα12 and Gα13 subunits define a fourth class of G protein α subunits. Biochemistry *88*, 5582-5586.

Su, B., Ceponis, P.J.M., Lebel, S., Huynh, H., and Sherman, P.M. (2003). *Helicobacter pylori* Activates Toll-Like Receptor 4 Expression in Gastrointestinal Epithelial Cells. Infection and immunity *71*, 3496-3502.

Suerbaum, S., and Josenhans, C. (2007). *Helicobacter pylori* evolution and phenotypic diversification in a changing host. Nature reviews Microbiology *5*, 441-452.

Sun, H.W., Tong, S.L., He, J., Wang, Q., Zou, L., Ma, S.J., Tan, H.Y., Luo, J.F., and Wu, H.X. (2007). RhoA and RhoC -siRNA inhibit the proliferation and invasiveness activity of human gastric carcinoma by Rho/PI3K/Akt pathway. World J Gastroenterol *13*, 3517-3522.

Tan, P., and Yeoh, K.G. (2015). Genetics and Molecular Pathogenesis of Gastric Adenocarcinoma. Gastroenterology *149*, 1153-1162 e1153.

Tang, D., Kang, R., Ill, H.J.Z., and Lotze, M.T. (2011). High-Mobility Group Box 1, Oxidative Stress, and Disease. Antioxidants & Redox Signaling *14*.

Tellmann, G., and Geulen, O. (2006). LightCycler 480 Real-Time PCR System_Innovative Solutions for Relative Quantification. Biochemica, 16-18.

Thakur, B.K., Dittrich, T., Chandra, P., Becker, A., Lippka, Y., Selvakumar, D., Klusmann, J.H., Reinhardt, D., and Welte, K. (2012). Inhibition of NAMPT pathway by FK866 activates the function of p53 in HEK293T cells. Biochemical and biophysical research communications *424*, 371-377.

The Angiogenesis Foundation (2015). Antiangiogenic Therapy for Advanced Gastric Cancer - Update for Oncologists. In Targeting Tumor Angiogenesis.

Thompson, J., Epting, T., Schwarzkopf, G., Singhofen, A., Eades-Perner, A.M., van Der Putten, H., and Zimmermann, W. (2000). A transgenic mouse line that develops early-onset invasive gastric carcinoma provides a model for carcinoembryonic antigen-targeted tumor therapy. International journal of cancer *86*, 863-869.

Tripathi, V., Popescu, N.C., and Zimonjic, D.B. (2012). DLC1 interaction with alpha-catenin stabilizes adherens junctions and enhances DLC1 antioncogenic activity. Molecular and cellular biology *32*, 2145-2159.

Tu, S., Bhagat, G., Cui, G., Takaishi, S., Kurt-Jones, E.A., Rickman, B., Betz, K.S., Penz-Oesterreicher, M., Bjorkdahl, O., Fox, J.G.*, et al.* (2008). Overexpression of interleukin-1beta induces gastric inflammation and cancer and mobilizes myeloid-derived suppressor cells in mice. Cancer cell *14*, 408-419.

Uemura, N., Okamoto, S., Yamamoto, S., Matsumura, N., Yamaguchi, S., Yamakido, M., Taniyama, K., Sasaki, N., and Schlemper, R.J. (2001). *Helicobacter pylori* infection and the development of gastric cancer. The New England Journal of Medicine *345*, 784-789.

Van Doorn, N.E.M., Namavar, F., Sparrius, M., Stoof, J., Van Rees, E.P., Van Doorn, L.-J., and Vandenbroucke-Grauls, C.M.J.E. (1999). *Helicobacter pylori*-associated gastritis in mice is host and strain specific. Infection and immunity *67*, 3040-3046.

Vetter, E., Kronast, M., Tolge, M., and Zimmermann, W. (2016). Lgr5-expressing stem cells are not the cells of origin of pyloric neuroendocrine carcinomas in mice. J Pathol *238*, 42-51.

Vickers, E.R., Kasza, A., Kurnaz, I.A., Seifert, A., Zeef, L.A., O'Donnell, A., Hayes, A., and Sharrocks, A.D. (2004). Ternary complex factor-serum response factor complex-regulated gene activity is required for cellular proliferation and inhibition of apoptotic cell death. Molecular and cellular biology *24*, 10340-10351.

Wang, F., Qu, N., Peng, J., Yue, C., Yuan, L., and Yuan, Y. (2017). CagA promotes proliferation and inhibits apoptosis of GES-1 cells by upregulating TRAF1/4-1BB. Molecular medicine reports *16*, 1262-1268.

Wang, K., Yuen, S.T., Xu, J., Lee, S.P., Yan, H.H., Shi, S.T., Siu, H.C., Deng, S., Chu, K.M., Law, S.*, et al.* (2014). Whole-genome sequencing and comprehensive molecular profiling identify new driver mutations in gastric cancer. Nature genetics *46*, 573-582.

Weigt, J., and Malfertheiner, P. (2009). Influence of *Helicobacter pylori* on gastric regulation of food intake. Curr Opin Clin Nutr Metab Care *12*, 522-525.

Wells, C.D., Gutowski, S., Bollag, G., and Sternweis, P.C. (2001). Identification of potential mechanisms for regulation of p115 RhoGEF through analysis of endogenous and mutant forms of the exchange factor. The Journal of biological chemistry *276*, 28897-28905.

Wessler, S., Gimona, M., and Rieder, G. (2011). Regulation of the actin cytoskeleton in *Helicobacter pylori*-induced migration and invasive growth of gastric epithelial cells. Cell Commun Signal *9*, 27.

Williams, J.A. (2011). Galpha12/13. The Pancreapedia: Exocrine Pancreas Knowledge Base.

Wilson, K.T., and Crabtree, J.E. (2007). Immunology of *Helicobacter pylori*: insights into the failure of the immune response and perspectives on vaccine studies. Gastroenterology *133*, 288-308.

Xia, Y., Cai, X.Y., Fan, J.Q., Zhang, L.L., Ren, J.H., Chen, J., Li, Z.Y., Zhang, R.G., Zhu, F., and Wu, G. (2015). Rho Kinase Inhibitor Fasudil Suppresses the Vasculogenic Mimicry of B16 Mouse Melanoma Cells Both In Vitro and In Vivo. Molecular cancer therapeutics *14*, 1582-1590.

Xiang, Z., Censini, S., Bayeli, P.F., Telford, J.L., Figura, N., Rappuoli, R., and Covacci, A. (1995). Analysis of expression of CagA and VacA virulence factors in 43 strains of *Helicobacter pylori* reveals that clinical isolates can be divided into two major types and that CagA is not neccessary for expression of the vacuolating cytotoxin. Infection and immunity *63*, 94-98.

Xu, W., Yang, Z., and Lu, N. (2016). Molecular targeted therapy for the treatment of gastric cancer. J Exp Clin Cancer Res *35*, 1.

Xu, X.T., Song, Q.B., Yao, Y., Ruan, P., and Tao, Z.Z. (2012). Inhibition of RhoA/ROCK signaling pathway promotes the apoptosis of gastric cancer cells. Hepato-gastroenterology *59*, 2523-2526.

Yam, J.W., Ko, F.C., Chan, C.Y., Jin, D.Y., and Ng, I.O. (2006). Interaction of deleted in liver cancer 1 with tensin2 in caveolae and implications in tumor suppression. Cancer research *66*, 8367-8372.

Yamahashi, Y., and Hatakeyama, M. (2013). PAR1b takes the stage in the morphogenetic and motogenetic activity of Helicobacter pylori CagA oncoprotein. Cell Adh Migr *7*, 11-18.

Yamaoka, Y. (2010). Mechanisms of disease: *Helicobacter pylori* virulence factors. Nature reviews Gastroenterology & hepatology *7*, 629-641.

Yanai, H., Ban, T., and Taniguchi, T. (2012). High-mobility group box family of proteins: ligand and sensor for innate immunity. Trends in immunology *33*, 633-640.

Yao, Y., Tao, H., Park, D.I., Sepulveda, J.L., and Sepulveda, A.R. (2006). Demonstration and characterization of mutations induced by Helicobacter pylori organisms in gastric epithelial cells. Helicobacter *11*, 272-286.

Ying, H., Biroc, S.L., Li, W.W., Alicke, B., Xuan, J.A., Pagila, R., Ohashi, Y., Okada, T., Kamata, Y., and Dinter, H. (2006). The Rho kinase inhibitor fasudil inhibits tumor progression in human and rat tumor models. Molecular cancer therapeutics *5*, 2158-2164.

Yuasa, Y. (2003). Control of gut differentiation and intestinal-type gastric carcinogenesis. Nature reviews Cancer *3*, 592-600.

Zaas, D.W., Duncan, M., Rae Wright, J., and Abraham, S.N. (2005). The role of lipid rafts in the pathogenesis of bacterial infections. Biochimica et biophysica acta *1746*, 305-313.

Zhang, S.J., Gao, J., Huang, Y., and Xu, W.R. (2009). Study on the pharmacokinetics of Fasudil, a selective Rho kinase inhibitor. Asian Journal of Pharmacodynamics and Pharmacokinetics *9*, 221-226.

7 Appendices

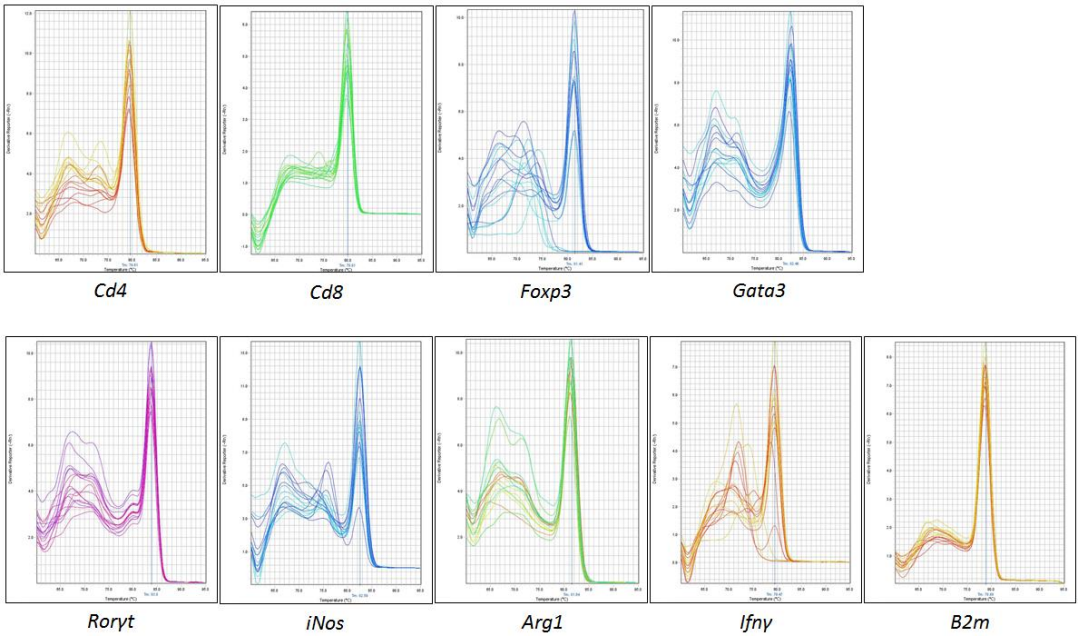

Fig. 7.1: Melting curves corresponding to the expression analysis of surface markers of immune cells and cytokines in DLC1$^{gt/+}$ mice compared to WT mice.

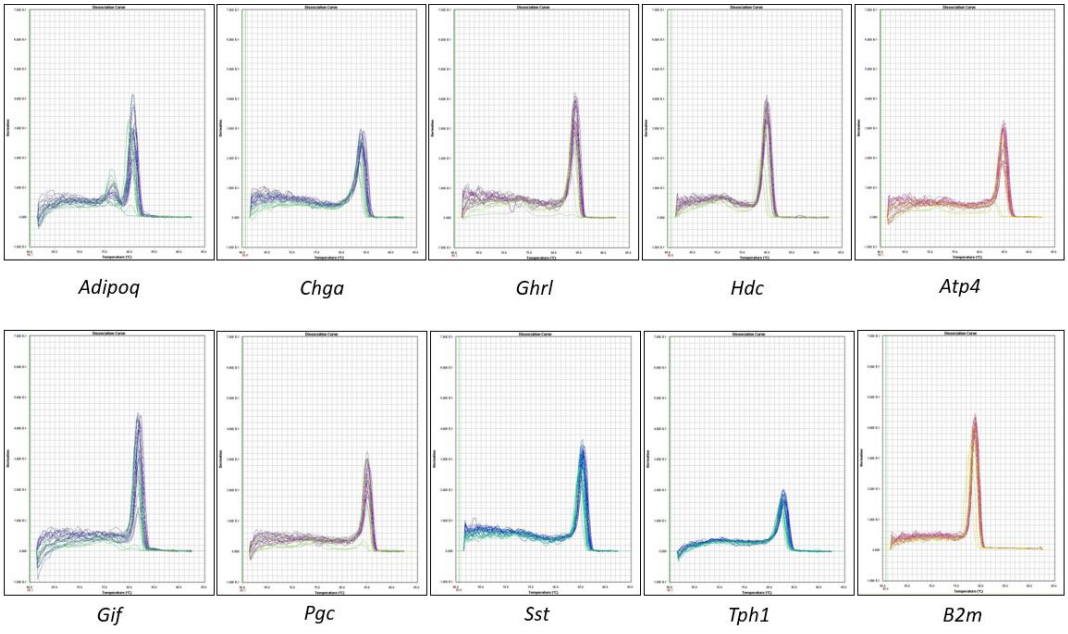

Fig. 7.2: Melting curves corresponding to the expression analysis of proteins involved in hormone balance and gastric acid secretion in DLC1$^{gt/+}$ mice compared to WT mice.

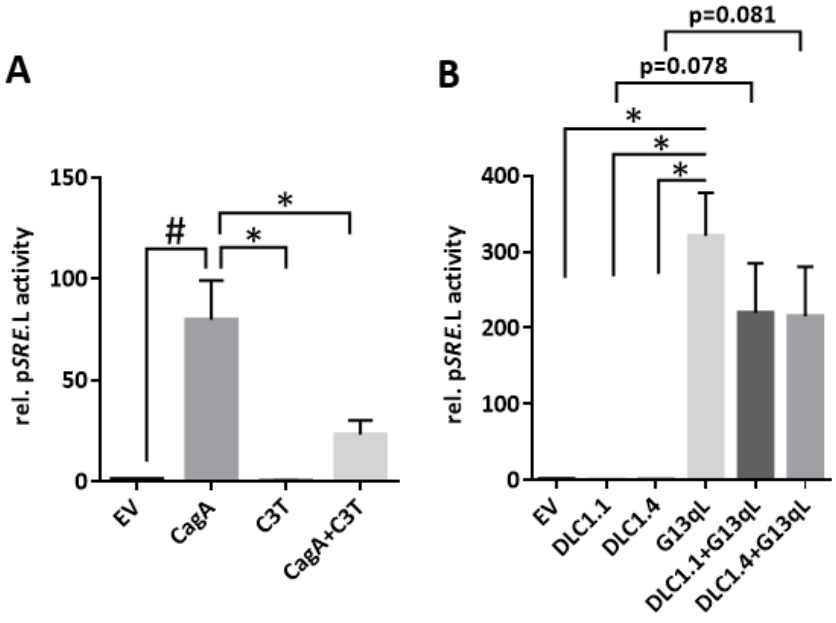

Fig. 7.3: CagA-mediated activation of mutated *SRE* is inhibited by C3T and DLC1-mediated inhibition of mutated *SRE* is abolished by constitutively activated Gα protein. A: TsA201 cells were transiently transfected with empty vector (EV), CagA, a plasmid containing C3T (C3 toxin of *Clostridium botulinum*) or a combination of CagA and C3T in addition to p*SRE*.L and pRL.TK. Luciferase activity was measured by dual luciferase assay. *Firefly* luciferase was normalized to *renilla* luciferase and calculated as -fold ± S.E. (n=6; *p<0.05: unpaired t-test; $^{\#}$p<0.05: one sample t-test). **B:** TsA201 cells were transiently transfected with empty vector (EV), DLC1.1, DLC1.4, a plasmid containing G13qL (constitutively active G-protein α subunit Gα13) or a combination of G13qL with DLC1.1/DLC1.4 in addition to p*SRE*.L and pRL.TK. Luciferase activity was measured by dual luciferase assay. *Firefly* luciferase was normalized to *renilla* luciferase and calculated as -fold ± S.E. (n=2; *p<0.05: 2way ANOVA G13qL vs. EV/DLC1.1/DLC1.4; p=0.078: unpaired t-test DLC1.1 vs. DLC1.1+G13qL; p=0.081: unpaired t-test DLC1.4 vs. DLC1.4+G13qL). Data jointly produced with the group of Prof. Wieland (Dept. of Experimental Pharmacology, Medical Faculty Mannheim of University Heidelberg).

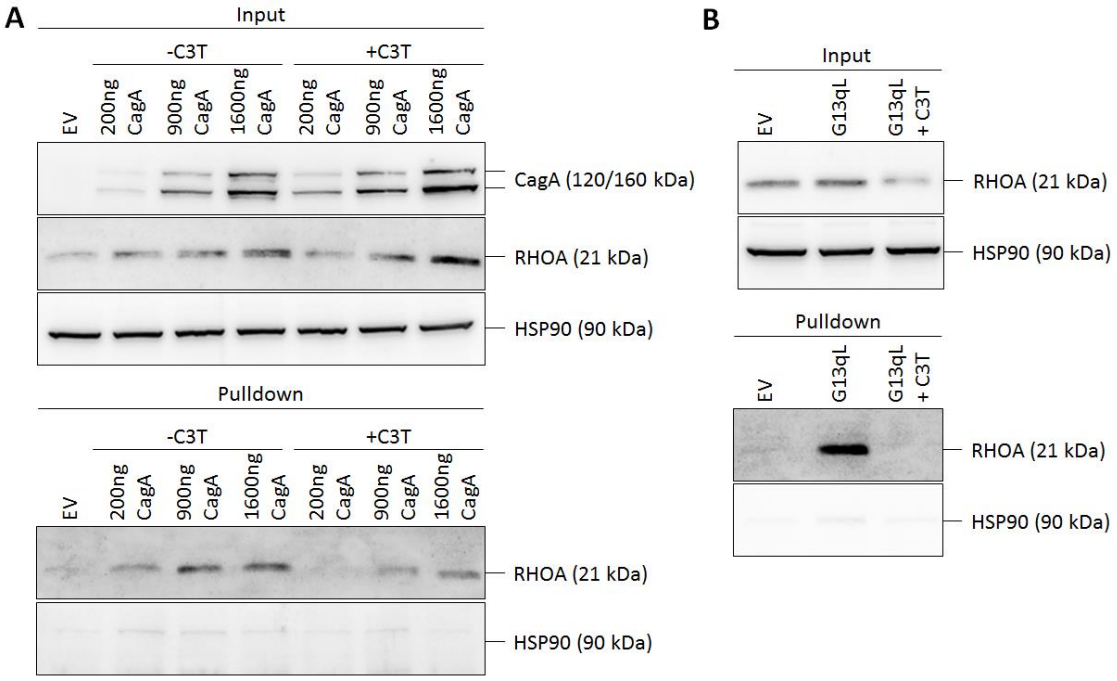

Fig. 7.4: C3T inhibits CagA- and G13qL-mediated G-protein coupled RHOA activation. A: TsA201 cells were transiently transfected with empty vector (EV) and increasing concentrations of CagA with or without co-transfection of C3T (C3 toxin of *Clostridium botulinum*) (n=1). **B:** TsA201 cells were transiently transfected with empty vector (EV), G13qL (constitutively active G-protein α subunit Gα13) or a combination of G13qL with C3T (n=1). RHOA pulldown assay was performed for analysis of RHOA activity. Total cell lysates (Input) were subjected to Western Blot for verification of transfection efficiency and detection of total RHOA amount. Data jointly produced with the group of Prof. Wieland (Dept. of Experimental Pharmacology, Medical Faculty Mannheim of University Heidelberg).

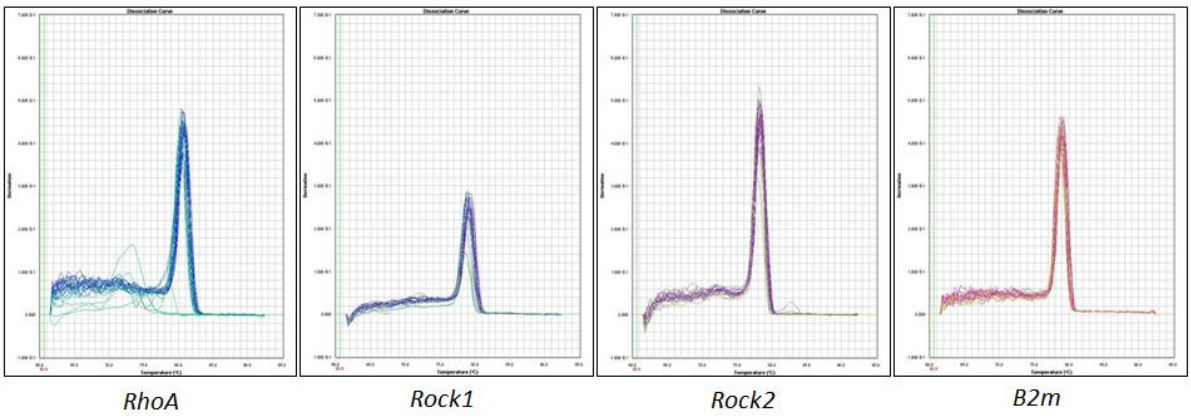

Fig. 7.5: Melting curves corresponding to the expression analysis of *RhoA* and *Rock1/2* in gastric tissue of CEA424-SV40 TAg mice.

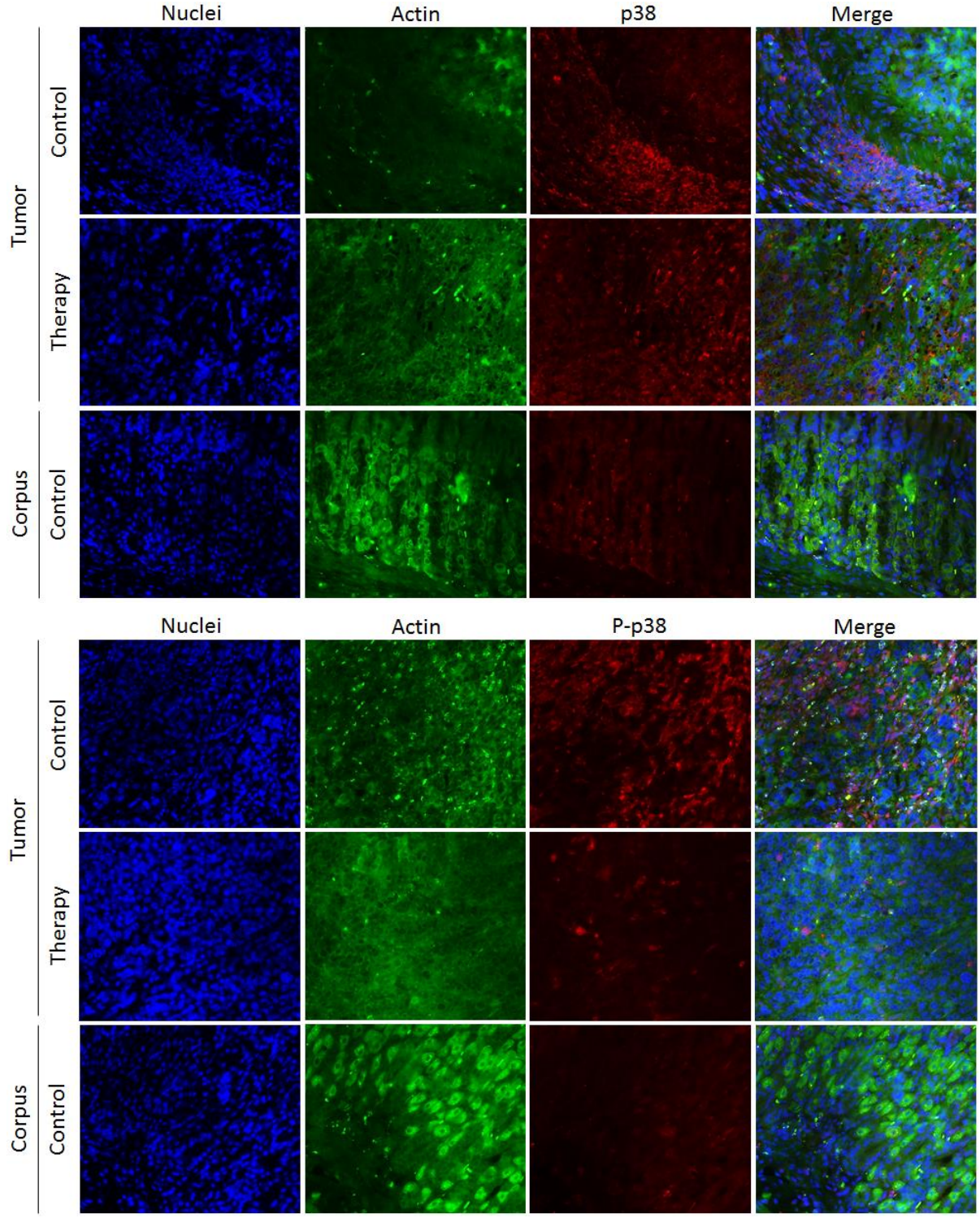

Fig. 7.6: Fasudil lowers P-p38 levels *in situ*. Paraffin embedded stomach tissues of fasudil (four weeks, Therapy) and PBS (Control) treated CEA424-SV40 TAg mice were subjected to (P)-p38 immunofluorescence staining. Gastric tumor tissue (pylorus) was compared with normal gastric tissue (corpus) of PBS treated mice. Blue: DAPI/nuclei; green: actin; red: (P)-p38; magnification 400x. n=1 mouse per group for p38, n=2 mice per group for P-p38, representative pictures are shown.

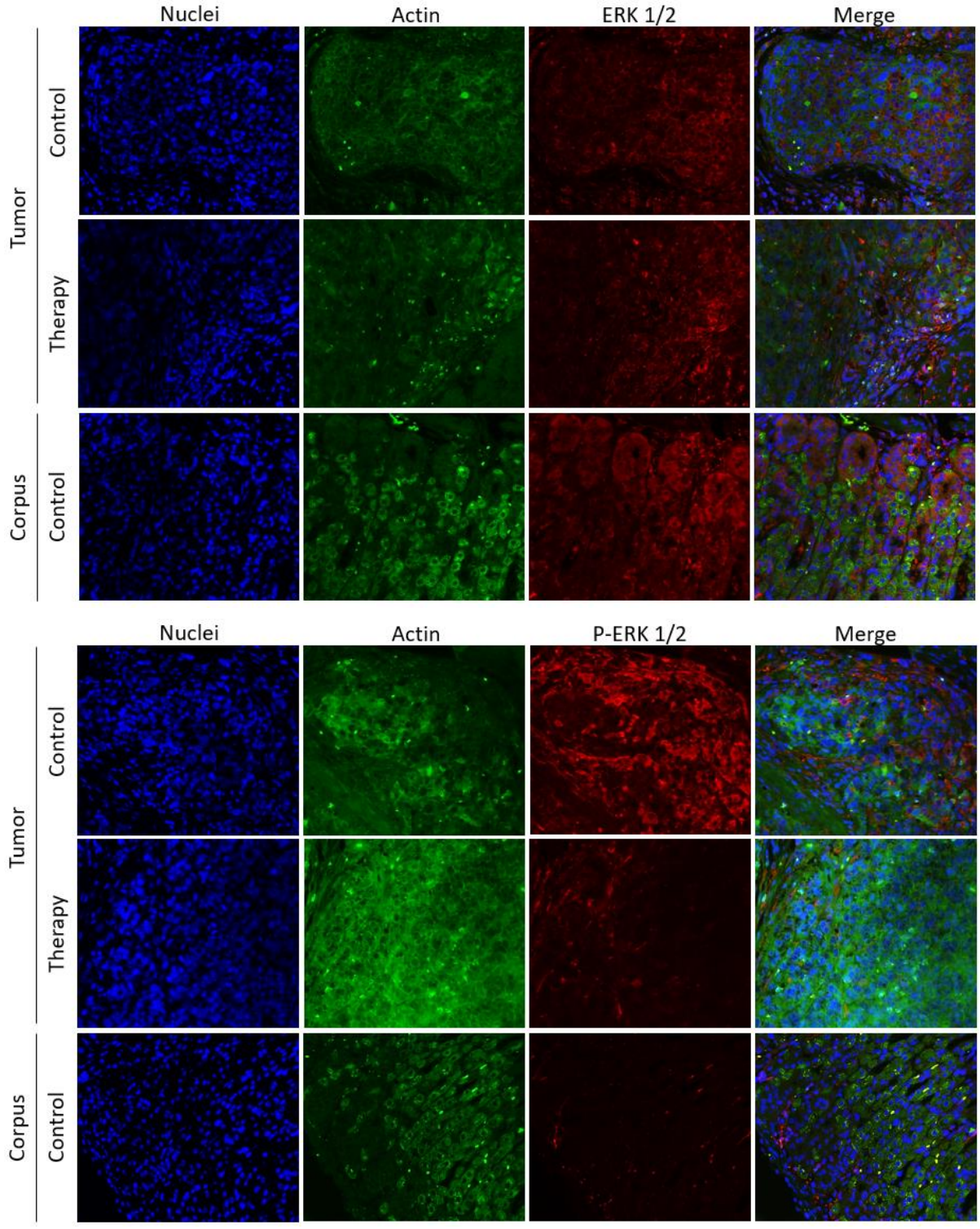

Fig. 7.7: Fasudil lowers P-ERK 1/2 levels *in situ*. Paraffin embedded stomach tissues of fasudil (four weeks, Therapy) and PBS (Control) treated CEA424-SV40 TAg mice were subjected to (P)-ERK immunofluorescence staining. Gastric tumor tissue (pylorus) was compared with normal gastric tissue (corpus) of PBS treated mice. Blue: DAPI/nuclei; green: actin; red: (P)-ERK; magnification 400x. n=1 mouse per group for ERK1/2, n=2 mice per group for P-ERK1/2, representative pictures are shown.

8 Acknowledgment

First, I want to thank Prof. Ebert for providing the opportunity to me to do research at the II. Medical Department, Medical Faculty Mannheim of the University Heidelberg, Mannheim, Germany.

I would like to thank the Deutsche Forschungsgemeinschaft (German Research Foundation, DFG) for financial support (BU2285) of my research project.

I want to thank my supervisors and evaluators Prof. Wink and Prof. Hofmann.

I especially want to thank my mentor and head of the laboratory PD Dr. rer. nat. Burgermeister for the development of the research concept and her scientific supervision.

I want to thank the groups of Prof. Wieland (Experimental Pharmacology) and Prof. Wängler (Dept. of Clinical Radiology and Nuclear Medicine) from the Medical Faculty Mannheim of the University Heidelberg and Prof. Hopf (Center for Applied Research in Biomedical Mass Spectrometry and Institute of Medical Technology of Heidelberg University and Mannheim University of Applied Sciences, Mannheim, Germany) for the kind cooperation.

I want to thank Dr. med. vet. Kränzlin (ZMF, group of Prof. Gretz, Medical Faculty Mannheim of the University Heidelberg, Mannheim, Germany) for organization of the mouse facilities, Stefanie Uhlig from FlowCore Mannheim for her support in FACS performance, Prof. Gaiser (Dept. of Pathology, Medical Faculty Mannheim of the University Heidelberg, Mannheim, Germany) for providing me with patient tissue sections, Prof. Mowat (Dept. of Biochemistry & Medical Genetics, University of Manitoba, Winnipeg, Canada) for supplying the DLC1$^{gt/+}$ mice and PD Dr. Vogelmann for his support concerning the experiments with *Helicobacter*.

Thanks to my past and present lab colleagues in Mannheim. Thank you for your constant help and creating a great working environment during the last years. I especially want to thank Frank Herweck and Sandra Schneider for excellent technical assistance and Friedrich Behne for his help concerning mouse work.

I appreciate the constant support of my parents, all my family members and friends. They played an important role in the accomplishment of this thesis.

Last but not least, I thank you, Florian, for your support and trust in me.